Extraction of Vanadium from New Zealand Titanomagnetite Sand and Vanadium Recovery Concentrate.

By

Lachlan Gaudin

A thesis submitted for the degree of

Master of Science in Chemistry

Victoria University of Wellington

2022

Abstract

This study explores the extraction of the vanadium from titanomagnetite ironsand (IS) from the West Coast of New Zealand, and a vanadium-rich concentrate (VRC) which is formed during the New Zealand steel-making process from this titanomagnetite resource. This extraction first involved an HCl leaching method, with acid concentrations ranging between 1M – 11.5M (concentrated) where the amount of Fe, Ti and V leached/dissolved from the VRC and titanomagnetite materials was determined with respect to leaching time. The concentrations of dissolved Fe, Ti and V in the leachates were measured by ICP-MS, and the solid residues by X-ray fluorescence spectroscopy. The morphology, chemical and individual component characterisation of the solid residues were carried out by X-ray diffraction and scanning electron microscopy and associated energy dispersive elemental and mapping analyses. The leaching results for the VRC showed no selective leaching of Fe, Ti, and V. The amount of Fe, Ti, and V leached increased with increasing HCl concentrations, up to about 50 % of the amount in the original VRC.

A different approach was then taken where the VRC material was roasted overnight at two different temperatures (900 and 1200 °C) wherein the V and Mn formed a manganese vanadate phase ($Mn_2V_2O_7$) and the Fe and Ti formed pseudobrookite (Fe_2TiO_5) within the VRC. The $Mn_2V_2O_7$ phase was found to leach much more readily in HCl, while the pseudobrookite phase, which is comparatively acid-resistant, did not leach to any extent. HCl leaching of the roasted VRC thus resulted in selective dissolution of the V (86.89 % amount leached) from the Fe and Ti (~3 % amount leached). This provides a potential new approach for extracting the vanadium from the VRC material.

In order to remove the small amount of Fe and Ti that did leach from the roasted VRC, an attempt to precipitate the dissolved Ti and Fe from the leachate was made. The dissolved Ti was seeded to promote hydrolysis and form TiO_2, and the Fe was precipitated by increasing the pH to form an iron hydroxide precipitate. ICP-MS analysis of the resulting filtrate showed a large decrease in the concentrations of Fe, Ti, and V compared to the starting leachate, indicating that the V in solution was removed alongside the Ti and Fe. This was likely caused by the V^{5+} forming V_2O_5 and/or being adsorbed onto the surface of the iron hydroxide precipitate. This method to separate the residual dissolved Fe and Ti in the roasted VRC leachate was deemed unsuitable for the extraction of vanadium.

The leaching experiments were repeated with the IS material, and again no selective leaching of Fe, Ti and V was found. Approximately 73 % of these elements were leached. A portion of the IS material was roasted (900 °C overnight) in an attempt to form an acid-soluble manganese vanadium phase similar to the one formed in the VRC roast. Only a small amount of this phase could be identified in the EDS and XRD analyses. HCl leaching of the roasted material similarly resulted in selective dissolution of

the V (29.26 % amount leached) from the Fe and Ti (~13 % amount leached), although total dissolution for these elements was decreased after roasting.

This research has therefore shown that V can be selectively leached from the IS and VRC materials, using a pre-roasting stage to form the manganese vanadate $Mn_2V_2O_7$ phase which is more readily soluble in HCl than the pseudobrookite Ti- and Fe- containing phase.

Acknowledgements

I offer my sincere appreciation to Prof. Jim Johnston, who graciously accepted me as a master's student. It has been a pleasure working with you.

The whole of Jim's research group has kept me well challenged and well entertained. I thank them deeply. From those who endured the year with me, to those who I only briefly met, you have all taught me the imperativeness of enjoying the company of your colleagues.

Abbreviations

EDS – Energy Dispersive X-ray Spectroscopy

ICP-MS – Inductively Coupled Plasma Mass Spectrometry

LOI – loss on ignition

PES – Polyethersulfone

ppm – parts per million

ppb – parts per billion

ppt – parts per trillion

RFB – Redox Flow Battery

RPM – revolutions per minute

SEM – Scanning Electron Microscopy

TTM - Titanomagnetite

VRC – Vanadium Recovery Concentrate

VRU – Vanadium Recovery Unit

XRD – X-ray Powder Diffraction

XRF – X-ray Fluorescence

Table of Contents

Introduction 1
1.1 New Zealand Ironsand 1
1.1.1 Ironsand Reserves in New Zealand 1
1.1.2 Titanomagnetite 2
1.2 NZ Steel 3
1.2.1 NZ Steel-making Process 3
1.2.2 Vanadium-rich Concentrate (VRC) 4
1.3 Vanadium 5
1.3.1 Overview 5
1.3.2 Vanadium Uses 5
1.3.3 Vanadium-manganese Chemistry 7
1.4 Overview of Analytical Methods 10
1.4.1 Energy-dispersive X-ray Spectroscopy 10
1.4.2 X-ray Powder Diffraction 11
1.4.3 X-ray Fluorescence 11
1.4.4 Inductively Coupled Plasma Mass Spectrometry 12
1.5 Extraction of Vanadium 12
1.5.1 Roasting 12
1.5.2 Leaching 14
1.5.3 Kinetics 14
1.5.4 Current Industry Methods 15
1.5.5 Solvent Extraction 16
1.6 Overview of Project 18
2 Experimental 19
2.1 Leaching 19
2.1.1 General Leaching Procedure 19
2.1.2 Leaching of Non-roasted Samples 19
2.1.3 Leaching of Roasted Samples 20
2.1 Precipitation of Material from Filtrate 21
2.2 Analysis and Characterisation 21
2.2.1 XRD 21
2.2.2 XRF 22
2.2.3 SEM/EDS 22
2.2.4 ICP-MS 22

3 Results and Discussion 23
3.1 Introduction 23
3.2 Vanadium Recovery Concentrate (VRC) 23
3.2.1 Analysis of Starting Material 23
3.2.2 Leaching of Non-roasted Samples 27
3.2.1 Titanium and Iron Precipitation from Leachate 41
3.2.2 Roasting of Samples 42
3.2.3 Leaching of Roasted Sample 49
3.3 Ironsand (IS) 63
3.3.1 Analysis of Starting Material 63
3.3.2 Leaching of Non-roasted Samples 65
3.3.3 Roasting of Samples 78
3.3.4 Leaching of Roasted Sample 82
4 Conclusions 87
5 Future Directions 88
5.1 Further Separation of V 88
5.2 Combination with H_2 Reduction 88
6 References 89

Introduction

1.1 New Zealand Ironsand

1.1.1 Ironsand Reserves in New Zealand

Iron-containing mineral deposits, in the form of ironsand, can be found on a 480 km stretch of the New Zealand (NZ) North Island's western coastline (Figure 1.1).[1] These beach and dune deposits are the largest known reserve of ferrous ore located in the country, containing an estimated 322 million tonnes of ore.[2] Currently, mining of this ore takes place at a number of mines on the west coast, north of Taranaki, and an estimated 1.8 million tonnes of this ore are recovered each year as of 2009.[2] These ironsand deposits have been determined to be of volcanic origin.[3] Specifically, the mineral content of the ironsand, as well as the dispersion of the minerals, points to the Mount Taranaki volcano as a major factor in their creation. Offshore ironsand reserves are also known, but estimates of their size are currently poor.[4, 5]

This content is unavailable. Please consult the reference for further details.

Figure 1.1. *Map of the west coast of the North Island of NZ. Indicated (green to red) is the concentration of offshore ironsand deposits. The inset (top left) is the region shown of the west coast. Figure is sourced from* Baker et.al.[4]

The iron in this sand exists mainly as a titanomagnetite ore (TTM), with the general structural formula $Fe_{3-x}Ti_xO_4$.[6] The sand also contains amounts of Ilmenite ($FeTiO_3$) and Magnetite (Fe_3O_4).[2] In

a typical mining process, a TTM concentrate is produced via magnetic and gravity separation, which enrichesthe iron content of the ore to ~70%.[7, 8] This TTM concentrate is used primarily used for the productionof steel, and much of it is sent overseas for this purpose.[9] The typical composition of NZ ironsand concentrate is listed below (Table 1.)

Table 1.1 *Typical composition of NZ ironsand.*[10]

This content is unavailable. Please consult the reference for further details.

1.1.2 Titanomagnetite

The structure of the titanomagnetite mineral is of crucial consideration when attempting to further the understanding of the acid leaching, and possible vanadium extraction from the TTM ore. For this reason, a consideration of the TTM mineral follows.

The TTM ore is a member of the spinel group of minerals, with an inverse-spinel structure.[11] The spinel group contains many ferrites and other magnetic oxides, and is described by the formula AB_2X_4, where A and B are metal ions occupying tetrahedral and octahedral sites, respectively, and X is an anion (Figure 1.2).[12, 13] An inverse-spinel contains a close-packed arrangement of the anions with the tetrahedral *A* site ions substituted for half of the octahedral *B* site ions, which can be formulated as $B(AB)O_4$.[14, 15] In the case of TTM, the regular inverse-spinel structure of magnetite, Fe_3O_4, has been interpolated with a fraction of Ti^{4+} ions populating the *B* site.[16] This can be understood as a magnetite structure substituted in places with some fraction of the mineral Ulvöspinel (Fe_2TiO_4). This leads to the general formula of TTM being $Fe_{3-x}Ti_xO_4$ (where *x* is the parameter giving the fraction of Ulvöspinel present in the structure). A standard unit cell for a spinel is shown below (Figure 1.2).

This content is unavailable. Please consult the reference for further details.

Figure 1.2. *a) Spinel crystal lattice of magnetite, showing atoms in a face-centred cubic structure, b) a close-up of an Fe^{3+} ion occupying a tetrahedral A site, and an Fe^{2+} ion occupying a B site. In TTM, some portion of the B ions is replaced by Ti^{4+}.*

It is expected that the small amount of vanadium impurity within NZ TTM ironsand is not present as V_2O_5. It has been shown that the vanadium within the structure of TTM exists in a solid solution of predominately V^{3+}, substituting the octahedral *B* site ions.[17-19] If this is the case, one expects to see little difference in the acid leaching rate of vanadium and iron from TTM, and this appears to be the case (see section 1.4). This is an important consideration, as it presents yet another research challenge: not only is vanadium present in such small quantities, but it is locked within the ore structure, and selective leaching may thus not be adequate for separation of the vanadium.

1.2 NZ Steel

1.2.1 NZ Steel-making Process

The ironsand used in this research is primarily used to produce steel, thus a brief overview of the NZ steel-making process follows. The development of the NZ steel industry was fraught with challenges, chief of them the fact that the ironsand feedstock contains other minerals, such as TiO_2 and SiO_2. For instance, blast furnaces which were historically used for the smelting of iron ores were deemed inadequate due to the build-up of titanium cyanonitride, TiCN. Early ore-processing plantsturned to direct reduction methods, using a reductant such as carbon, yet this method was more challenging, and relied heavily on the skill of the iron-maker.[20]

Currently, the Waikato North Head mine employs four multi hearth furnaces for the drying of the ore, and the driving off of unwanted impurities such as oils, tars and other hydrocarbons.[21] The ironsand is initially mixed with coal and a small amount of limestone ($CaCO_3$), before being added to

the furnaces. Also employed are four reduction kilns, which turn the iron oxide into pig iron.[22] The main chemical reactions that take place in the kilns are

$$C + O_2 \rightarrow CO_2 \tag{1.1}$$

$$CO_2 + C \rightarrow 2CO \tag{1.2}$$

$$Fe_3O_4 + CO \rightarrow 3FeO + CO_2 \tag{1.3}$$

$$FeO + CO \rightarrow Fe + CO_2 \tag{1.4}$$

$$Fe_3O_4 + 4C \rightarrow 3Fe + 4CO \tag{1.5}$$

Reactions (1.1) and (1.2) work to convert any CO_2 produced into CO gas as long as there is carbon remaining, which can continue to participate in the reduction process.[22] As per reactions (1.4) and (1.5), the primary product that is removed from the kilns is iron metal, which contains carbon and multiple impurities. This product is moved into smelters, where the iron is converted to its molten form. The molten iron is then moved to the vanadium recovery unit (VRU), where the slag is separated from the molten iron.[23] The iron-making process then yields its final product, a liquid iron, which can be transported to the steel-making plant.

1.2.2 Vanadium-rich Concentrate (VRC)

First commissioned in 1986, the VRU contains large metal containers, called ladles, into which the raw molten iron from the smelters is pumped.[23] The VRU is made economical by the fact that the presence of impurities such as vanadium and manganese make other steel-making processes less cost-effective, requiring larger amounts of reagents to process. Not only this, but vanadium is a very useful and costly metal, for which special effort needs to be made in order to extract.[24] In order to extract the metalloids, oxidation is required, which can either be achieved at high temperatures (~1400 °C) via use of a gaseous O_2 stream produced by an oxygen lance, or by the addition of solid millscale powder (a powder of mixed iron oxides). The process takes advantage of the fact that vanadium is preferentially oxidised over the iron and carbon.[25] The oxidised vanadium and the other lower-density materials, such as Si and Ti containing minerals, are allowed to form a slag on the top of the ladle, which can then be mechanically scraped from the surface and collected.

The vanadium-rich slag that this process generates was tested during this research, thus the expectedqualities of this slag are discussed. The following equations represent the important oxidation reactions for iron and vanadium, for both oxidation with O_2 (1.6) and millscale (1.7).[26] The presence of millscalein such high heat also results in the production of oxygen indirectly, which can then perform the required oxidation.

$$2Fe + O_2 \rightarrow 2FeO \quad (1.6)$$

$$2V + 3FeO \rightarrow V_2O_3 + 3Fe \quad (1.7)$$

$$2V + Fe_2O_3 \rightarrow V_2O_3 + 3Fe \quad (1.8)$$

From this, one can expect the vanadium present in the slag to be in the form of vanadium oxide, V_2O_3. However, this is a simplified view, as multiple valences are available to many of the metals contained within pig iron, and vanadium may exist instead as V_2O_5. Information on the composition of this slag produced in NZ is not available, but similar steel production processes have produced vanadium- rich slags with a vanadium concentration of 10-15%, some order of magnitude larger than that containedwithin NZ TTM ironsand.[26] This will provide a large benefit to the research proposed herein, as the biggest challenge for extracting vanadium from TTM is the detection and chemical manipulation of such small quantities. Any extraction method may first be applied to this vanadium-rich slag to determine their efficacy more efficiently.

1.3 Vanadium

1.3.1 Overview

Vanadium, first discovered in 1801 by Spanish-Mexican scientist Manuel Del Rio, was named after the Norse goddess of beauty Vanadis.[27] This was not the name he gave it, however, as his discovery was not recognised until 1831, when Swedish chemist Nils Sefström produced vanadium chlorides from iron ores.[28] Later, the English chemist Henry Roscoe first generated the metallic form of vanadium via the reduction of vanadium dichloride.[29]

The element itself, atomic number 23, takes on a steel-grey appearance with a blueish tinge in itsmetallic form.[30] The element exhibits two isotopes, ^{51}V and ^{50}V, with the former at 99.75% abundance. The metallic form is stable at temperatures below 250 °C, and above this temperature oxidation takes place readily.[31] Other than its metallic V(0) oxidation state, vanadium displays compounds of oxidation state II, III, IV, and V. The major commercial product of vanadium is the V(V) compound V_2O_5.[32] It occurs in the earth's crust at an abundance of 150 g/t, and thus it is a more abundant metal than copper and zinc.[31]

1.3.2 Vanadium Uses

The first application of vanadium was discovered in 1903, when the first vanadium-steel alloy was manufactured.[31] In later years, this alloy would go on to enable the revolution of many technologies. A major example of this was in 1905, when automobile manufacturer Henry Ford recognised the potential of the vanadium-alloyed steel for use in his Model N and S cars.[33] The lighter and stronger

steel alloy was prime for use in areas such as the crankshaft and the axle, where a high-tensile strength material is crucial. This was one of the factors that led the later model, the Model T, become such a financial success, leading to the revolution of the automobile industry.[34] The material went on to find use in a wider range of areas, including machine gears, high-impact tools, and bicycle frames.[31]

This content is unavailable. Please consult the reference for further details.

Figure 1.3. *Henry Ford standing by his Model T (left), spanners made from chrome-vanadium steel alloy (right).*

Other applications of vanadium do not derive from the metallic form of vanadium. In fact, the many oxidation states which vanadium displays offers a unique set of properties that enable applications such as catalysis and energy storage. In particular, the redox flow battery (RFB) is a forthcoming and potentially ground-breaking technology for the storage of renewable energy.[35] The vanadium RFB operates with two electrolyte tanks, each containing a vanadium solution, each of which is fed through a half cell of the battery, where the charging/discharging of the electrolyte takes place (Figure 1.4).[36] Vanadium is well suited for use in RFB technology, due to its many oxidation states, lower levels of gas evolution in quick charges, and good efficiency compared to other RFBs.[37] The positive and negative cell equations are

Positive cell reaction: $$VO_2^+ + 2H^+ + e^- \rightleftharpoons VO^{2+} + H_2O \quad (1.9)$$

Negative cell reaction: $$V^{2+} \rightleftharpoons V^{3+} + e^- \quad (1.10)$$

Overall cell reaction: $$VO_2^+ + 2H^+ + V^{2+} \rightleftharpoons VO^{2+} + H_2O + V^{3+} \quad (1.11)$$

This content is unavailable. Please consult the reference for further details.

Figure 1.4. *Schematic diagram of an RFB, showing the anodic electrolyte (blue) and the cathodic electrolyte (red).*

1.3.3 Vanadium-manganese Chemistry

Many studies have reported either the coextraction, or the solid-state combination of vanadium and manganese in metallurgical contexts.[38-40] For this reason, and for reasons which pertain to the results of this thesis, a brief overview of the Mn-V literature is warranted. While not many studies have been conducted into Mn-V systems, there are two categories which is considered: Mn-V alloys, and Mn-V oxides. Further to this, a short exploration of Mn-V coextraction is presented in the roasting and solvent-extraction sections of this thesis (Section 1.4.1 and 1.4.5, respectively)

A study by Smith and Carlson sought to elaborate on the Mn-V alloy system phase diagram developed by Watersrat in 1962 (Figure 1.5).[41] This diagram shows the phases for annealing a Mn-V alloy at a range of temperatures and compositions. For the sake of this thesis, it is worth considering whatphases are likely to be present if a Mn-V phase were to be formed during the roasting of Ironsand and VRC. From the XRF analysis of the VRC material, the ratio of Mn to V is 3:4 (or 43 %Mn).At this molar ratio, there are two possible annealed phases available above 600 °C. The first is a CsCl-like phase, which is a primitive cubic lattice. (Figure 1.5.a) This phase is formed up to temperatures of roughly 800 °C, and above this, a body-centred-cubic structure is formed (Figure 1.5.b).

This content is unavailable. Please consult the reference for further details.

Figure 1.5. *a) Composite phase diagram for the Mn-V alloy system. Sourced from Smith and Carlson.*[41] *b) Primitive cubic crystal structure. c) Body-centred cubic structure.*

Like the Mn-V alloy system, not much is reported on Mn-V oxides, aside from their use in advanced materials, which will not be covered herein.[42, 43] Instead, the existence of the two most researched Mn-V oxide materials is covered, MnV_2O_6 and $Mn_2V_2O_7$. The first Mn-V oxide to be considered, MnV_2O_6, has potential for application as a catalyst.[44, 45] The structure of this oxide is a brannerite-type structure (UTi_2O6) (Figure 1.6) and can be formed under mild conditions from solutions ofammonium vanadate, NH_4VO_3, and manganese nitrate, $Mn(NO_3)_2$.[46, 47]

This content is unavailable. Please consult the reference for further details.

Figure 1.6. *Brannerite structure of Mn_2VO_6. The unit cell for is indicated by black lines, and the colours designate elements (red = O, grey = Mn, blue = V).*

$Mn_2V_2O_7$ is a paramagnetic oxide which crystallises in two phases (α and β) with a transition between the two around room temperature (~296 K).[48] Its α-phase is triclinic (Figure 1.7.a) whilst the β-phase takes on a monoclinic distorted-honeycomb thortveitite structure ($(Sc,Y)_2Si_2O_7$, Figure 1.7.b).[49, 50] This material has also been studied for its potential in catalysis, particularly as it shows promise for use as a light absorber.[51] It can be grown at room temperature from a solution of $MnCl_2$ and VCl_3.[51] Some literature could be found for the existence of the $Mn_2V_2O_7$ compound being generated via the roasting of a vanadium-rich slag similar to the one studied in this thesis (see section 1.5.1).[52] This material is of particular interest to the results of this thesis, as evidence was found for the existence of this material in the roasted VRC (see section 3.2.2)

This content is unavailable. Please consult the reference for further details.

Figure 1.7 *a) Crystal structure of α-$Mn_2V_2O_7$. b) Crystal structure of β-$Mn_2V_2O_7$. The unit cell for each is indicated by black lines, and the colours designate elements (red = O, grey = V, purple = Mn).*

1.4 Overview of Analytical Methods

Before going into the existing literature on vanadium extraction, it is necessary to explain the relevant analytical methods employed in this research.

1.4.1 Energy-dispersive X-ray Spectroscopy

This technique is usedto generate elemental data of a sample surface, by exploiting the unique atomic structure of each element.[53] A beam of electrons is generated, which ejects an inner-shell electron via excitation (Figure1.8). After ejection, an electron hole is formed in its place, which promotes the relaxation of a higher-energy electron into the K shell. This relaxation results in the emission of a specific frequency of energy (X-rays), which can be used to identify elements in the sample. Three main transitions are used for this analysis.First are the Kα and Kβ transitions, which refer to transitions which result at the K shell of the atom. Also detected is the Lα transition, which involves a relaxation from the M to the L shell.

This content is unavailable. Please consult the reference for further details.

Figure 1.8. *Cartoon representation of atomic transitions probed in EDS analysis.*

The EDS setup consists of an electron source (emitter) and a collector, which are often paired with an electron microscope in order to probe the elemental composition at a specific location. In this thesis, EDS is used in two major ways. The first of which is the generation of elemental maps, giving insight into the arrangement and distribution of mineral phases present in both the starting materials and the acid-leaching residues. Coupled with this are EDS point analyses, where a single point is chosen, and elemental data is collected with nanoscopic resolution. This enables semi-quantitative analysis of individual mineral phases present in the solid materials.[54]

Some limitations are however present.[54, 55] X-rays can only penetrate thoughseveral nanometres of solid material, therefore only surface analysis can be done with this technique. This makesthe technique highly sensitive to surface contamination, as well as shielding effects due to topographical features. Additionally, oxygen is known for being a challenge when trying to gather even semi-quantitative

results from EDS, for many reasons.[56] First is the oxidation of the material, primarily on the surface, which will overinflate oxygen emission datacompared to a bulk solid. Oxygen also suffers from being a relatively small element, resulting in its small weight percentage of the sample, requiring higher precision. A further issue surrounding oxygenEDS detection is that oxygen produces relatively soft X-rays compared to the rest of the elements investigated in this thesis (O-Kα = 0.525 keV), which EDS detectors have historically been inefficient at measuring.

Finally, two of the elements of interest to this research, Ti and V, have overlapping emission energies (Ti-Kβ = 4.93 keV, V-Kα = 4.95 keV).[57] One has to rely upon the EDS analysis software to deconvolute the overlapping data in order to produce reliable elemental maps.

1.4.2 X-ray Powder Diffraction

The EDS results, which provide elemental analysis of individual mineral phases, are paired with X-ray Powder Diffraction (XRD). In the same way that visible light passed through a nanometre diffraction grating will produce a diffraction pattern, the crystal lattice of a mineral phase can act as a diffraction grating for X-rays.[58, 59] This produces a unique set of diffraction patterns, which can be used to identify crystalline phases. In order to achieve this, X-rays are generated in an X-ray tube, which are then directed toward the sample, and any diffracted X-rays are measured with a detector. The detector moves through the range of diffraction angles, and since the sample is a powder, and the phases are randomly orientated, all diffractions should be collected. These diffraction patterns are then compared to a reference library of diffraction patterns, in order to assign specific crystalline phases to the sample.

Some limitations are present for the analysis of the materials concerned in this thesis.[60] First, the samples considered herein are often heterogeneous samples, with many micro- and nano-sized particulate phases to be identified. These can be hard to detect, if a dominant amount of another phase is present. Another limitation is the amount of powder required; in this thesis, much of the solid material was dissolved in concentrated HCl, thus a small amount of substance may be all that is left forXRD analysis, which will lower the sensitivity of the measurement. Despite its limitations, XRD will pair well with EDS for the identification of the phases present in the solid samples concerned in this thesis.

1.4.3 X-ray Fluorescence

Another analysis technique utilised in this thesis is X-ray Fluorescence (XRF). This is a powerful methodwhich can provide accurate elemental analysis of a sample.[61] This technique also relies on the same principles as EDS, but is highly quantitative, where EDS is not.[62] A primary electron beam is directed at a sample, generating inner electron holes which are filled with outer electrons, emitting frequenciesof energy specific to the atomic structure of that element. Since XRF is conducted with the aid of certified standards, the elemental analysis can be calibrated, and precision in the ppm range is often achieved. A typical presentation of the results for mineral samples includes the major elements expressed in their oxide form after heating at 1000 °C.

In this thesis, XRF is a crucial component of the analysis of the starting materials, roasted materials, and leaching residues. Compared with EDS, a quantitative result can be obtained, allowing for the composition of these materials to be determined. This is essential for calculating certain values, such as the percentage leaching of a particular element.

1.4.4 Inductively Coupled Plasma Mass Spectrometry

The final technique discussed is inductivelycoupled plasma mass spectrometry (ICP-MS). This is a mass spectrometric technique, which enables the detection of the elemental composition of a sample to a high degree of precision (up to the ppt range).[63] In this technique, a liquid sample is converted into an ultra-fine mist (nebulised) and introduced into an argon-plasma at extremely high temperature (6000 – 8000 K). This atomises and ionises the sample, preparingit for mass spectrometry. The atomised sample is then passed into the mass spectrometer, where the species are separated and detected based on their mass.

The aspects of ICP-MS that are of interest to this thesis are as follows. First, ICP-MS allows for the analysis of solution samples. Experiments in this thesis involve acid-leaching, and both the solid residue and the leachate will need to be analysed. ICP-MS analysis of the leachate will thus enable the determination of relative leaching rates for each element. Furthermore, the sensitivity and precision of ICP-MS analysis will lend itself well to this thesis, as the vanadium content of the TTM ironsand is so low.

1.5 Extraction of Vanadium

1.5.1 Roasting

A potential pre-treatment process useful in this research is roasting of the TTMore. Roasting is a commonly employed treatment step in metallurgical processes, involving high-temperature treatment of ore in a controlled atmosphere to encourage favourable reactions.[64, 65] In the case of vanadium extraction, one procedure currently employed is roasting of the TTM orewith a sodium salt, to generate a water-soluble sodium metavanadate ($NaVO_3$), which can be extractedwith a water leaching step.[66, 67] This, however, results in a low extraction ratio of vanadium (< 45% total extraction) as well as generation of environmental pollution through the water leaching step.

A recent study by Zheng *et. al.* examined the additive-free roasting of titanomagnetite ore, in the range of 800-1250 °C, with a focus on the oxidative transformations of vanadium species.[68] The thermodynamic results showed that the oxidation of V^{3+} to V^{5+} would occur at temperatures exceeding 327 °C, and the phases of the spinel structure which have vanadium present (vanadium-iron spinel phase, FeV_2O_4) are oxidised more easily than magnetite (Fe_3O_4). In addition, liquids were generated upon high-temperature roasting (including V_2O_5), and temperatures above 1200 °C should be avoided to limit over-roasting. This study provides a justification for attempting a roastingstep prior to acid-leaching, since the vanadium-containing phases were more readily oxidised. However, due to the potential environmental impact of high-temperature roasting procedures,direct acid leaching without

pre-roasting is a more attractive solution.

A 2017 study by Li *et. al.* sought to extract vanadium from a vanadium slag similar to the one studied in this thesis.[52] The slag was provided by Chengde Iron and Steel Group Co. in China, and the elemental composition of this slag is presented below (Table 1.2). This study continued the additive-free roasting pathway of vanadium extraction by roasting the slag in the 800 – 1000 °C range, followed by leaching in ammonium carbonate, $(NH_4)_2CO_3$. An investigation of the roasting process was conducted, and the results showed that the oxidation of the vanadium spinel occurred in three steps. Initially, the spinel phase was broken up, and a solid solution of $Fe_2O_3 \cdot V_2O_3$ is formed (Equation 1.12). Following this, the solid solution was oxidised to form $Fe_2O_3 \cdot V_2O_4$ (Equation. 1.13), and some of the V(IV) is reacted with basic oxides like MgO and MnO_2 to form low-valence vanadates, such as Mg_2VO_4. The final oxidation step resulted in the formation of the highest-valence vanadates, $Mg_2V_2O_7$ and $Mn_2V_2O_7$ (Equation. 1.14). This Mn complex oxide was the material considered earlier in this thesis (see section 1.3.3). The evidence for the formation of $Mn_2V_2O_7$ was the presence of its characteristic reflections in the XRD pattern of the roasted slag.

$$FeV_2O_4 + O_2 \rightarrow Fe_2O_3 \cdot V_2O_3 \qquad (1.12)$$

$$2Fe_2O_3 \cdot V_2O_3 + O_2 \rightarrow Fe_2O_3 \cdot V_2O_4 \qquad (1.13)$$

$$Fe_2O_3 \cdot V_2O_4 + 4MnO + O_2 \rightarrow 2Mn_2V_2O_7 + 2Fe_2O_3 \qquad (1.14)$$

Table 1.2. *Elemental composition of vanadium slag used by Li* et.al. *determined by XRF.* [52]

This content is unavailable. Please consult the reference for further details.

A study, published in March 2020 by Wen *et.al*,sought to co-extract vanadium and manganese from two sources simultaneously.[40] A vanadium-rich slag was obtained from XiChang Steel Vanadium Co. Ltd. in Sichuan and mixed with the manganese-rich mineral pyrolusite (elemental compositions in Table 1.3). The motivation behind this study was the idea that, as the V^{3+} in the slag needs to be oxidised to $V^{5+}$to form $Mn_2V_2O_7$, while the Mn^{4+} in thepyrolusite needs to be reduced to Mn^{2+}, the co-roasting of a mixture of these two materials should facilitate the formation of the desired complex oxide. This is akin to adding MnO_2 as an additive tovanadium slag in order to facilitate the formation of $Mn_2V_2O_7$. This study continued with an acid leaching experiment, with H_2SO_4 used as the acidic extractant. A reasonably good extraction result was

reported, with 93.86% of vanadium content extracted to a 91.98% purity. This study provides ample evidence for the possibility of extracting vanadium from the VRC used in the thesis herein.

Table 1.3. *Elemental composition of materials used by Wen* et.al. *determined by XRF*.[40]

This content is unavailable. Please consult the reference for further details.

1.5.2 Leaching

An important initial consideration for this research is as follows: what happens when TTM is dissolved in HCl? A study by Sedneva *et. al.* attempted to dissolved titaniferous magnetite with HCl solutions, with acid concentrations between 15-25%.[69] This was done to determine the recovery efficiency of the metal components in the resulting leach solution. The main products from HCl digestion were determined to be an HCl solution of $FeCl_2$, which contained the majority of the vanadium component (87-99%), and also a solid TiO_2/SiO_2 residue. Reductive HCl leaching (using Feor Fe/HF as the reductant) was determined to be more effective for the total recovery of the Fe and V components. In this experiment, a precipitation of iron and vanadium was performed using aqueous ammonia. The precipitation process for vanadium removal in this research resulted in a sorption of vanadium ions to the freshly precipitated $Fe(OH)_3$. Some enrichment of vanadium was observed via this method, which varied as a function of pH, but only a low level of enrichment could be achieved,from 1.4% to 3.2% vanadium content. For the herein proposed research, this method of vanadium enrichment is not adequate due to its low level enrichment, and also has the implication that any methodrelying on the removal of iron via precipitation of $Fe(OH)_3$ will lead to unwanted partial V extraction.

1.5.3 Kinetics

A study by the co-supervisor of the proposed project, Chris Bumby, was conducted into the kinetics of TTM ironsand HCl dissolution kinetics (Nusheh *et.al*).[70] This study compared the component leaching efficiencies over time across a range of factors, including HCl concentration, particle size, and leaching temperature. The study showed that the dissolution kinetics can be described using the shrinking core model (cube root model), as the rate-limiting step for dissolution is the surface chemical reactions. The dissolution rate was shown to be strongly related to the acid strength, with very little difference in the extraction ratios of Ti:V:Fe (Figure 1.9.). This supports the claim that the vanadium is present as an impurity within the TTM structure, as it is co-extracted with Fe and Ti. This study also examined the milled TTM ironsand using SEM and EDS mapping (Figure 1.9.a and b). As the source of the ironsand used in the proposed project is the same, a brief review is necessary. The SEM images

show that the majority of the particles are featureless magnetite, and a small number of particles with lamellae of titanohematite (TTH).

This content is unavailable. Please consult the reference for further details.

Figure 1.9. *(Top) Chart from Nusheh et. al. showing leaching behaviour at a range of HCl concentrations. (Bottom) a) TTM particle having undergone leaching in 6M HCl b) TTM particle with Hematite lamellae having undergone leaching in 6M HCl.*

1.5.4 Current Industry Methods

Whilst the early hydrometallurgical experiments in the proposed project will focus on the initial dissolution of the ore in HCl, the focus of this research is to direct the development of a vanadium separation method that can inform industry processes. To achieve this, a brief review of currently employed industry methods as well as novel exploratory methods is necessary. The method which is

utilised in the NZ Steel-making process has already been covered earlier in this thesis (Section 1.2.2), as this generates the VRC studied herein.

One recent industrial development in vanadium extraction and purification comes from the Mount Peak Project (TNG Limited).[71] Their proprietary process, named TIVAN, is a patented hydrometallurgical treatment process, which can produce, three product streams (TiO_2, Fe_2O_3, V_2O_5) from magnetite.[72] Limited information on the chemistry of this process is available. The magnetite ore isinitially leached with acid, which is followed by a selective solvent extraction process to extract the Ti, Fe, and V as three separate products. The key to the success of the Mount Peak Project is the recovery of vanadium via TIVAN, which provides further justification for the research proposed herein. To see if a solvent extraction pathway is suitable for this thesis project, an investigation into current solvent extraction research is warranted.

1.5.5 Solvent Extraction

Solvent extraction is a method which involves addition of a compatible solvent to a digested ore, in order to selectively remove a target for purification.[73] In the case of vanadium extraction, it is important to know what form the vanadium is found in solution. A range of different species are available to vanadium, depending on factors such as pH and chemical potential. In certain industry processes, the TTM ore is roasted in the presence of sodium, forming a vanadate species that can be extracted with water as the solvent.[74] This method has been explored earlier in this thesis (Section 1.5.1), along with the additive-free roasting method, followed by $(NH_4)_2CO_3$ extraction.

Many solvent systems have also been attempted in laboratory settings, such as amine and organophosphorus extractants, yet these have not adequately shown efficient selectivity of V over Fe on their own, due to the complexity of the system (valances, redox effects, etc.).[75-77] Some solvent systems, including one studied by Tavakoli and Dreisinger, have shown separation of V^{4+} over Fe^{2+} via extraction of VO^{2+}, yet does not show suitable separation for any of the other oxidation states of the metal ions.[78] Dreisinger tested a range of organophosphorus extractants, including phosphinic and phosphoric acids (Figure 1.10) on an acidic vanadium leachate. This study showed promise for the extraction of vanadium, but not in the presence of iron ions. In particular, Cyanex 923 showed the best selectivity of V(V) over Fe(III), and D2EHPA showed selectivity of V(IV) over Fe(II), but no extractant was selective for V(V) over Fe(II), or for V(IV) over Fe(III). It should also be noted that these extractions were performed in a sulphated media (i.e. mimicking an H_2SO_4 leachate), and thus the V and Fe species in solution will differ for this thesis, which will utilise HCl. For this reason, if it is decided that the herein research requires a solvent extraction experiment, a range of extractants will need to be tested, rather than relying on this research by Tavakoli and Dreisinger.

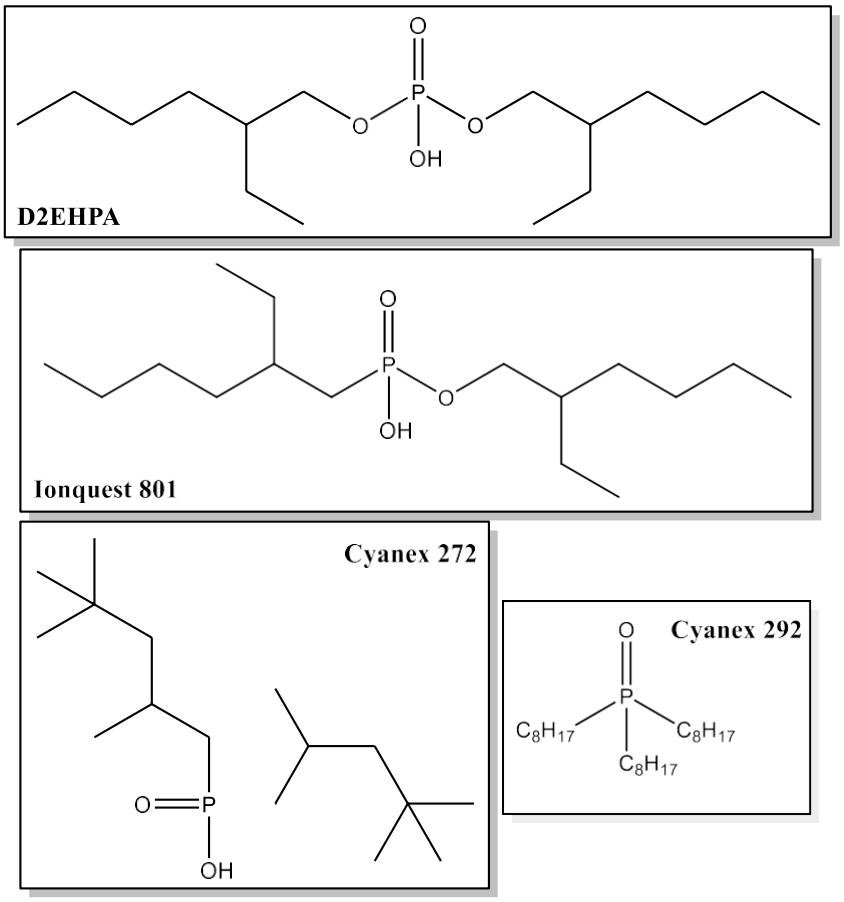

Figure 1.10. *Structures of organic extractants studied by Tavakoli and Dreisinger.*

To round off the earlier exploration of Mn-V chemistry, a brief look is taken at the coextraction of these elements using solvent extraction. A recent study has been published in this area by Liu *et.al.*, who provides a novel method for coextracting Mn and V from high-manganese-containing wastewater.[38] Such wastewater is commonly produced via the vanadium extraction process from TTM ores. Heavy metals (including Mn^{2+} and V^{5+}) in the water make this an environmental pollutant,and thus hard to reuse or discharge directly. In this study, a solvent-extraction process was developed, followed by a precipitation step, in order to remove both the Mn and V from this waste. The solvent used in the extraction process was D2EHPA, previously used above (Figure 1.10.). This extracted the V from the wastewater, and the Mn along with it. Following this, Na_2CO_3 was added to precipitate the Mn as $MnCO_3$. This process was completed with 98.15% of vanadium extracted, to a purity of 98.60%.This study reveals that, if a method of coextracting Mn and V from the VRC were to be developed, thata highly pure product of V can be produced from this to a high degree of efficiency.

1.6 Overview of Project

This project seeks to explore potential methods of selectively extracting V first from VRC and then from IS materials.This will be achieved by leaving other major elements (such as Fe and Ti) behind, or by precipitation of these elements. Three treatments were applied to VRC during the research conducted in this thesis. Procedures and findings from the VRC treatment were also applied to ironsand:

1. Selective leaching of V was attempted for 120 min in HCl at a rangeof concentrations (2M – 12M). This was conducted on both the IS and VRC materials. Theleachate and solid residues were analysed for their elemental and mineral compositions.

2. In another attempt, Ti and Fe were precipitated from a leachate generated in the leaching experiments. Ti was hydrolysed from the leachate, and Fe was precipitated upon manipulation of the pH.

3. The IS and VRC materials were roasted at 900 °C in air (3 hr), and the same HCl leaching procedure was conducted on the resulting roasts with a 4M HCl concentration. The roasting was conducted again on the VRC material at 1200 °C (overnight), and the roasts were compared. Following this, the new roast was leached at a lower range of HCl concentrations (1M – 3M)

2 Experimental

2.1 Leaching

2.1.1 General Leaching Procedure

All leaching experiments were conducted according to the following procedure, unless otherwise specified. Where the term “conc. HCl” is used, this refers to a concentration of 11.5M. HCl was added to a flask equipped with a stirrer, condenser, and thermocouple. The HCl was heated to 80 °C under stirring. The solid to be leached was added, and the experiment was left for 120 min under constant temperature and stirring. Aliquots of ~2 mL were taken at fixed time intervals (2, 4, 6, 8, 10, 15, 20, 30, 45, 60, 90, and 120 min), and these were filtered with a syringe filter. The experiment was removed from the heat, and the solid residue was filtered and washed with water (3 x 2 mL), before being air dried. Leachate aliquots were submitted for ICP-MS analysis. The solid residue was analysed via XRD XRF, and EDS.

Heating was supplied by a Labmaster Isopad LMUL/ER/500, and thermal regulation was achieved by an Omron E5CSZ Temperature Controller. Stirring was achieved with a Heidolph RZR overhead stirrer. Leachate aliquots were filtered, unless otherwise specified, through PES membrane syringe filters of a 0.45 µm pore size. Where stated, samples were centrifuged with an Eppendorf Centrifuge 5424.

2.1.2 Leaching of Non-roasted Samples

The first run of experiments was conducted with 20 g of material and 150 mL of HCl. The leaching was conducted as per the general experimental procedure. For the conc. HCl attempts, syringe filters were inadequate for filtering, due to breakdown of the PES membrane. Instead, the aliquots were filtered through a glass wool plug in a Pasteur pipette. Upon addition of the solid material to the higher-concentration (8M, conc.) HCl, over-heating of the reaction was observed up to 95 °C, before returning to 80 °C over 6 – 10 min. The leachates for the VRC experiments ranged in colour from light green (2M) to dark green (conc.). The leachates for the IS experiments ranged from pale yellow (2M) to dark yellow (conc.). Over time, most filtrates accrued a small amount of white precipitate.

Table 2.1. *Leaching experiments on non-roasted samples. Samples labelled [a] were filtered through glass wool.*

Material used (mass used, g)	HCl Concentration (mol L^{-1})	HCl Volume (mL)	Remaining material (wt%)
VRC (20)	2	150	76.5
	4		59
	8		53.5
	conc. [a]		43
Ironsand (20)	2		81.5
	4		26.5
	8		3.5
	conc. [a]		1.5

2.1.3 Leaching of Roasted Samples

Roasting of the IS and VRC samples was conducted in an induction furnace. Samples were left in a roller mill with steel balls at 52 RPM overnight, prior to leaching experiments.

Table 2.2. *Roasting experiments.*

Sample Name	Material	Mass (g)	Temperature (°C)	Duration (hr)
IS-R	Ironsand	30.1	900	3
VRC -R1	VRC	30.1	900	3
VRC-R2	VRC	59.8	1200	o/n

The roasted materials were leached as per the general experimental procedure. The leachates for the VRC experiments ranged in colour from light green (2M) to dark green (conc.). The leachates for the IS experiment were a dark yellow/gold colour. The leachates for the VRC experiments ranged from pale yellow (1M) to yellow (4M).

Table 2.3. *Leaching experiments of roasted samples.*

Material used (mass used, g)	HCl Concentration (mol L^{-1})	HCl Volume (mL)	Remaining material (wt%)
IS-R (20)	4	150	58
VRC -R1 (20)	4	150	78.5
VRC-R2 (10)	1	75	67
	2	75	70
	3	75	62

2.1 Precipitation of Material from Filtrate

Seeding and precipitation of Ti was attempted with 100 mL of the filtrate resulting from the 8M dissolution experiment. 100 mL of water was brought to a boil, and 1 mL of the filtrate was added to this dropwise. This was left to boil until a cloudy suspension formed. The remaining filtrate was then added,and left to boil for 3 hr, at which point it was taken off the heat and cooled. Then the mixture was filtered, andthe solid was resuspended in water. This new suspension was centrifuged at 4500 RPM for 30 min,and the resulting solid was separated from the pale blue supernatant. The recovered solid was left in a vacuum desiccator overnight, resulting in a grey-white product. This product was then characterised using XRD.

The supernatant above was then used to attempt a precipitation of the Fe. The pH of the supernatant was slowly altered by dropwise addition of 2M NaOH, until a dark green precipitate had formed. Afew mL of pre-prepared flocculant (KW 10 HB) was then added, and this was centrifuged at 4500 RPMfor 20 min. The dark solid was separated from the colourless supernatant and analysed using XRD.A small amount of orange solid was found in the supernatant, and this was also centrifuged at 4500RPM for 20 min and collected.

2.2 Analysis and Characterisation

2.2.1 XRD

XRD data was collected on a PANalytical X'Pert PRO, with a Cu Kα1 emitter. Data was collected with a continuous scan in the $10° \leq 2\theta \leq 80°$ range, with a fixed step size of 0.013°, and a step time of 111 s. The XRD samples were loaded onto flat-plate spinner sample holders and measured using a Bragg-Brentano geometry.

2.2.2 XRF

XRF data was collected by SpectraChem Analytical (Verum Group, Wellington, NZ). Samples were oven dried at 110 °C before analysis. Two analyses were carried out, a loss-on-ignition analysis using a furnace/gravimetric method up to 1000 °C, and a major oxide analysis using borate fusion/X-ray fluorescence.

2.2.3 SEM/EDS

SEM/EDS data was collected on a JEOL JSM-6610LA system, with a JEOL EX-230**BU EX37001 Energy Dispersive X-ray Analyser. Samples were analysed with a working distance of 1 mm at 20 kV, with spot size SS60. Samples were affixed to stubs with carbon tape, and carbon-coated with a Quorum Q150T E coater. The samples were coated with 2 pulses, at a current of 65 A and a pulse time of 3 seconds. After coating, samples were stored under vacuum in a PELCO 2251 Vacuum Desiccator.

2.2.4 ICP-MS

Concentration determinations were carried out using a ThermoFisher Element II sector field ICP-MS. Leached aliquots were diluted using 3% HNO3 in a two-stage gravimetric dilution procedure, to yield final solutions containing analytes of interest at the 0.5 to 20 ppb range. A suite of commercially available certified reference materials (Inorganic Ventures, USA) for the elements Fe, Ti, and V, and Mn were mixed and diluted to encompass similar concentrations to those expected in the diluted leachates. The diluted leachates were then run against the calibration lines given by the gravimetrically diluted reference standards for each element in order to calculate their concentrations in the diluted samples. After subtraction of the procedural blank, a dilution factor was then applied to the concentration determinations for the diluted samples in order to calculate the concentration in the original undiluted leachate material.

Each analysis consisted of an initial three-minute wash cycle, with a 90 s sample uptake followed by three minutes of analysis. The suite of elements was measured using a combination of different instrument resolution modes in order to attenuate the dynamic range encountered within the samples. This is particularly the case for Fe where the 98% beam attenuation afforded by the high-resolution mode permitted collection of the large Fe ion beam alongside the small ion beams for other elements measured at lower resolutions.

3 Results and Discussion

3.1 Introduction

In this section, the results of the VRC and IS leaching experiments are presented, alongside a discussion of the main findings. This section is split into two parts, one for each of the materials studied. The first material covered herein is the VRC, followed by the IS, as the VRC may act as a testing ground for the potential vanadium extraction procedures, owing to its higher vanadium content. It should be noted that the main mineral components of the VRC are different to the IS, as is explainedfurther in this section.

Initially, an analysis of the starting material was conducted, as this formed a basis for interpreting the results of any leaching and roasting experiments. To achieve this, XRF was used to determine the elemental composition, and XRD was used to determine the major mineral phases. To harmonise these two sets of results, and to determine any phases which did not appear in the XRD, EDS was also employed.

Following this, leaching data for the unroasted materials was analysed, and in the case of VRC, an attempt at precipitating the Ti and Fe from the leachate was considered. For this, ICP-MS has been used to determine the elemental composition of the leachate across the course of the leaching, and this has been coupled with the XRF results of the starting materials to determine the leaching efficiencies of the elements in question. XRD, XRF, and EDS were also used to analyse the solid residues remaining after leaching. Following this, the roasting of the materials is covered, and special consideration is taken to the effect of roasting on the leaching behaviour of the materials.

3.2 Vanadium Recovery Concentrate (VRC)

3.2.1 Analysis of Starting Material

Before analysing the leaching and roasting results, it is essential to have a sound understanding of the starting materials. To begin, the XRF results are examined (Table 3.1). The main elemental components are Fe, Mn, Ti, Si, and V. When compared to the composition of the IS (see section 1.1.1), it should be noted that most of the Fe component has been removed. This is no surprise, as the VRC is the side-product of iron smelting, and it is desirable that minimal Fe is withdrawn in the vanadium-recovery process.

Table 3.1. *XRF major oxide analysis results for VRC, and the VRC used by* Li et. al.[52] *Values are expressed as weight % on oven dried (110°C) basis. LOI = loss on ignition at 1000°C. Negative LOI indicates positive mass gain due to oxidation. Values for SO_3, P_2O_5 and K_2O have been omitted due to low value (<0.11). Dashes indicate values not reported.*

Sample	Fe_2O_3	MnO	TiO_2	CaO	SiO_2	Al_2O_3	MgO	V_2O_5	LOI	SUM
VRC	37.72	14.17	14.66	2.81	16.88	1.63	1.1	14.1	-6.7	96.56
VRC from Li *et. al.*	This content is unavailable. Please consult the reference for further details.									

An important consideration to make is how the composition of the VRC material compares to that covered in the literature presented in the introduction. This is because VRC products will differ due to the natural variation in ore compositions between locations. In particular, this study will make comparisons to the Li *et. al.* research, where the slag was roasted and leached with a NH_4CO_3 solution (see section1.5.1).[52] The compositions are somewhat comparable, with one major exception. The slag that Li *et. al.* used had comparable wt% of Mn and Mg, whereas the VRC studied herein contained less Mg, and markedly more Mn, than the Li *et. al*. slag. This is significant, as this study reported the formation of two vanadium oxides upon roasting, $Mg_2V_2O_7$ and $Mn_2V_2O_7$. This leads to the assumption that, if the roasting conditions from Li *et. al.* were to be replicated with our VRC, formation of the $Mn_2V_2O_7$ material should be expected, and formation of the $Mg_2V_2O_7$ material should be less expected.

To determine how the elemental composition of the VRC is reflected in its major crystalline phases, the XRD pattern was considered (Figure 3.1). The major phase of the material appears to be Jacobsite, a Mn-containing spinel mineral, which accounts for the high Mn composition observed in the XRF data. This phase, along with Ilmenite, also accounts for the Fe and Ti components, and the Cristobalite phase accounts for most of the Si component. The shape of the background in the XRD pattern indicated lower amounts of amorphous phases were present. The Olivine phase, judging by the low Mg component of the material, was likely on the Fe-rich end of the Mg/Fe solid solution series(i.e. Fayalite).

What remained unaccounted for was the high V component of the material, and the EDS results were considered to determine whether it was found in the amorphous phase, or as a solid solution in the titaniferous minerals. Furthermore, no Ca- or Al-containing minerals were present in the XRD pattern. The later XRD analyses of the leaching residues revealed an Augite phase, a pyroxene mineral with the general formula $(Ca,Na)(Mg,Fe,Al,Ti)(Si,Al)_2O_6$. This mineral was more resistive to the HCl leaching, and consequently the Ca and Al components of the VRC can be attributed to this mineral. However, corroboration with the EDS results was necessary to confirm this.

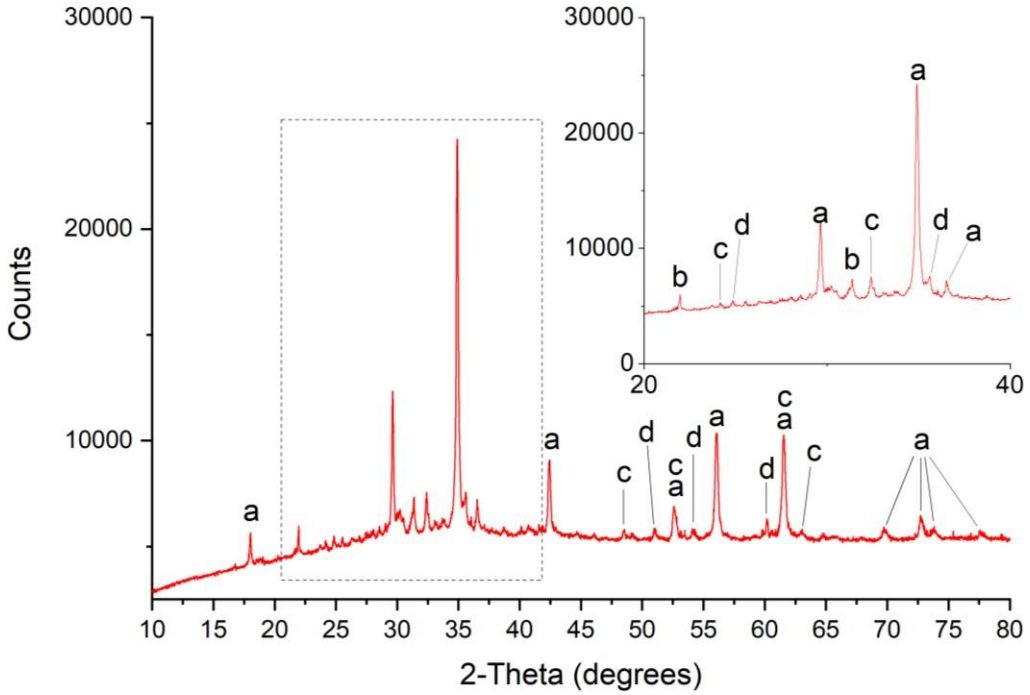

Figure 3.1. *XRD pattern of VRC with major reflections labelled a) Jacobsite, $MnFe_2O_4$ b) Cristobalite,SiO_2 c) Ilmenite, $FeTiO_3$ d) Olivine, $MgFe(SiO_4)$*

EDS maps were taken of the VRC material, and a representative section of the material, along with EDS point analyses, is shown below (Figure 3.2). The EDS point analyses can be largely assigned to the phases identified in the XRD, with a few exceptions. Notable exceptions are EDS points 5, 9, and 10, which contained large Mn, Fe, and Si components. These were assigned to the Rhodonite phase $(Mn,Fe,Mg,Ca)SiO_3$, which appeared in the XRD patterns of the leaching residues reported later in this thesis. The SiO_2 phase was not represented by any EDS point, but can be observed as red regions in the colour map (Figure n, a). A Ti-rich phase with very little Fe was also observed (EDS point 4) and assigned to a TiO_2 phase. Small TiO_2 particles appeared to be frequent in the VRC and its leaching residues. As expected, the Olivine phase (EDS point 3) displayed a small Mg:Fe ratio (17.5:1.6 atomic%). This could be due to a small Mg inclusion in a titaniferous particle, but as this EDS point contained no Ti or V, it was most likely due to Olivine.

The most important takeaway from the EDS results is the location of the V component. Most of the V component appeared to be locked up in a solid solution of the titaniferous minerals, as evidenced by EDS points 2 and 6-9. However, one standout region of the EDS map (EDS point 1) contained an overwhelming predominance of Mn and V, with little to no Fe or Ti observed. As this phase was not present in the XRD, it was assumed that either the phase was not abundant enough to be identified in the XRD, or this phase was amorphous. A particular quality of note is the ratio of Mn to V in this region. The ratio was roughly 2:3 (Mn:V), and this fact became crucial in later sections in this thesis, where this Mn-V region is revisited.

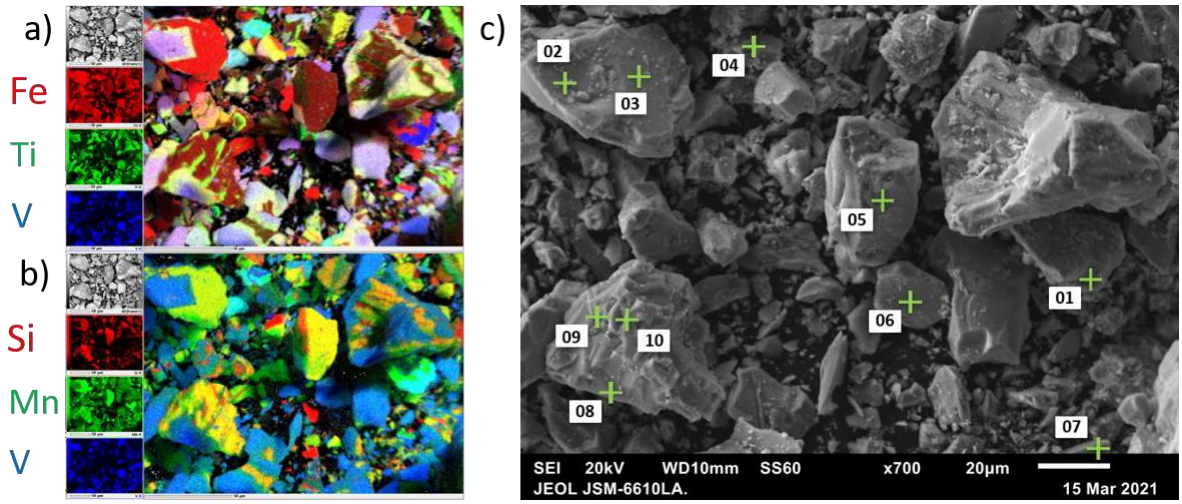

EDS Point	EDS Data for Element							Assignment
	Fe	**Ti**	**V**	**O**	**Mn**	**Si**	**Mg**	
1	2.10	0.93	42.12	27.29	26.32	0.88	0.37	Manganese-vanadium phase
2	25.60	8.10	23.50	34.76	6.69	0.71	0.64	Vanadium-bearing Jacobsite
3	22.67	0.67	0.71	43.02	11.13	19.74	2.06	Olivine
4	7.48	32.05	13.42	36.73	7.24	1.87	1.22	TiO_2
5	18.52	1.50	2.32	50.02	7.98	18.42	1.25	Iron-bearing Rhodonite
6	37.62	14.14	26.31	10.31	9.85	1.63	0.14	Vanadium-bearing Ilmenite
7	21.50	14.01	50.91	3.23	10.07	0.25	0.03	Vanadium-bearing Jacobsite
8	34.37	12.75	36.48	7.03	8.17	1.11	0.07	Vanadium-bearing Jacobsite
9	26.72	1.65	1.11	20.76	20.42	28.75	0.59	Iron-bearing Rhodonite
10	26.93	4.47	0.80	18.65	19.86	28.46	0.82	Iron-bearing Rhodonite

Figure 3.2. *SEM maps of VRC. a) elemental colour map (red: Fe, green: Ti, blue: V) b) elemental colour map (red: Si, green: Mn, blue: V) c) corresponding SEM image at x700 with EDS points labelled. Table shows the mineral phases assigned to each EDS point, and the raw EDS data for each of the major elements in atomic% (rescaled to 100 %).*

Summary

The main component of the VRC was Jacobsite, a Mn-bearing titaniferous spinel. Other minor components were Ilmenite, Cristobalite, Rhodonite, Olivine, and TiO_2. The elemental composition of the material showedsimilarities to VRC materials studied elsewhere, with the exception of the richness of Mn in this VRC. Of particular note was the presence of a yet-unidentified Mn-V phase, with a ~2:3 (Mn:V) atomic ratio. Apart from this phase, the overwhelming majority of the vanadium appeared to be found as a solid solution in the Jacobsite and Ilmenite phases.

3.2.2 Leaching of Non-roasted Samples

Having analysed the starting material, one can consider the HCl leaching data. First it should be noted that the liquid to solid ratio (7.5 ml/g) was chosen as a rough estimate of the amount required to convert all the metal species into their highest oxidation-state chloride forms. After addingthe solid to the 80 °C HCl, aliquots of the leachate were taken at fixed intervals, and the ICP-MS resultsof these aliquots are shown below (Figure 3.3). The values reported in the ICP-MS results were given as concentrations, and these have been modified to show the amount leached as a molar percentage of the element in the initial VRC material.

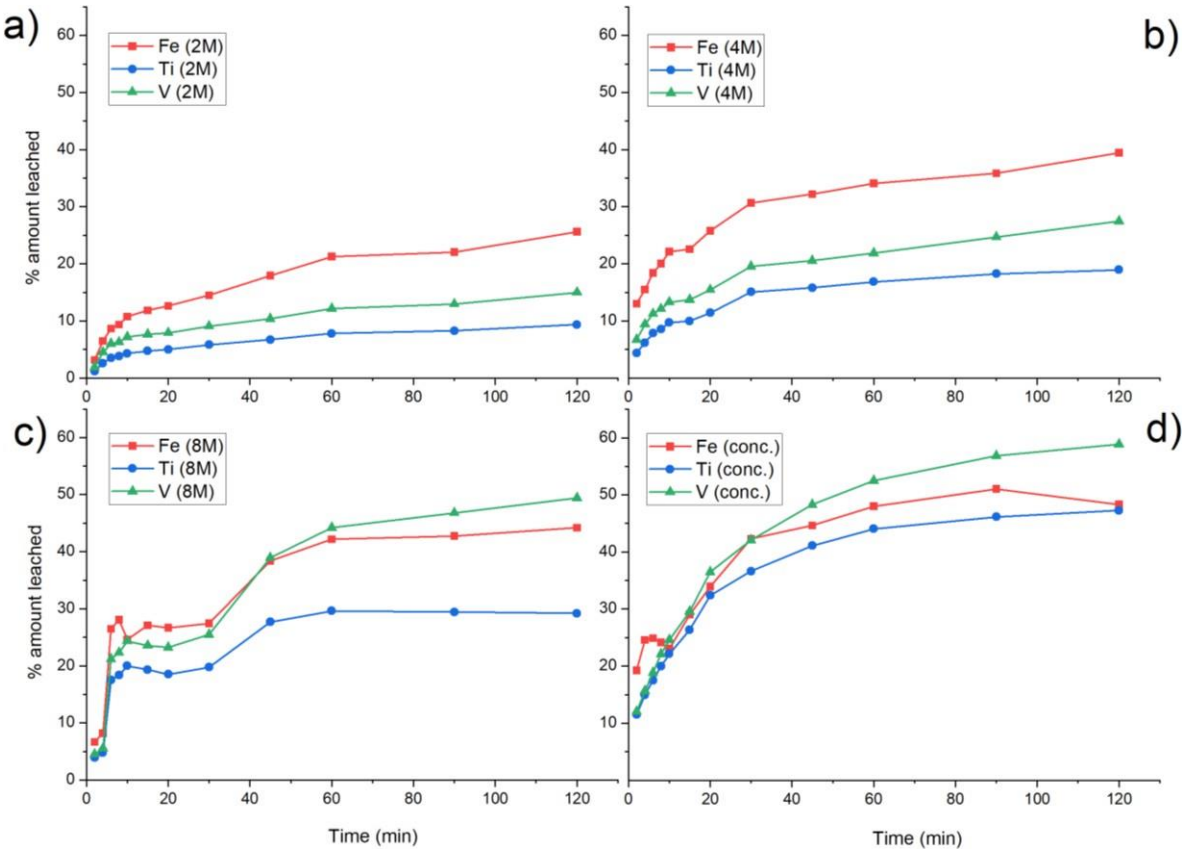

Figure 3.3. *HCl Leaching of VRC over time, comparing the effect of HCl concentration. a) 2M leaching b) 4M leaching c) 8M leaching d) conc. leaching. The % amount leached is the moles of element leached compared to the moles of element in initial solid material.*

There was no considerable difference in leaching rate for the three elements of interest across the course of the experiment. Ti appeared to have slower leaching kinetics, which was likely because Ilmenite and TiO_2 are more resistiveto HCl attack compared to Jacobsite. The leaching rate of Fe and V at lower HCl concentrations differed, with Fe leaching faster than V. At higher concentrations this reversed, with V leaching faster than Fe. The inconsistent leaching curve in the 8M experiment was taken to be a result of anomalous values at 15, 20, and 30 min, as when these were omitted a smooth curve similar to the other results was found. For all the higher concentration leaching experiments in this thesis, addition of the solid materialto the HCl resulted in an increase in temperature as the leaching

reactions are exothermic. This had the general effect of inflating the initial results, as the higher temperature leachate raised the solubility of the metal ions.

The other main result from the leaching data was the total % amount (yield) leached as a function of acidstrength. At a 2M concentration, only a small amount (25.64 %) of the Fe, and even smaller amounts of Ti and V, were leached (9.35 and 14.98 %, respectively). As the HCl concentration was increased, the total amount leached increased to approximately half of the amount in the initial material. These values are reported as leaching efficiencies in Table 3.2. The change in leaching efficiency as a function of acid strength is exemplified in Figure 3.4. This figure shows clearly the reversal in the comparative leachingrates of Fe and V. At lower concentrations, the Ilmenite appeared to be selectively leached, leading to a higher amount of Fe in the leachate. At higher concentrations, this behaviour was not as significant, as the acid strength was high enough to leach Ilmenite and spinel phases alike, leading to a higher amount of V present in the leachate.

Table 3.2. *Leaching efficiencies for Fe, Ti, and V in VRC leaching experiments. Values are the maximum percentage amount leached from solid material.*

Sample	**Fe Leaching Efficiency (%)**	**Ti Leaching Efficiency (%)**	**V Leaching Efficiency (%)**
VRC 2M Leach	25.64	9.35	14.98
VRC 4M Leach	39.46	18.95	27.46
VRC 8M Leach	44.19	29.61	49.41
VRC conc. Leach	51.01	47.25	58.88

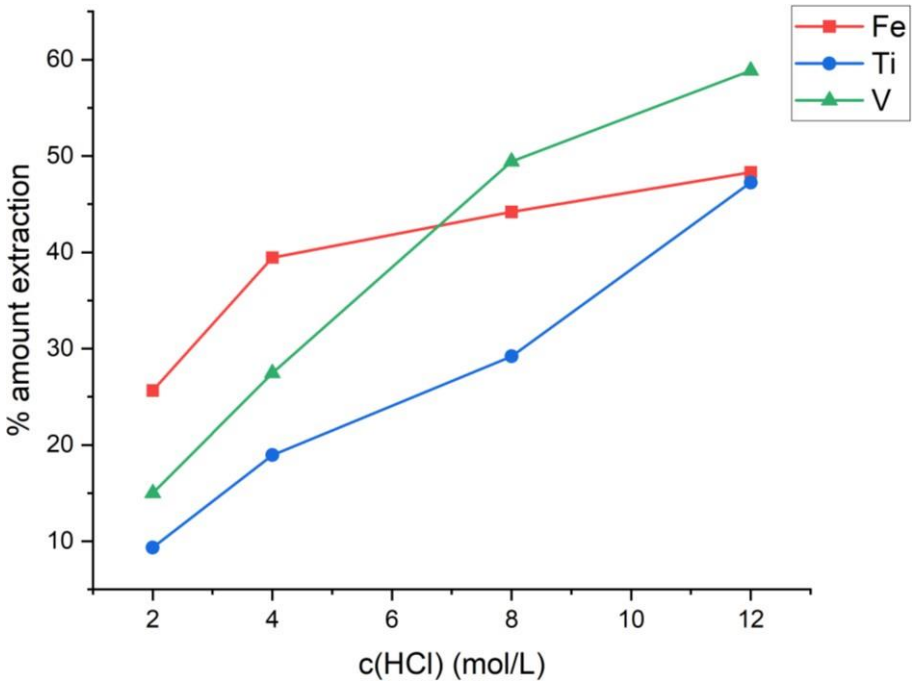

Figure 3.4. *Final extraction values at 120 min as a function of HCl concentration.*

In order to fully understand the leaching process, careful analysis of the solid residue which remains after leaching is warranted. Comparison of this data to the initial VRC material gave insight into which phases were being leached, and which phases were resistant to HCl attack. The first data to consider is the elemental data provided by XRF. This is compared to the starting material below (Table 3.3). Elements which became lower in weight % as the acid strength was increased were the elements that were being leached most. These elements were Fe, Ti and V. Theseelements were most likely found in the minerals which were not resistive to HCl attack, such as Jacobsite and Ilmenite. The elements which increased in their weight % values are the elements which were comparatively not being leached. These were Ca, Si, Al, and Mg. These elements were most likely found in phases which were resistive to HCl attack, such as Rhodonite, Augite, and Cristobalite. Analysis of theXRD and EDS results for the residue samples was required to confirm this. Mn appeared to maintain its weight % across the range of experiments, and this was likely due to the fact that it was locatedin both an HCl soluble phase (Jacobsite) and a more resistive phase (Rhodonite).

Table 3.3. *XRF major oxide analysis results for VRC and leached VRC residues. Values are expressed as weight % on oven dried (110°C) basis. LOI = loss on ignition at 1000°C. Negative LOI indicates positive mass gain due to oxidation. Values for SO_3, Na_2O, K_2O, and P_2O_5 have been omitted due to low value (<0.13).*

Sample	Fe_2O_3	MnO	TiO_2	CaO	SiO_2	Al_2O_3	MgO	V_2O_5	LOI	SUM
VRC	37.72	14.17	14.66	2.81	16.88	1.63	1.1	14.1	-6.7	96.56
VRC 2M Leaching Residue	32.21	13.71	16.6	2.73	19.14	1.59	0.99	14.88	-5.6	96.45
VRC 4M Leaching Residue	24.3	13.57	18.95	3.55	26.36	1.66	1.05	10.73	-3.32	97.06
VRC 8M Leaching Residue	22.9	13.19	17.13	3.74	30.3	1.78	1.08	8.8	-1.58	97.49
VRC conc. Leaching Residue	20.96	13.99	12.52	4.44	37.96	1.89	1.22	6.39	-1.66	97.88

These results were corroborated by the ICP-MS leaching data, as the mol of any element in the leachate and the mol of that element in the solid residue should total to the mol in the initial VRC sample. This value was always comparable to the mol in the initial material; however, it was consistently lower. This was due to material lost during the filtration process, and in handling of the material post-experiment. This value was calculated for each experiment, and while not presented herein, an example is as follows (from the 2M experiment).

n(V) in leachate (from ICP-MS) = 4.64 mmol

n(V) in residue (from XRF) = 25.03 mmol

total n(V) in leachate and residue = 29.67 mmol

n(V) in initial VRC material (from XRF) = 31.01 mmol

To continue the analysis of the residue samples, the XRD patterns and EDS data were considered. These allowed the identification of the phases which remained after dissolution at different acid strengths, and in turn revealed which phases had dissolved during the leaching experiments.

2M Leaching Residue

When compared to the XRD pattern of the initial VRC material, the reflections associated with Ilmenite and Olivine peaks disappeared, due to their dissolution during the leaching experiment. Rhodonite and Cristobalite reflections emerged, indicating that the major spinel phase became a much less prevalent phase due to dissolution. Thisalso indicated that the Cristobalite and Rhodonite phases

were more resistive to HCl leaching than the spinel phase. Another point of note is the assignment of the spinel phase diffraction lines as $Mn_{0.336}Ti_{0.942}Fe_{1.722}O_4$, a spinel mineral closer to the Ti end of the Mn/Ti spinel solid solution series. This was likely due to slight selective leaching of Mn-rich spinels. The diffraction patterns of spinel minerals are, however, very similar, thus determination of the composition of the spinel phase with XRD alone cannot be relied upon.

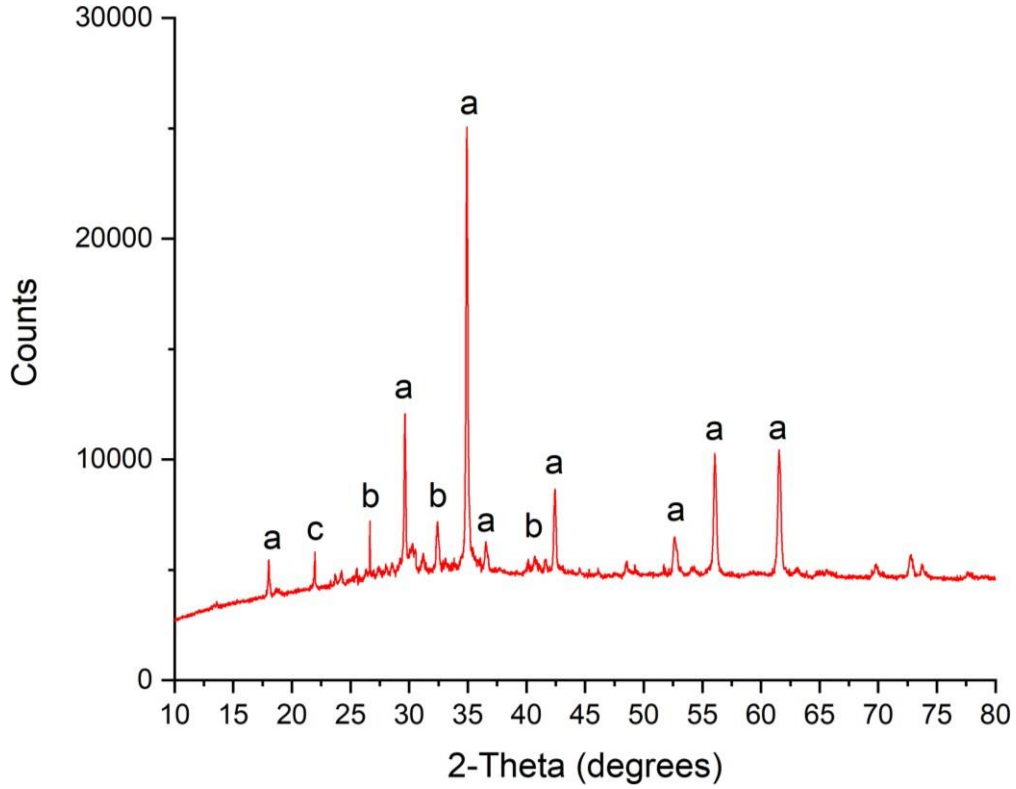

Figure 3.5. *XRD pattern of VRC residue after leaching with 2M HCl, major reflections labelled a) Titanomagnetite,* $Mn_{0.336}Ti_{0.942}Fe_{1.722}O_4$ *b) Rhodonite,* $MnSiO_3$ *c) Cristobalite,* SiO_2*.*

The EDS map of this residue material was considered and compared to the XRD. The main phase identified was a TTM phase. The colour map of Mn (Figure 3.6.b, green), as well as EDS points 1, 4 and 5, indicate that the Mn was correlated with the TTM phase, confirming the XRD results. Of particular interest are EDS points 4 and 5, where a large amount of V was found in the spinel phase, indicating V-rich areas of TTM. EDS point 4 indicated the presence of TiO_2 particles in the residue. The colour map of Si indicated the presence of SiO_2 particles, as well as a particular area of interest onthe righthand side of the colour map, where a network of SiO_2 appeared to be cementing particles together (Figure 3.6.b, red). A closer analysis of a particle (Figure 3.6.c, green box) is shown in Figure 3.7.

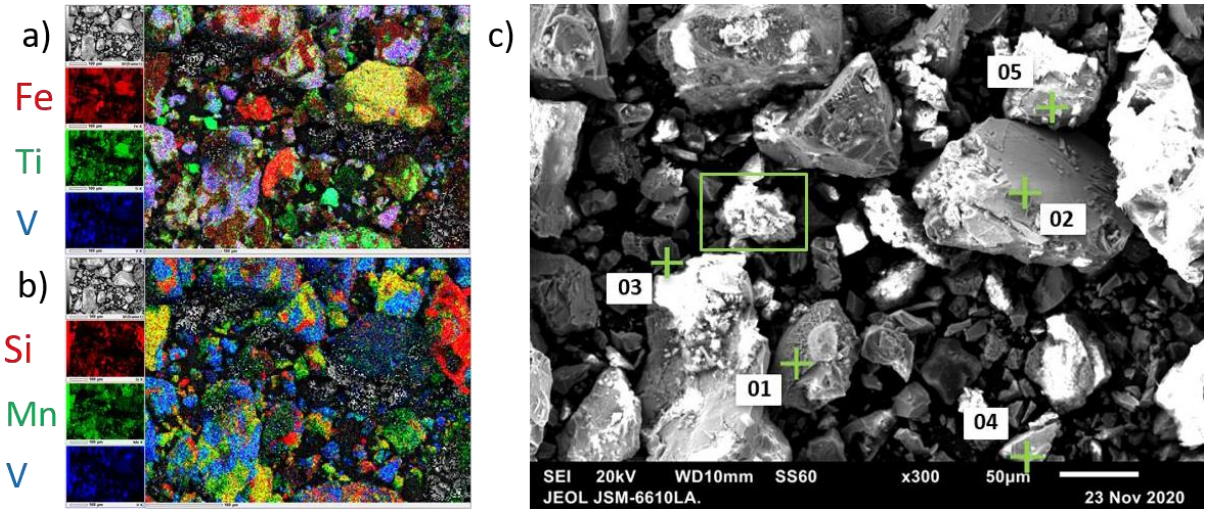

EDS Point	EDS Data for Element							Mineral Phase
	Fe	**Ti**	**V**	**O**	**Mn**	**Si**	**Mg**	
1	68.34	17.93	5.27	2.74	4.77	0.81	0.01	Mn-containing TTM
2	22.75	13.08	3.77	54.74	2.15	2.96	0.43	TTM
3	0.72	43.40	0.71	45.75	0.73	1.07	7.46	TiO_2
4	29.22	9.72	24.69	27.68	5.47	2.64	0.47	V-rich Mn-containing TTM
5	27.48	10.79	35.92	13.77	10.37	1.17	0.35	V-rich Mn-containing TTM

Figure 3.6. *SEM maps of VRC residue after leaching with 2M HCl. a) elemental colour map (red: Fe, green: Ti, blue: V) b) elemental colour map (red: Si, green: Mn, blue: V) c) corresponding SEM image at x300 with EDS points labelled. Table shows the mineral phases assigned to each EDS point, and the raw EDS data for each of the major elements in atomic% (rescaled to 100 %).*

This particle shows mainly the spinel phase, with Mn-rich, V-rich, and Ti-rich areas. At the top-left section of the particle, a Ti-rich region was present, which appeared to be nested in an SiO_2 network(EDS point 2). At the top-right section of the particle, the SiO_2 network was most prominent, and EDS point 3 indicated only the presence of Si, Fe, and O. This is likely due to a small region of Ilmenite which remained after the leaching, surrounded by SiO_2. The most interesting section of this map is at thetop-left, where a highly V-rich spinel phase was found (EDS point 1). All phases of spinel with differentamounts of Mn or V were assumed to have overlapping diffraction lines in the XRD pattern.

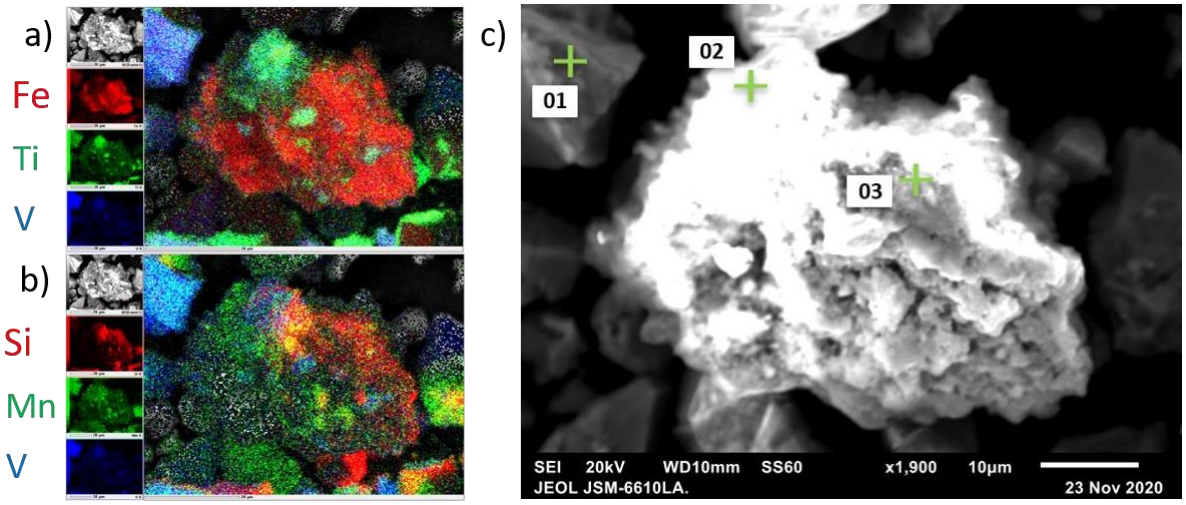

EDS Point	EDS Data for Element							Mineral Phase
	Fe	**Ti**	**V**	**O**	**Mn**	**Si**	**Mg**	
1	21.85	7.43	27.36	31.98	8.59	1.85	0.91	V-rich TTM
2	18.17	22.52	10.14	28.20	6.98	13.22	0.33	SiO_2 and TTM
3	78.20	0.76	0.59	12.56	0.62	7.21	0.00	SiO_2 and Iron

Figure 3.7. *SEM maps of VRC residue after leaching with 2M HCl. a) elemental colour map (red: Fe, green: Ti, blue: V) b) elemental colour map (red: Si, green: Mn, blue: V) c) corresponding SEM image at x1900 with EDS points labelled. Table shows the mineral phases assigned to each EDS point, and the raw EDS data for each of the major elements in atomic% (rescaled to 100 %).*

4M Leaching Residue

The major reflections in the XRD pattern of the 4M leaching residue were still assigned to the spinel phase pattern, but now the Rhodonite reflections were becoming much more prominent. This indicated that the spinel phase was being dissolved in the leaching process. Still visible were the Cristobalitereflections, and many other signals which could not be identified. It became more apparent that amorphous material was present in the residue, due to the increasing size of the background hump.

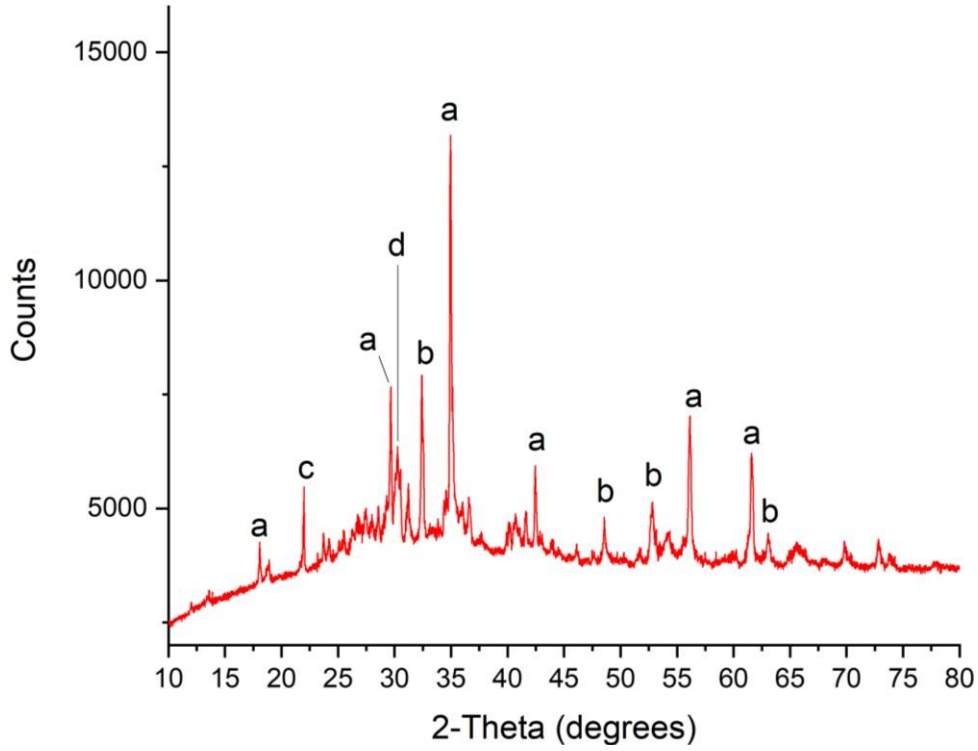

Figure 3.8. *XRD Pattern of VRC residue after leaching with 4M HCl, major reflections labelled a)Titanomagnetite,* $Mn_{0.336}Ti_{0.942}Fe_{1.722}O_4$ *b) Rhodonite,* $MnSiO_3$ *c) Cristobalite,* SiO_2*.*

The EDS maps of the 4M residue were similar to that of the 2M residue. EDS points 2-3 indicatedthe presence of the TTM spinel phase, including the V-rich TTM. EDS points 1-3 indicated the presenceof TiO_2, Rhodonite, and SiO_2. Qualitatively, it appeared that TiO_2 and SiO_2 phases were more prominent in these maps compared to the 2M maps, based on the presence of Ti-rich regions (Figure 3.9.a, green) and Si-rich regions (Figure 3.9.b, red). This was expected, as the spinel phase dissolved in the leaching process. A closer analysis of a particle (Figure 3.9.c, green box) is shown in Figure 3.10.

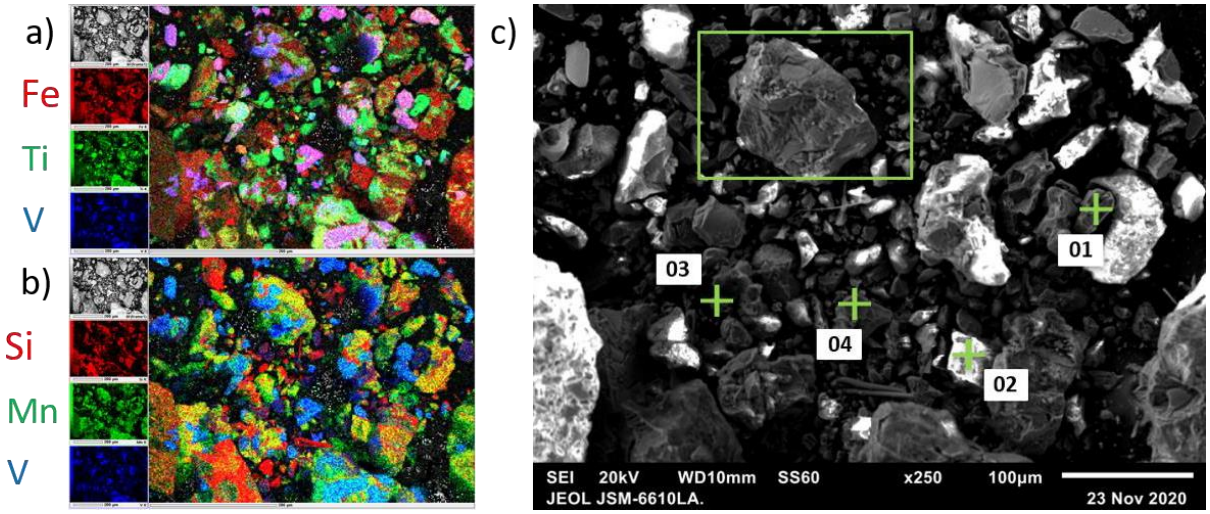

EDS Point	EDS Data for Element							Mineral Phase
	Fe	**Ti**	**V**	**O**	**Mn**	**Si**	**Mg**	
1	3.96	33.78	1.06	42.08	4.13	8.31	6.08	TiO_2
2	16.19	32.49	3.42	20.50	10.87	15.60	0.13	TTM and Rhodonite
3	46.07	21.28	6.72	15.12	2.58	7.23	0.22	TTM and SiO_2
4	24.48	10.82	25.48	30.52	6.31	2.04	0.21	V-rich TTM

Figure 3.9. *SEM maps of VRC residue after leaching with 4M HCl. A) elemental colour map (red: Fe, green: Ti, blue: V) b) elemental colour map (red: Si, green: Mn, blue: V) c) corresponding SEM image at x250 with EDS points labelled. Table shows the mineral phases assigned to each EDS point, and the raw EDS data for each of the major elements in atomic% (rescaled to 100 %).*

This particle contained multiple mineral phases of interest. EDS point 1 contained a large amountof V, Fe, and Ti, and was assigned as a V-rich TTM phase. These are the purple regions in the colourmap (Figure 3.10.a). EDS point 2 corresponded to the TiO_2 phase, of which many particles are visible inthe colour map. EDS point 3 contained mostly Si and Mn and has been assigned as a Rhodonite phase. EDS point 4 contains Si, Mn, Mg, Fe and Ca, and thus has been assigned as Augite. This phase was not found in the XRD map of this residue but was a phase which appeared in later residues from stronger acidleaching, thus was expected to be present in this residue as well. Finally, regions of SiO_2 were identifiedin the colour map (Figure 3.10.b, red), and found to be present in EDS point 5.

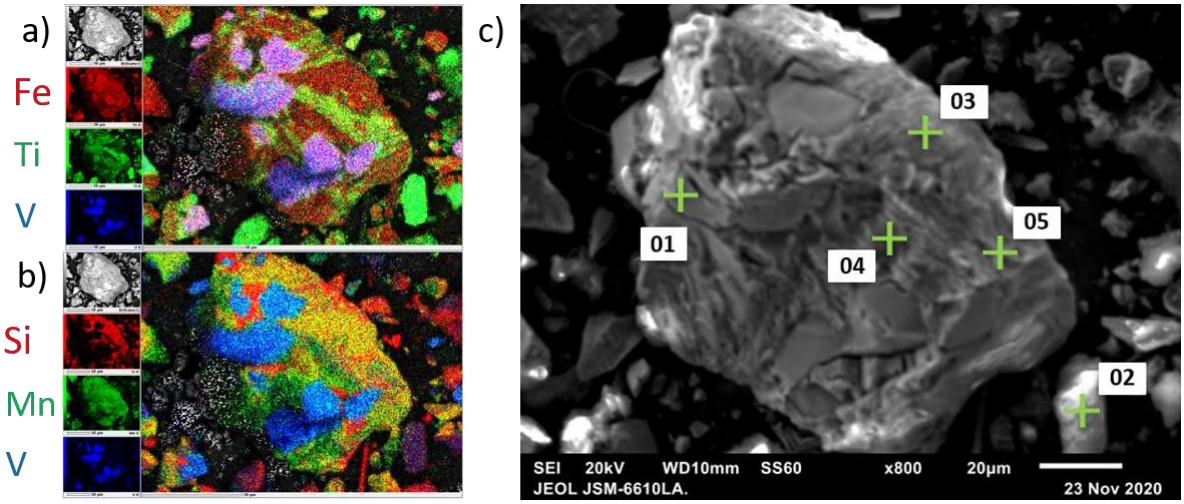

EDS Point	EDS Data for Element							Mineral Phase
	Fe	**Ti**	**V**	**O**	**Mn**	**Si**	**Mg**	
1	14.77	12.53	40.73	17.25	10.55	3.94	0.23	V-rich TTM
2	2.91	31.89	2.53	52.62	1.08	8.95	0.03	TiO_2
3	6.28	2.57	0.54	47.15	10.29	26.23	6.94	Rhodonite
4	16.22	6.13	1.51	25.53	24.30	24.49	1.82	Augite
5	5.45	12.47	1.30	59.77	5.79	14.74	0.47	TiO_2 and SiO_2

Figure 3.10. *SEM maps of VRC residue after leaching with 4M HCl. a) elemental colour map (red: Fe, green: Ti, blue: V) b) elemental colour map (red: Si, green: Mn, blue: V) c) corresponding SEM image at x800 with EDS points labelled. Table shows the mineral phases assigned to each EDS point, and the raw EDS data for each of the major elements in atomic% (rescaled to 100 %).*

8M Leaching Residue

The next solid residue analysed was the 8M leaching residue. From this point, the XRD patterns became more complex and harder to assign, as much of the spinel phase was dissolved. The TTM diffraction lines in the XRD pattern are now minor reflections, indicating that much of the TTM had been dissolved (Figure 3.11). In its place, the major phases identified in the XRD pattern were Rhodonite and Cristobalite. This corroborated the XRF data for this residue (Table 3.3), as the Si composition was much more dominant than in the initial VRC material. A new phase, Augite, became visible in the XRD, owing to its higher composition in the residue as the spinel phase was leached.Finally, the background hump of the XRD was much more pronounced, indicating a larger amount of amorphous material compared to the previous residues.

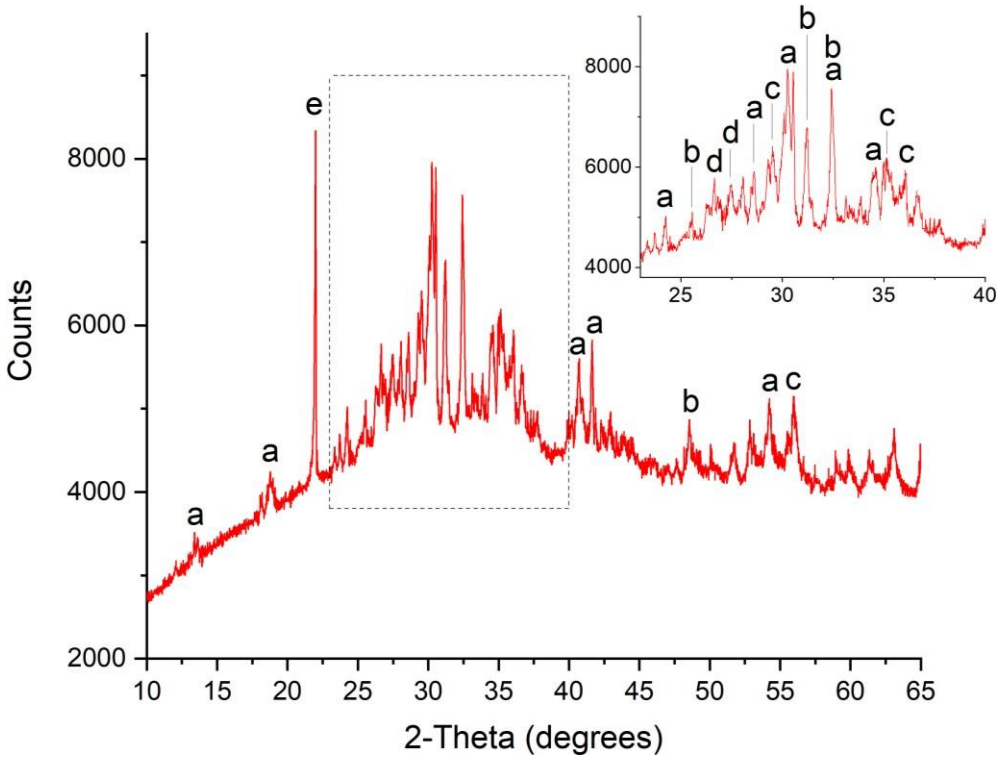

Figure 3.11. *XRD Pattern of VRC residue after leaching with 8M HCl, major reflections labelled a) Rhodonite, $MnSiO_3$ b) Pseudobrookite, $FeTi_2O_5$ c) Titanomagnetite, Fe_2TiO_4 d) Augite, $(Ca,Na)(Mg,Fe,Al,Ti)(Si,Al)_2O_6$ e) Cristobalite, SiO_2.*

In the EDS analysis of the residue, domains of the V-rich spinel phase were still visible (EDS point 1), although its prevalence in the residue was much lower. Regions of TiO_2 were much more common (EDS point 2). EDS point 3 contained a considerable amount of Mn and Si, as well as the expected amountsof Fe and Ti to identify this as the TTM phase. Thus, this point has been assigned to both the Rhodonite phaseand the TTM phase. EDS point 4 indicated the presence of SiO_2, and this phase was also more prevalent in the residue.

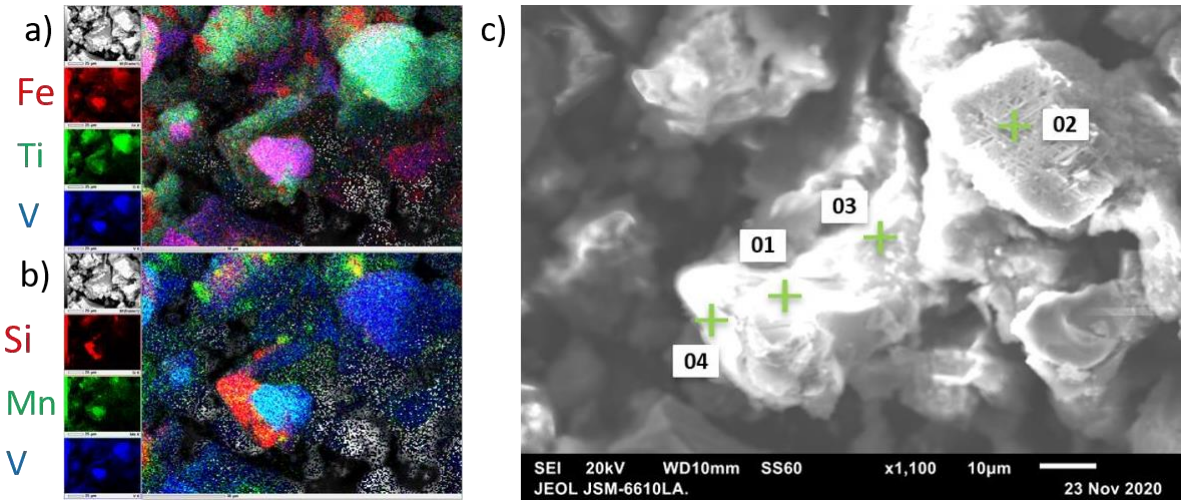

EDS Point	EDS Data for Element							Mineral Phase
	Fe	**Ti**	**V**	**O**	**Mn**	**Si**	**Mg**	
1	21.75	12.69	27.80	26.34	9.39	1.63	0.41	V-rich TTM
2	5.87	52.27	10.28	29.05	0.72	1.74	0.05	TiO_2
3	15.11	29.12	8.01	28.48	11.48	7.76	0.04	TTM/Pseudobrookite and Rhodonite
4	1.39	7.02	1.22	44.09	1.48	44.69	0.11	SiO_2

Figure 3.12. *SEM maps of VRC residue after leaching with 8M HCl. a) elemental colour map (red: Fe, green: Ti, blue: V) b) elemental colour map (red: Si, green: Mn, blue: V) c) corresponding SEM image at x1100 with EDS points labelled. Table shows the mineral phases assigned to each EDS point, and the raw EDS data for each of the major elements in atomic% (rescaled to 100 %).*

Conc. Leaching Residue

Again, it was much more difficult to assign phases to the XRD pattern, as many minor phases resistant to HCl attack were left after dissolution of the majority of the titaniferous minerals. Furthermore, the background hump of the pattern was much larger, owing to the higher composition of amorphous material compared to the previous residues. The main phases were Cristobalite and TTM, with Rhodonite and Augite also present.Additionally, a Pseudobrookite phase was identified in the pattern. It may be the case that EDS points in previous residues labelled TTM were in fact Pseudobrookite.

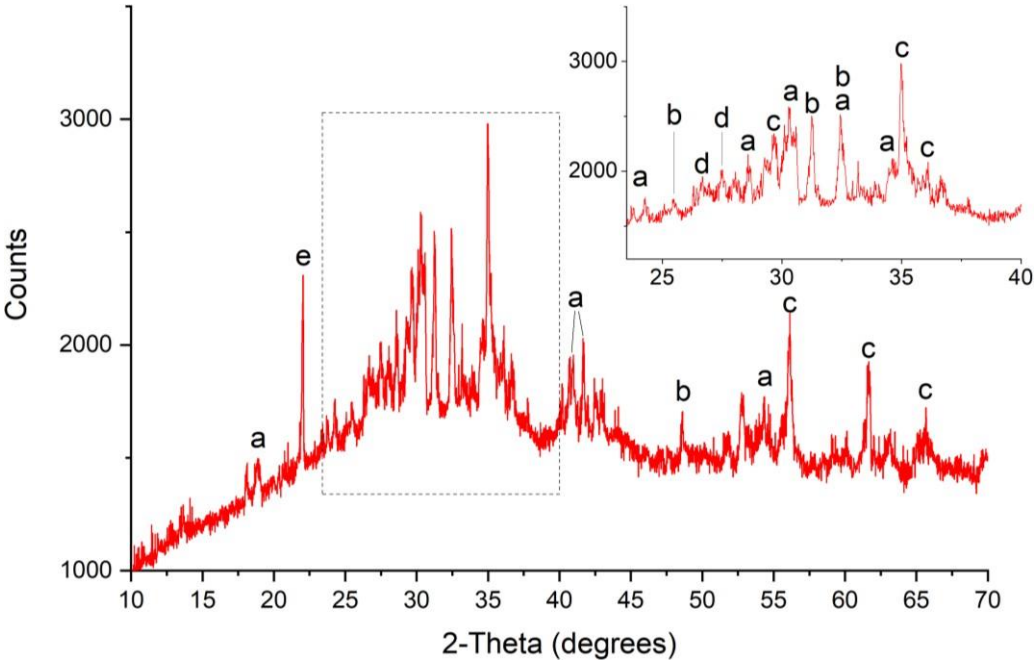

Figure 3.13. *XRD Pattern of VRC residue after leaching with conc. HCl, major reflections labelled a)Rhodonite, $MnSiO_3$ b) Pseudobrookite, $FeTi_2O_5$ c) Titanomagnetite, Fe_2TiO_4 d) Augite, $(Ca,Na)(Mg,Fe,Al,Ti)(Si,Al)_2O_6$ e) Cristobalite, SiO_2.*

The EDS map of the residue still displayed V-rich spinel phases (EDS point 1). However, Si-containing phases were much more dominant (Figure 3.14.b, red), as exemplified in EDS points3 and 4. EDS point 3 also indicated the presence of TiO_2 in the large agglomeration of SiO_2. The only other phase identified in the EDS map was Rhodonite (EDS points 1 and 5). The results of the EDS mapping agreed well with the XRF data for this sample, as the main component in the XRF data for thisresidue was Si, followed by Fe, Ti, and Mn.

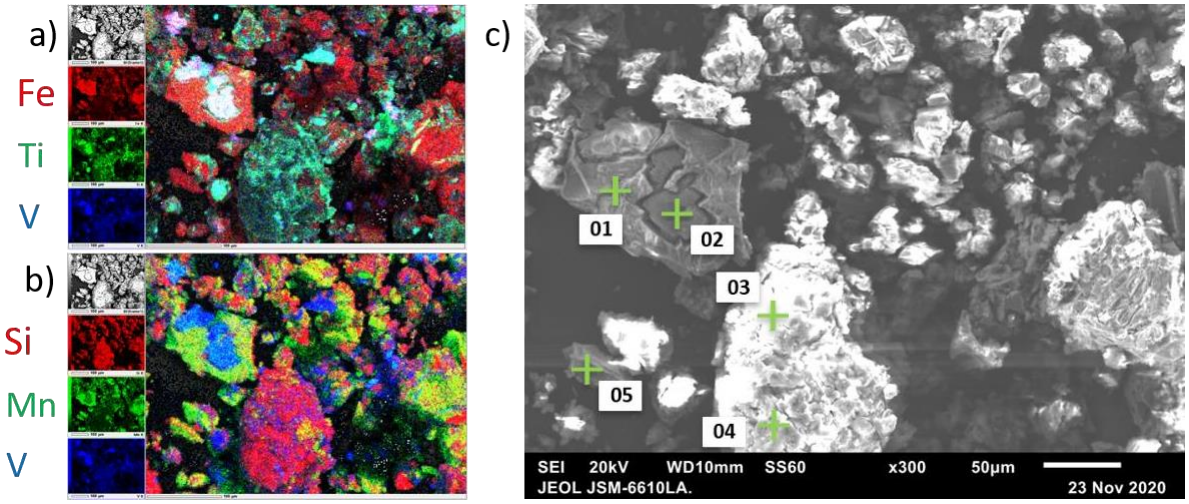

EDS Point	EDS Data for Element								Mineral Phase
	Fe	Ti	V	O	Mn	Si	Ca	Mg	
1	22.82	5.77	0.66	20.71	15.37	29.43	4.86	0.37	Rhodonite
2	22.93	18.35	20.92	29.88	6.54	1.10	0.09	0.19	V-rich TTM
3	4.36	20.17	3.25	47.55	1.43	22.85	0.30	0.08	TiO_2 and SiO_2
4	1.97	5.27	1.43	47.56	0.93	42.59	0.19	0.06	SiO_2
5	17.56	0.76	0.26	25.04	14.23	28.23	13.42	0.49	Rhodonite

Figure 3.14. *SEM maps of VRC residue after leaching with conc. HCl. a) elemental colour map (red: Fe, green: Ti, blue: V) b) elemental colour map (red: Si, green: Mn, blue: V) c) corresponding SEM image at x300 with EDS points labelled. Table shows the mineral phases assigned to each EDS point, and the raw EDS data for each of the major elements in atomic% (rescaled to 100 %).*

Summary

Analysis of theleaching data revealed no major differences in leaching rates for the major metals of concern in this thesis: Fe, Ti, and V. As the concentration of HCl was increased, a higher maximum % amount extractedwas observed, with the highest values being ~50 % in the conc. HCl experiments. Analysis of the residues with EDS and XRF enabled determination of which phases were undergoing dissolution, and which were resistive. The spinel phases (Jacobsite, TTM) were selectively leached over the other phases, including TiO_2, SiO_2, Augite, and Rhodonite. Finally, the mol of any particular element in the leachate (from ICP-MS) and the mol of the element in the residue (XRF) were comparable, but consistently lower, than the mol in the initial VRC material. This was taken to be evidence that some residue material was lost in the experimental procedure, most likely in the filtration step. These results indicated no reliable way to separate Fe, Ti, and V using direct HCl leaching.

3.2.1 Titanium and Iron Precipitation from Leachate

Briefly, results from the Ti and Fe precipitation attempts are considered. The attempts weremade using the leachate from the 8M HCl leaching experiment above. TiO_2 seeding yieldeda white product, which was analysed using XRD (Figure 3.15). Two phases were identified in the XRDpattern, with the major phase being Rutile, and the minor phase Anatase. This demonstrated the successful precipitation of Ti from the leachate.

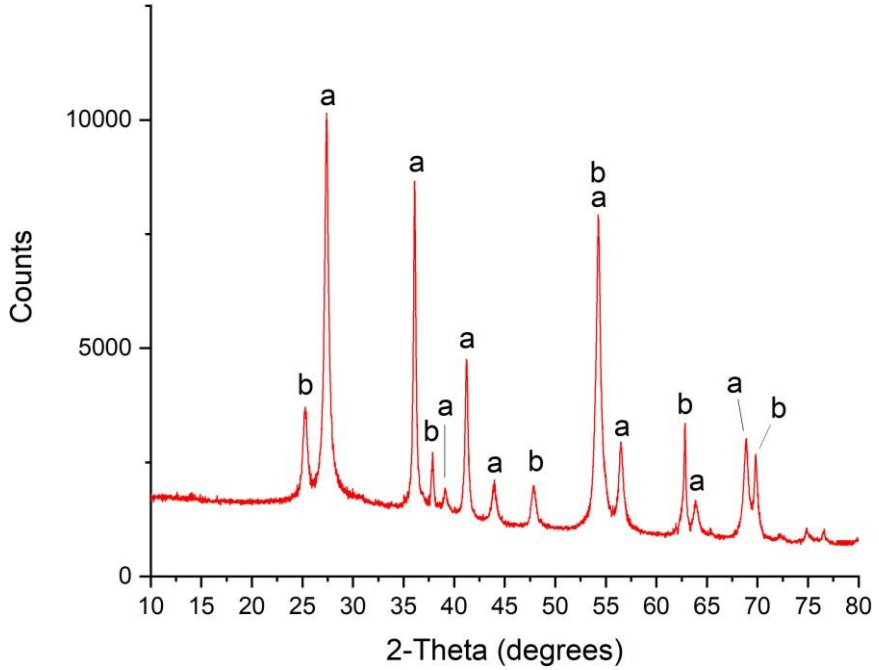

Figure 3.15. *XRD pattern of the first precipitated material, with major reflections labelled a) Rutile, TiO_2 b) Anatase, TiO_2.*

The filtrate from the TiO_2 seeding experiment was kept, and the pH of the filtrate was raised with NaOH inorder to precipitate Fe. This resulted in a black/green precipitate, which was flocculated. Upon centrifugation and drying the precipitate transformed into an orange solid. This was then analysed with XRD. As only a very small amount of this material could be recovered, this was analysed on an amorphous silica stage, resulting in the large background hump seen in the XRD pattern (Figure 3.16). The only phase identifiedfrom the XRD pattern was iron oxide-hydroxide. This proved that Fe was successfully precipitated fromthe filtrate. The orange material, when desiccated, reverted to a black solid. This was taken to be a transition between the polymorphs of iron oxide-hydroxide. The β-polymorph (Akaganéite) was initiallyformed, and took on an orange colour. When this was dried in a desiccator, it reverted to the black α-polymorph(Goethite).

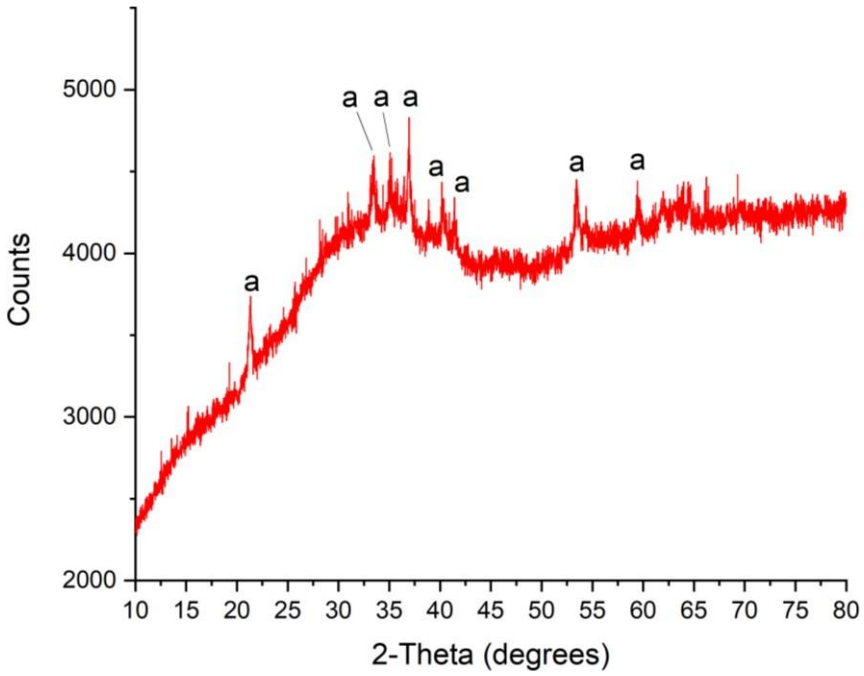

Figure 3.16. *XRD pattern of the second precipitated material, with major reflections labelled a) iron oxide-hydroxide, FeO(OH).*

As explained in the introduction of this thesis (see section 1.5.2), the prospect of precipitating Fe to separate it from V, according to Sedneva *et. al.*, faces the challenge of avoiding adsorption of the positive V ions to the surface of the forming FeO(OH) particles. To see if this was the case in the above attempts, the ICP-MS elemental results are compared before and after the precipitation (Table 3.4). The Fe and Ti values were a fraction of what they were in the 8M HCl leachate, indicating good extractionof these metals. However, the value for V in the final filtrate was miniscule, indicating that the V has been coextracted with the Fe. This showed that Ti and Fe precipitation, as a method of isolating the V, was not adequate.

Table 3.4. *ICP-MS elemental results for Fe, Ti, and V before and after precipitation experiments. Values are reported in mmol.*

Sample	**^{56}Fe**	**^{47}Ti**	**^{51}V**
VRC 8M Leachate	41.75	10.72	15.32
Filtrate after Ti and Fe precipitation	0.73	2.45×10^{-5}	1.77×10^{-6}

3.2.2 Roasting of Samples

For the VRC roasting experiments, two roasting conditions were investigated. The first one covered in this section produced roasts by heating samples for 3 hr at 900 °C, and the other sample was roasted overnight at 1200 °C.

Before investigating the XRD and EDS data for these roasts, the XRF is considered (Table 3.5). Therewere minor differences present in the elemental compositions of both roasts, and it was not known why thisshould be the case. It was assumed that these differences were due to compositional variation in the VRC material. The LOI value for the roasts was positive, indicating loss of mass during the XRF experiment, while the LOI value for the VRC was negative, indicating mass gained. This was because elements in the VRC were oxidised, leading to mass gain, while the elements in the roasted materials were already saturated, leading to no further gain by addition of oxygen.

Table 3.5. *XRF major oxide analysis results for VRC and both VRC roasts. Values are expressed as weight % on oven dried (110°C) basis. LOI = loss on ignition at 1000°C. Values for SO_3, Na_2O, P_2O_5, and K_2O have been omitted due to low value (<0.05).*

Sample	Fe_2O_3	MnO	TiO_2	CaO	SiO_2	Al_2O_3	MgO	V_2O_5	LOI	SUM
VRC	37.72	14.17	14.66	2.81	16.88	1.63	1.1	14.1	-6.7	96.56
VRC Roast (3 hr, 900 °C)	40.74	12.06	12.91	2.4	13.99	1.74	1.25	11.95	0.21	97.39
VRC Roast (overnight, 1200 °C)	35.55	13.22	13.79	2.53	15.68	1.71	1.07	13.01	0.22	96.91

3-hr Roast at 900 °C

The XRD and EDS for the 3-hr roast was first considered. The main phases present in the XRD pattern are Hematite and Pseudobrookite (Figure 3.17). Phases in lower quantities that are present in the pattern are Cristobalite, Rutile, manganese(III) oxide and Rutile. A set of reflections present at 27-28° (Figure 3.17, right inset) mirrored reflections present in the Wen *et. al.* study (see section 1.5.1). These reflections were due to a manganese vanadate phase $Mn_2V_2O_7$, thus the reflections herein have been identified as such. There was no indication of a spinel phase present in the material.This indicated that the Fe and Ti content of the VRC, present as Jacobsite, Ilmenite, and TTM, were converted to Hematite, Pseudobrookite, and Rutile. The Mn content of the VRC, present in the VRC as Jacobsite, formed the manganese vanadate under roasting, and the rest partitioned as an Mn_2O_3 phase.

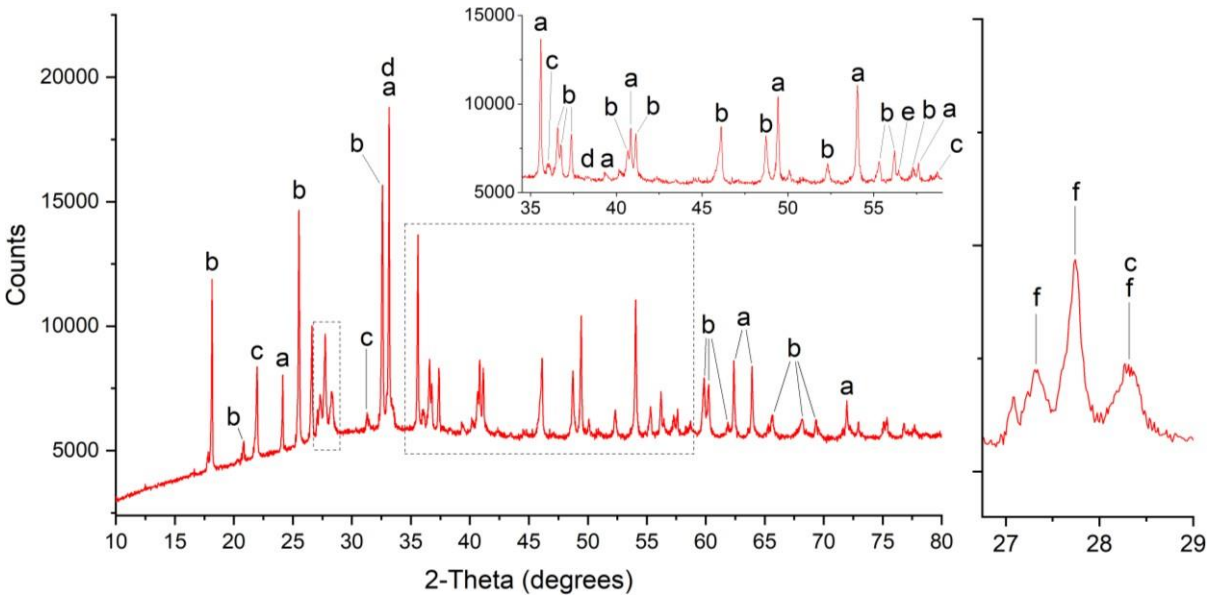

Figure 3.17. *XRD Pattern of VRC after roasting at 900 °C for 3 hr, with major reflections labelled a) Hematite, Fe_2O_3 b) Pseudobrookite, $Ti_{1.10}Fe_{1.90}O_5$ c) Cristobalite, SiO_2 d) Manganese Oxide, Mn_2O_3 e) Rutile, TiO_2 f) Manganese Vanadate, $Mn_2V_2O_7$.*

The EDS data was now consulted to corroborate the XRD results. The material appeared rife witha phase which contained only V and Mn, in a 2:3 ratio (Mn:V) (EDS point 1). The vanadium present in the colour map (Figure 3.18.a and b, blue) no longer appeared to be associated with the Fe andTi, and only seemed to be associated with the Mn. This was taken to be an indication that, during the roasting process, the V and Mn partitioned from the Fe and Ti spinel phase and formed their own phase. This phase was assigned as the manganese vanadate phase identified in the XRD pattern. From the XRD pattern, the Fe and Ti which remained was in the formed Pseudobrookite.

An Fe- and Ti-containing phase was identified and assigned as Pseudobrookite (EDS point2). A phase containing only Fe was also identified (EDS point 3), which corresponded to the Hematite phase present in the XRD pattern. Particles containing only Si were present in the colour map (Figure 3.18.b, red). EDS points were assigned to a predominantly manganese vanadate phase, with some SiO_2 phase present. The final EDS point contained Fe and Ti, and thus was another Pseudobrookite particle.

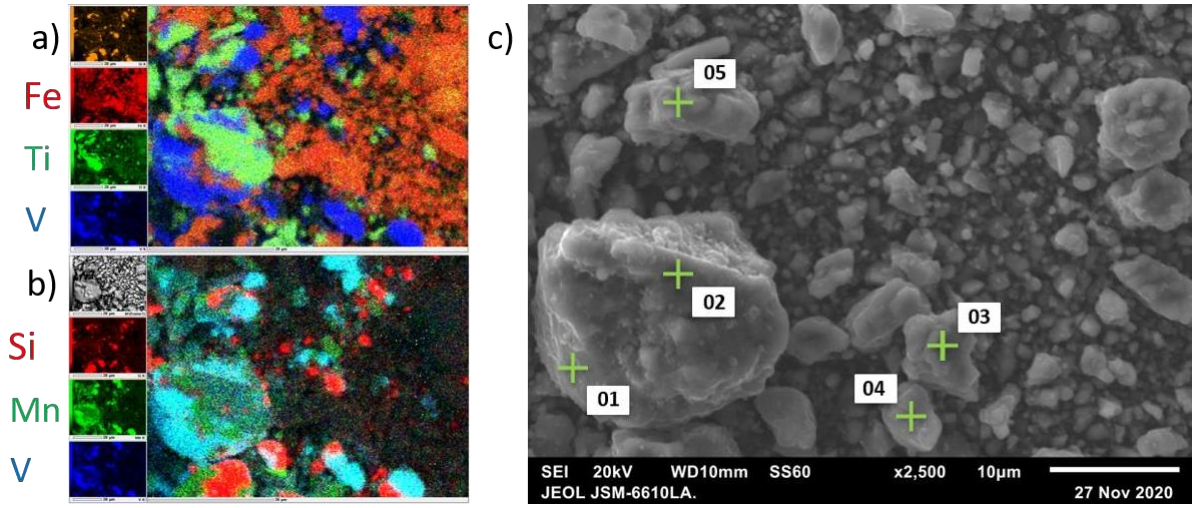

EDS Point	EDS Data for Element								Mineral Phase
	Fe	**Ti**	**V**	**O**	**Mn**	**Si**	**Ca**	**Mg**	
1	4.30	1.93	42.17	13.88	30.16	1.40	6.04	0.13	Manganese vanadate
2	33.29	22.63	5.02	29.73	6.73	0.57	0.71	1.33	Pseudobrookite
3	47.87	4.06	0.72	43.09	0.69	0.38	0.04	3.16	Hematite
4	2.33	0.57	25.66	37.83	19.44	7.53	5.25	1.39	Manganese vanadate with SiO_2
5	27.28	15.92	3.23	43.06	4.41	4.57	0.49	1.03	Pseudobrookite

Figure 3.18. *SEM maps of VRC roast (3 hr, 900 °C). a) elemental colour map (red: Fe, green: Ti, blue: V) b) elemental colour map (red: Si, green: Mn, blue: V) c) corresponding SEM image at x2500 with EDS points labelled. Table shows the mineral phases assigned to each EDS point, and the raw EDS data for each of the major elements in atomic% (rescaled to 100 %).*

To further investigate the correlation of Mn with V in the 3-hr roasted sample, a range of EDS points were taken, and their Mn and V values were plotted against each other (Figure 3.19, left). This resulted in a high degree of correlation, with a ratio to 2:3 (slope = 0.71). This indicated that the V was found almost entirely in the same phase as the Mn in the roasted sample. Furthermore, two distinct groups can be identified in the chart, one with a high amount of both Mn and V, and one with low amounts. This indicated that the Mn and V were found in distinct regions, separate from the other main elements: Fe andTi. Another point to note is that there was a larger amount of Mn than V in theareas which contained little of each, indicated by the bump in Mn atomic % values near the bottom left of the chart. This indicated that a small amount of Mn remained in the Fe and Ti phase, Pseudobrookite.

The same correlative analysis was performed for Fe and V and the opposite result was found. An inverse correlation was found, indicating that the V and the Fe existed in separate phases. Again, two distinct groupings were found in the data, representative of the Fe-rich/V-poor phase and the Fe-

poor/V-rich phase. These correlation plots, together with the EDS colour maps, showed a clear and distinct redistribution of the Mn and V during the roasting process, separating them from the Fe and Ti into their own phase.

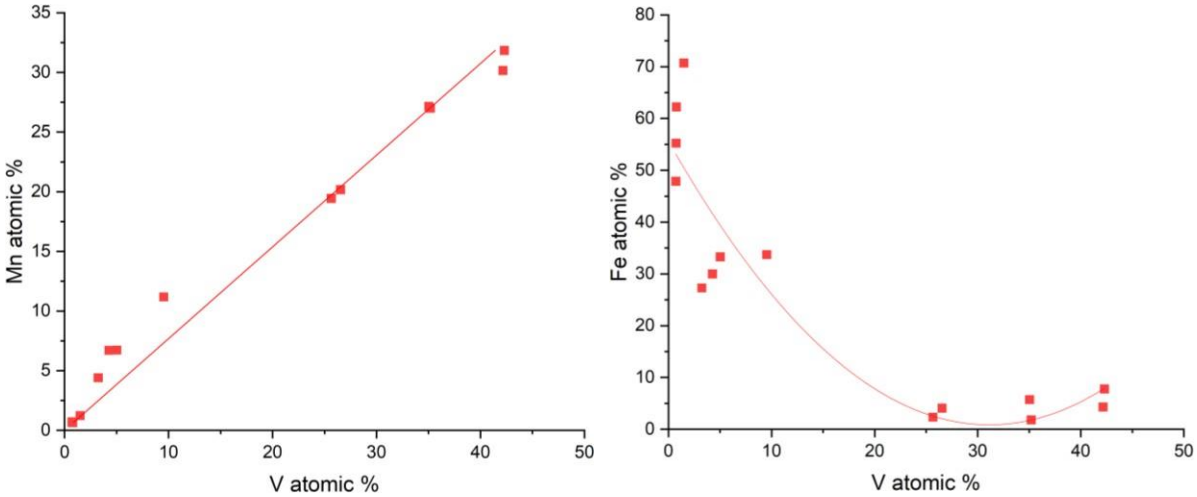

Figure 3.19. *Correlation data for EDS points showing Mn-V correlation (left) with a linear regression (R_2 = 0.99), and the Fe-V inverse correlation (right) with a polynomial fit (R^2 = 0.83).*

Overnight Roast at 1200 °C

Having analysed the 3-hr roast at 900 °C, it was decided that the roast should be taken as far to completion as possible in order to fully convert all V to the new Mn-V phase. To this end, a sample of VRC was roasted overnight at 1200 °C. The XRD pattern of this new roast material was taken and compared to the 3-hr roast (Figure 3.20). All the major phases that were previously identified in the 3-hr roast were also identified in the overnight roast. Importantly, the manganese vanadate phase was still present, with reflections in the 25-29° range (Figure 3.20, labelled f).

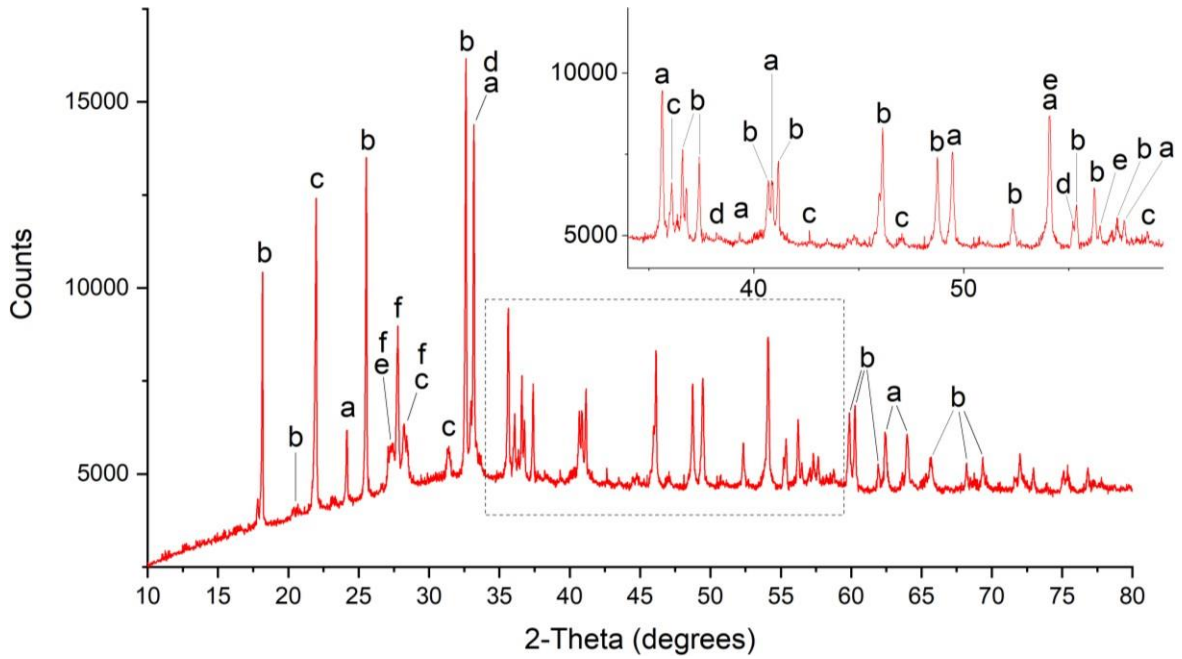

Figure 3.20. *XRD Pattern of VRC after roasting at 1200 °C overnight, with major reflections labelled a) Hematite, Fe_2O_3 b) Pseudobrookite, $Ti_{1.10}Fe_{1.90}O_5$ c) Cristobalite, SiO_2 d) Manganese Oxide, Mn_2O_3 e)Rutile, TiO_2 f) Manganese Vanadate, $Mn_2V_2O_7$.*

The EDS of the overnight roast is now considered. All the same phases appeared to be present inthe overnight roast as compared to the 3-hr roast. The Mn and V partitioned into their own phase, leaving the Fe and Ti as Pseudobrookite and Hematite. The presence of manganese(III) oxide was also found, and this was a phase identified in the XRD. This was identified based on the presence of Mn and Fe in EDS point 6, with very little Ti and V to accompany it.

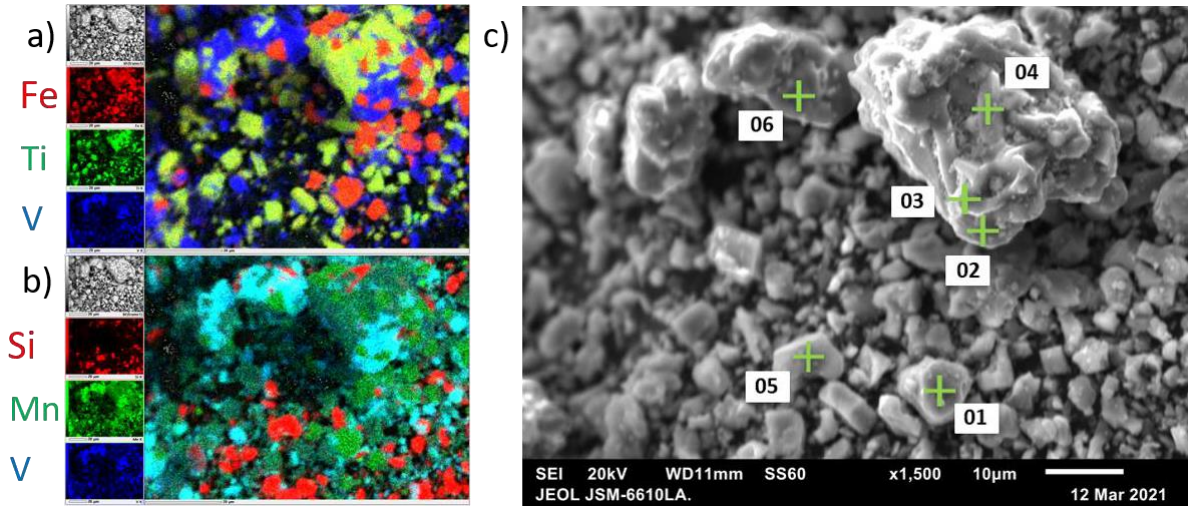

EDS Point	EDS Data for Element							Mineral Phase
	Fe	Ti	V	O	Mn	Si	Mg	
1	49.78	4.46	0.95	34.37	9.06	0.28	1.10	Hematite
2	5.26	2.52	46.00	10.50	33.72	1.78	0.21	Manganese vanadate
3	51.11	4.80	2.14	30.85	8.89	0.87	1.33	Hematite
4	48.95	27.07	4.54	11.07	7.15	0.63	0.58	Pseudobrookite
5	0.69	0.53	1.83	44.26	1.21	51.40	0.07	SiO_2
6	63.63	5.91	2.44	14.51	12.53	0.40	0.58	Hematite and Mn_2O_3

Figure 3.21. *SEM maps of VRC roast (overnight, 1200 °C). a) elemental colour map (red: Fe, green: Ti, blue: V) b) elemental colour map (red: Si, green: Mn, blue: V) c) corresponding SEM image at x1500 with EDS points labelled. Table shows the mineral phases assigned to each EDS point, and the raw EDS data for each of the major elements in atomic% (rescaled to 100 %).*

Summary

Two sets of roasts were conducted, oneat 900 °C for 3-hr, and the other at 1200 °C overnight. No noticeable difference could be found in theirXRD pattern, XRF data, or EDS maps. Comparison of the XRF results with the initial unroasted material showed that the elements in the roasted material were in a higher oxidation state. The main phases of the initial unroasted VRC, namely Jacobsite and Ilmenite, were converted into Hematite, Pseudobrookite, Rutile and Mn_2O_3. The Cristobalite phase remained unchanged in the roast, and no spinelphase was identified. Importantly, the existence of a manganese vanadate was demonstrated, due to XRD reflections which conferred with $Mn_2V_2O_7$ XRD reflections in the literature. During the roasting process, V and Mn were partitioned from the Ti and Fe and formed their own phase. This phase had a Mn:V ratio of approximately 2:3.

3.2.3 Leaching of Roasted Sample

Having roasted the VRC samples, HCl leaching studies were conducted. Initially, the 3-hr roast was leached with just 4M HCl, in order to compare the leaching behaviour to the unroasted VRC. Following this, the overnight roast was leached with a range of lower HCl concentrations, in order to determine the effect of acid strength. This was considered appropriate as no significant difference between the roasts was found in the previous chapter. In this section, the 3-hr roast is discussed first.

3-hr Roast Leaching at 4M HCl

The leaching results of the 3-hr VRC roast are shown below, with the unroasted results shown as dashed lines for comparison (Figure 3.22). The obvious result was an increase in the % amount of V leached over the course of the experiment. For the unroasted material, the % amount of Vstarted at approximately 7 %, and increased to ~30 % at the end of the experiment. In contrast,over 80 % of the V in the roasted VRC material was leached in the first 2 min, and this peaked at close to 90 % after 6 min of leaching time. This was due to the new manganese vanadate phase formed during roasting, which appeared to be much less resistant to HCl attack compared to the spinel phase of the initial unroasted material. This is the key finding of this thesis, as it provides a method of selectively extracting V from the VRC material.

Furthermore, the leaching behaviour of Fe and Ti in the roasted VRC was remarkably different to that in the unroasted VRC. The leaching behaviour of Fe and Ti in the unroasted VRC mimics the V leaching, as all three were found in the same spinel phase. However, during the roasting, the Fe and Ti from the Jacobsite and Ilmenite phases formed the new Pseudobrookite and Hematite phases, which were more resistive to HCl leaching. This leads to the behaviour shown below, where less than 4 % of the Fe and Ti was leached after roasting.

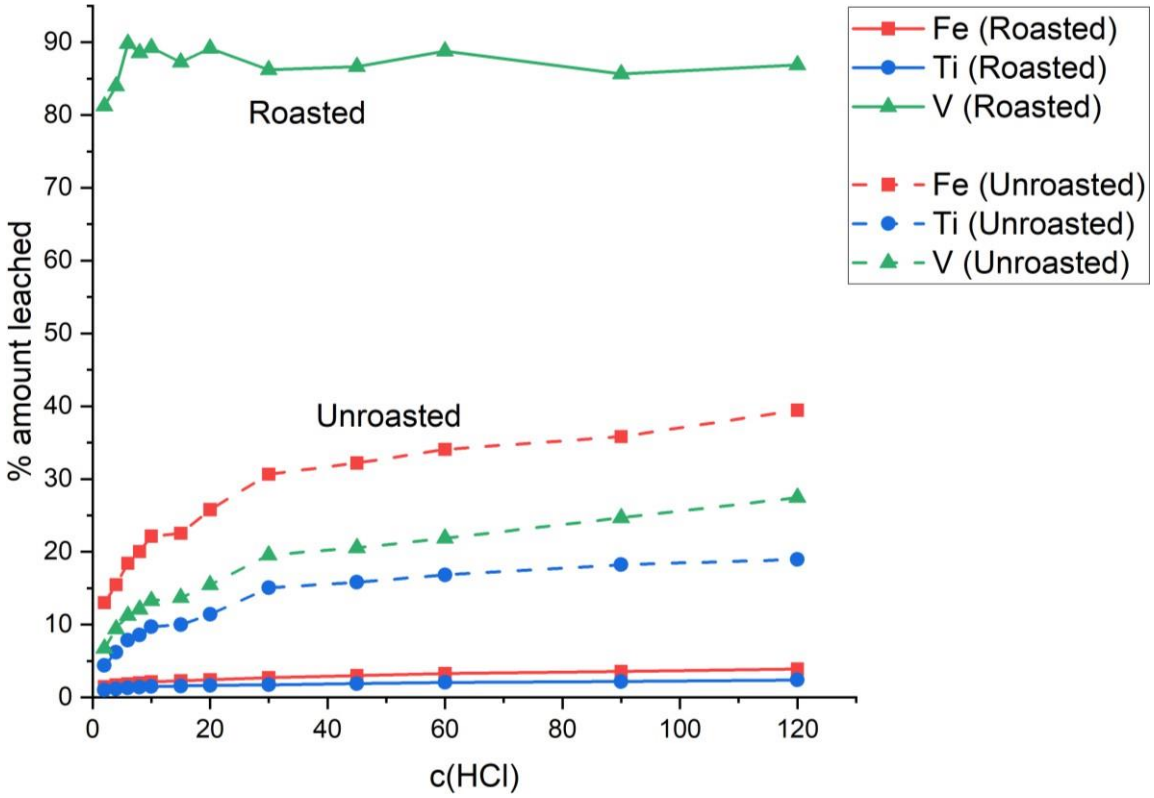

Figure 3.22. *HCl Leaching of VRC over time, comparing the effect of roasting (3 hr, 900 °C) prior to leaching. Unroasted comparison is 4M leaching of unroasted VRC. The % amount leached is the moles of element leached compared to the moles of element in initial solid material.*

The general result from the leaching experiment is exemplified below, where the leaching efficiencies are compared (Table 3.6). The Fe and Ti leaching efficiencies drop from 39.46 % and 18.95 %, respectively, to below 4 %. The V leaching efficiency increases from 27.46 % for the unroasted VRC, to 86.89 % after roasting. This result revealed a pathway for selective extraction of Vfrom the Fe and Ti. Yet, some Fe and Ti were leached along with the V, so some improvements are required. The XRF results of the leaching residue were next considered, to determine which other elements were leached in this process.

Table 3.6. *Leaching efficiencies for Fe, Ti, and V in roasted VRC leaching experiment, compared to unroasted. Values are the maximum percentage amount leached from solid material.*

Sample	Fe Leaching Efficiency (%)	Ti Leaching Efficiency (%)	V Leaching Efficiency (%)
VRC 4M Leach	39.46	18.95	27.46
VRC Roast Leach (3 hr, 900°C)	3.92	2.40	86.89

The XRF results for the roasted material and the leaching residue are shown below (Table 3.7). The weight % of V_2O_5 in the analysis decreased from 11.95 to 2.07, indicating that almost all of the V was leached from the roasted material. The other elements leached include Mn, Ca, and a small amount of both Al and Mg. The leaching of Mn is expected in this experiment because the V, which is being leached so successfully, is locked up with Mn in the manganese vanadate phase. The elements which were not leached in the experiment were Fe, Ti, and Si.

Table 3.7. *XRF major oxide analysis results for roasted VRC and its 4M HCl leaching residue. Values are expressed as weight % on oven dried (110°C) basis. LOI = loss on ignition at 1000°C. Values for SO_3, Na_2O, P_2O_5, and K_2O have been omitted due to low value (<0.06).*

Sample	Fe_2O_3	MnO	TiO_2	CaO	SiO_2	Al_2O_3	MgO	V_2O_5	LOI	SUM
VRC Roast (3 hr, 900 °C)	40.74	12.06	12.91	2.4	13.99	1.74	1.25	11.95	0.21	97.39
4M Leaching residue	46.55	7.31	18.42	0.12	21.17	1.48	0.98	2.07	0.34	98.45

To corroborate the XRF analysis of the residue, the XRD and EDS results have been analysed. The Pseudobrookite, Hematite, and SiO_2 phases were still present in the XRD pattern of the leaching residue (Figure 3.23). This was expected, from the lack of Fe and Ti in the leachate, as well as the presence of Fe, Ti, and Si in the XRF results above. The only notable difference between this pattern and that of the roasted starting material was the disappearance of the manganese vanadate reflections in the 25-29° range.This not only demonstrated the dissolution of the Mn-V phase, but also supported the analysis of these patterns in the roasted material.

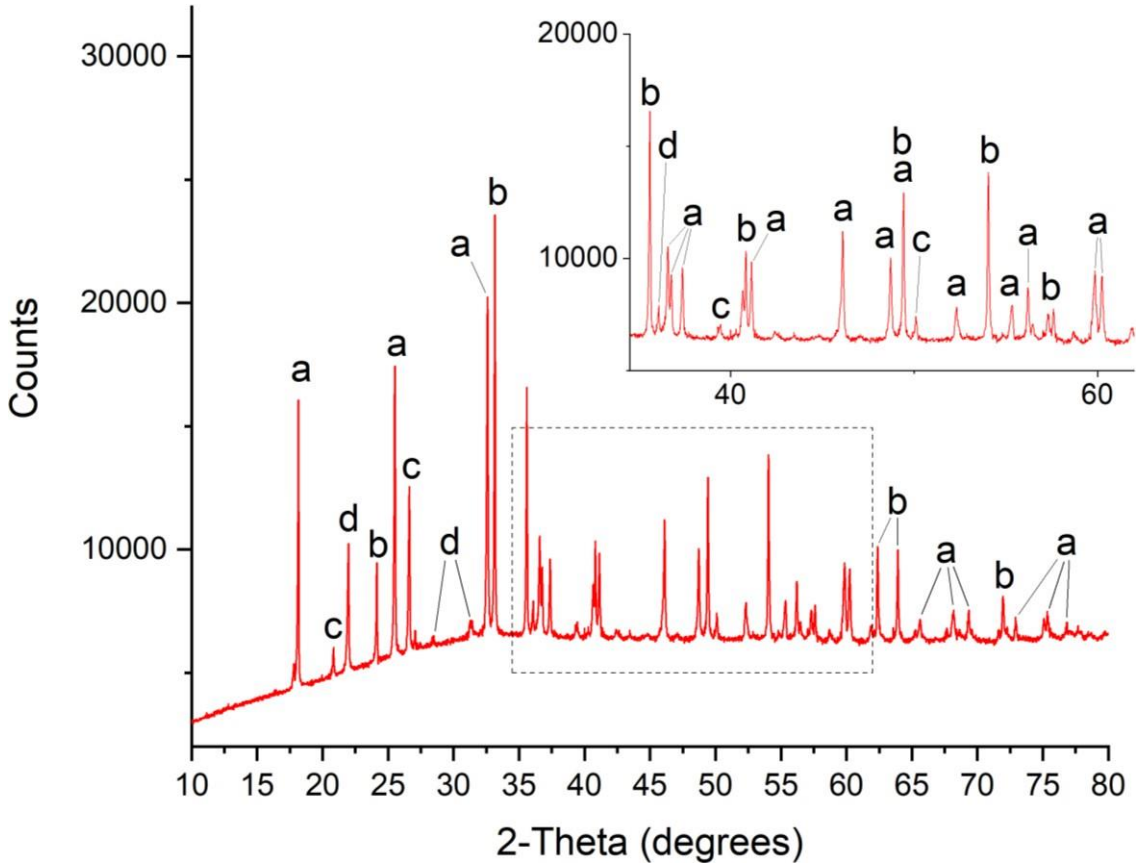

Figure 3.23. *XRD Pattern of residue after leaching roasted VRC (3 hr, 900 °C) with 4M HCl, with major reflections labelled a) Pseudobrookite, $Ti_{1.10}Fe_{1.90}O_5$ b) Hematite, Fe_2O_3 c) Quartz, SiO_2 d) Cristobalite, SiO_2.*

The EDS maps of the leached residue indicated no regions of co-located V and Mn, and in fact no regions of V were found separate from the Fe and Ti (Figure 3.24.a and b). The remaining V was found only in the Pseudobrookite phase (EDS point 2), and the only other Fe-containing phase found was Hematite (EDS point 3). The other phase of note was an SiO_2 phase (EDS point 1). The colour maps provided a key visual confirmation of the dissolution of the manganese vanadate phase. Whereas in the roasted pre-leached material, where large regions of co-located V and Mn were found, no such regions were visible in the leaching residue. This further confirmed the XRD reflections identified in the 25- 29° range as a manganese vanadate and agreed perfectly with the ICP-MS results of the leachate.

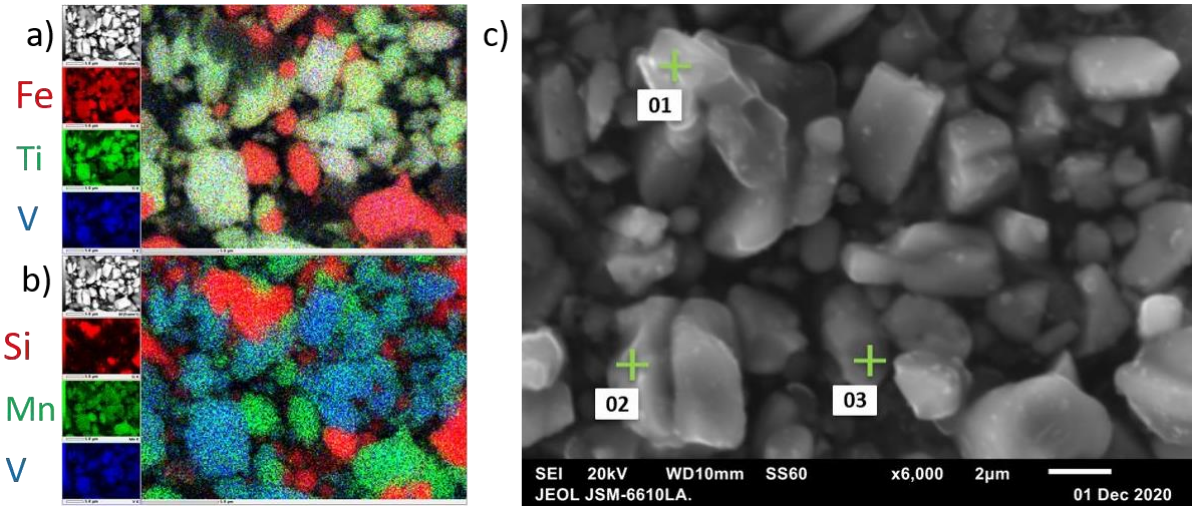

EDS Point	EDS Data for Element						Mineral Phase
	Fe	Ti	V	O	Mn	Si	
1	2.82	1.83	0.13	64.32	0.54	30.35	SiO_2
2	36.87	23.41	3.87	27.93	5.40	2.53	Pseudobrookite
3	43.35	4.47	0.28	43.50	6.63	1.76	Hematite

Figure 3.24. *SEM maps of residue after leaching VRC roast (3 hr, 900 °C) with 4M HCl. a) elemental colour map (red: Fe, green: Ti, blue: V) b) elemental colour map (red: Si, green: Mn, blue: V) c) corresponding SEM image at x6000 with EDS points labelled. Table shows the mineral phases assigned to each EDS point, and the raw EDS data for each of the major elements in atomic% (rescaled to 100 %).*

Overnight Roast at 1200 °C Leaching

To determine the effects of acid strength on the leaching behaviour of the roasted VRC, the experiment was repeated with a range of HCl concentrations between 1M -3M. The material used for these experiments was roasted overnight at 1200 °C. This was done under the expectation that a more complete roast would enable all of the Mn and V to partitionand form the manganese vanadate phase. The results from the ICP-MS analysis of the leachates for eachexperiment are shown below (Figure 3.25).

The leaching results of the overnight roast mirrored the results of the 3-hr roast. The % amount leached for V was much higher in all experiments, while the Fe and Ti leaching amounts were considerablylower, as compared to the unroasted VRC. The 1M experiment leached a lower amount of V (~ 50 %),as expected for a less concentrated acid leaching. After the leaching of V had stopped, the amount in the leachate appeared to steadily drop, indicating precipitation may have been taking place. The V % amount values for the 2M and 3M experiments were higher than that of the 1M experiment, but confusingly the order was not what is expected. The 2M experiment appeared to have leached a higher amount of V fromthe roasted sample, but it was not clear if this was a reliable result or due to

experimental error.

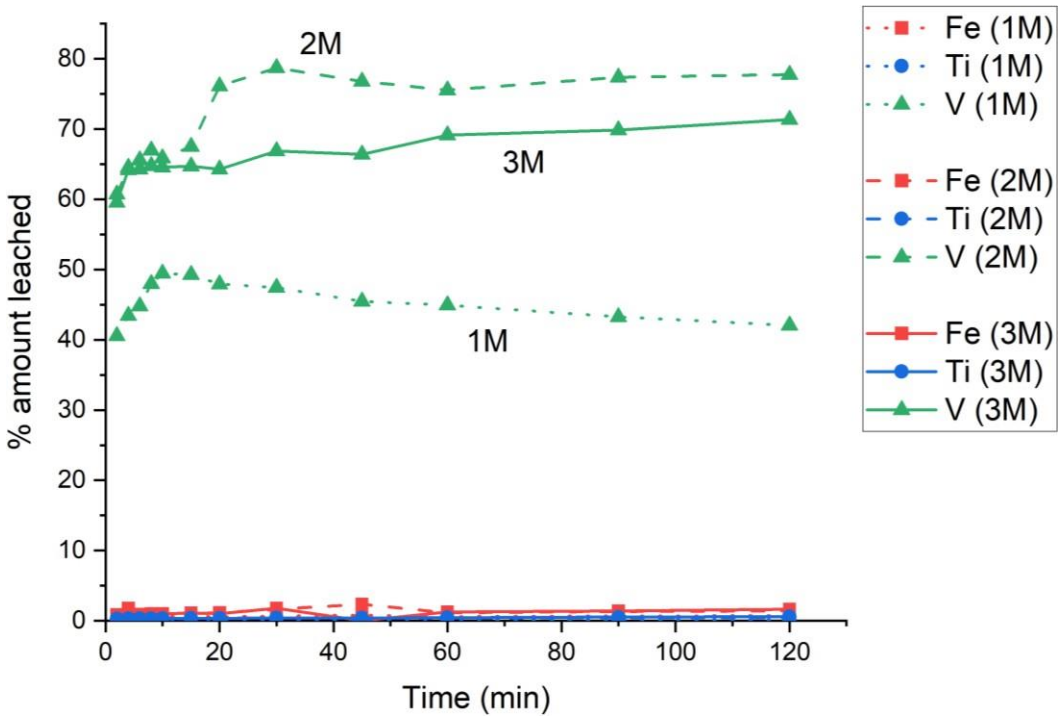

Figure 3.25. *HCl Leaching of roasted VRC (overnight, 1200 °C) over time, comparing the effect of HCl concentration. The % amount leached is the moles of element leached compared to the moles of element in initial solid material.*

The leaching efficiencies are shown below (Table 3.8) and these also reflect the results obtained from the 3-hr roast experiment. Across the range of HCl concentrations, only a very minimal change wasobserved in the total leaching amounts of Fe and Ti. The leaching efficiency for V jumped from 49.45 % in the 1M leachate, to values in the 70's for 2M and 3M.

Table 3.8. *Leaching efficiencies for Fe, Ti, and V in roasted VRC (overnight, 1200 °C) leaching experiments, compared to unroasted. Values are the maximum percentage amount leached from solid material.*

Sample	Fe Leaching Efficiency (%)	Ti Leaching Efficiency (%)	V Leaching Efficiency (%)
VRC 4M Leach	39.46	18.95	27.46
VRC Roast 1M Leach	0.81	0.19	49.45
VRC Roast 2M Leach	1.64	0.45	77.76
VRC Roast 3M Leach	1.80	0.60	71.36

The analysis of the leaching residues follows, beginning with the XRF analysis. The elements leached were Mn, Ca, V, and a small amount of Al and Mg. A small amount of the V component remained in the VRC material after each of these leaching experiments. Leaching of the Mn was expected, as the V was co-located with the Mn in the vanadate phase. Interestingly, the Mn weight % values remained constant throughout the range of experiments and matched the value for the 4M leaching experiment reported above (Table 3.9.). This due to the Mn found in the manganese(III) oxide and titaniferous mineral phases. Once the amount in these was comparable to that remaining in the vanadate phase, no large change in weight % was expected. The elements resistant to leaching were Fe, Ti, and Si, which conferred well with the above results.

Table 3.9. *XRF major oxide analysis results for roasted VRC (overnight, 1200 °C) and its 4M HCl leaching residue. Values are expressed as weight % on oven dried (110°C) basis. LOI = loss on ignition at 1000°C. Values for SO_3, Na_2O, P_2O_5, and K_2O have been omitted due to low value (<0.06).*

Sample	Fe_2O_3	MnO	TiO_2	CaO	SiO_2	Al_2O_3	MgO	V_2O_5	LOI	SUM
VRC Roast (overnight, 1200 °C)	35.55	13.22	13.79	2.53	15.68	1.71	1.07	13.01	0.22	96.91
1M Leaching residue	42.32	7.21	16.44	0.26	17.87	1.45	0.88	9.23	1.65	97.31
2M Leaching residue	45.69	7.52	17.77	0.14	18.99	1.54	0.92	4.54	0.97	98.08
3M Leaching residue	46.11	7.52	17.92	0.13	19.5	1.52	0.94	3.65	0.83	98.12

Overnight Roast at 1200 °C 1M Leaching Residue

To continue the analysis of the residues, the XRD pattern and EDS maps were compared for each leaching experiment, beginning with the 1M experiment. The XRD pattern displayed the main phases of the residue, including Hematite, Cristobalite, and Pseudobrookite, which matched expectations given the XRF results above (Figure 3.26). Minor reflections for manganese(III) oxide were also identified. Importantly, the pattern displayed none of the reflections in the 25-29° range, mirroring the result found in the 4M experiment.

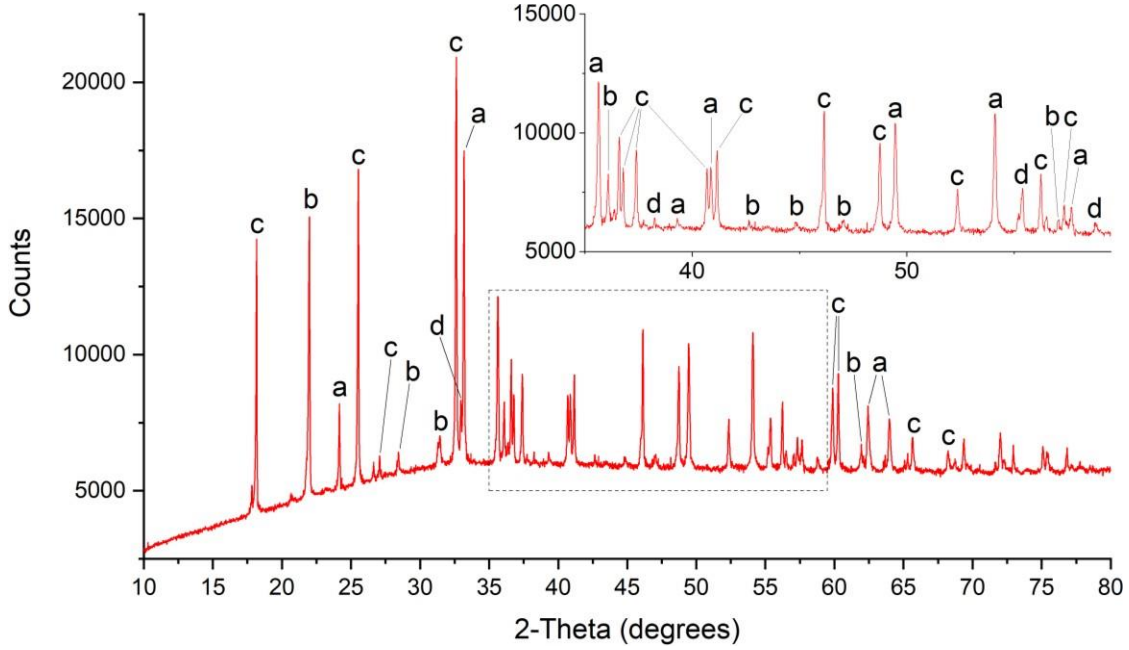

Figure 3.26. *XRD Pattern of residue after leaching roasted VRC (overnight, 1200 °C) with 1M HCl, with major reflections labelled a) Hematite, Fe_2O_3 b) Cristobalite, SiO_2 c) Pseudobrookite, $Ti_{1.10}Fe_{1.90}O_5$ d)Manganese Oxide, Mn_2O_3.*

The EDS results for the 1M residue are considered. The three main phases identified in theXRD pattern (Pseudobrookite, Hematite, and Cristobalite) were identified in the EDS map (Figure 3.27.EDS points 1-3). By observing the EDS colour map, a network of a V-rich, Mn-containing phase was identified, which appeared to cement several other particles together. This might be a vanadate phase, but itshould be noted that this phase was not identified in the XRD pattern for this residue. Furthermore, nosign of this phase was present in the EDS analysis of the starting material. This might be due to precipitationof the V during the leaching experiment; V^{5+} can precipitate as V_2O_5, and this might be the material present in the EDS map.[79] In order to confirm the nature of this phase, a higher magnification image of the region in the green box (Figure 3.27.c) is presented below.

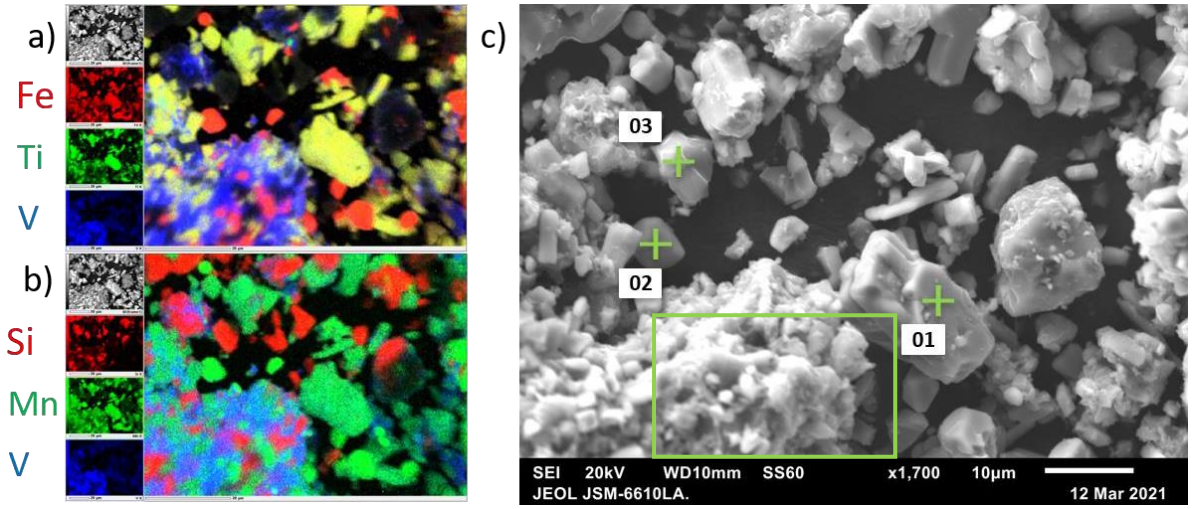

EDS Point	EDS Data for Element							Mineral Phase
	Fe	Ti	V	O	Mn	Si	Mg	
1	24.09	16.13	2.77	50.80	3.60	1.33	1.27	Pseudobrookite
2	47.66	4.99	1.69	36.10	7.13	1.44	0.99	Hematite
3	1.61	1.18	0.65	62.34	0.29	33.89	0.03	SiO_2

Figure 3.27. *SEM maps of residue after leaching VRC roast (overnight, 1200 °C) with 1M HCl. a) elemental colour map (red: Fe, green: Ti, blue: V) b) elemental colour map (red: Si, green: Mn, blue: V) c) corresponding SEM image at x1700 with EDS points labelled. Table shows the mineral phases assigned to each EDS point, and the raw EDS data for each of the major elements in atomic% (rescaled to 100%).*

From the colour maps below (Figure 3.28.a and b), it appeared that the vanadium was acting as a cement to hold together multiple particles of Fe-, Ti-, Si-, and Mn-containing particles. None of the V was co-located with the Mn in any meaningful way, thus the manganese vanadate phase appeared to have been fully leached. It is unknown what this V-only phase is, but the best guess was a V_2O_5 phase, due to the expected high oxidation state of V after roasting. For the sake of the EDS analysis, this is assumed to be the present phase.

A collection of EDS points was taken across the collection of particles in the SEM image below (Figure 3.28.c). EDS point 1 contained a predominant amount of Fe, with amounts of Mn and V. This region was assigned as a Mn-rich Hematite within the V cementing phase. EDS point 2 contained predominately Fe, with an amount of Mn present, so this was assigned as a Mn-rich Hematite. EDSpoint 3 contained Fe and Ti, and so deemed to be Pseudobrookite. Two regions were identified which contained only Si and V (EDS points 4 and 6). This was assigned as SiO_2 particles within the V cementing phase. EDS point 5 contained Fe, V, Mn, and Si, and was identified as SiO_2, with an amount of Mn-rich Hematite, both stuck in the V cementing phase. EDS point 7 contained mostly Fe, Ti,

and V, and so was assigned as Pseudobrookite within the V phase. EDS point 8 contained only Si, and so was assigned as an SiO_2 particle. EDS point 9 contained a predominance of Fe, with an amount of Mn, and so was identified as a Mn-rich hematite phase. The analysis of these points confirmed that the Hematite contained an amount of the Mn content, agreeing with the earlier analysis of theXRF results for the roasted leaching residues (i.e. why the weight % results for Mn stabilise).

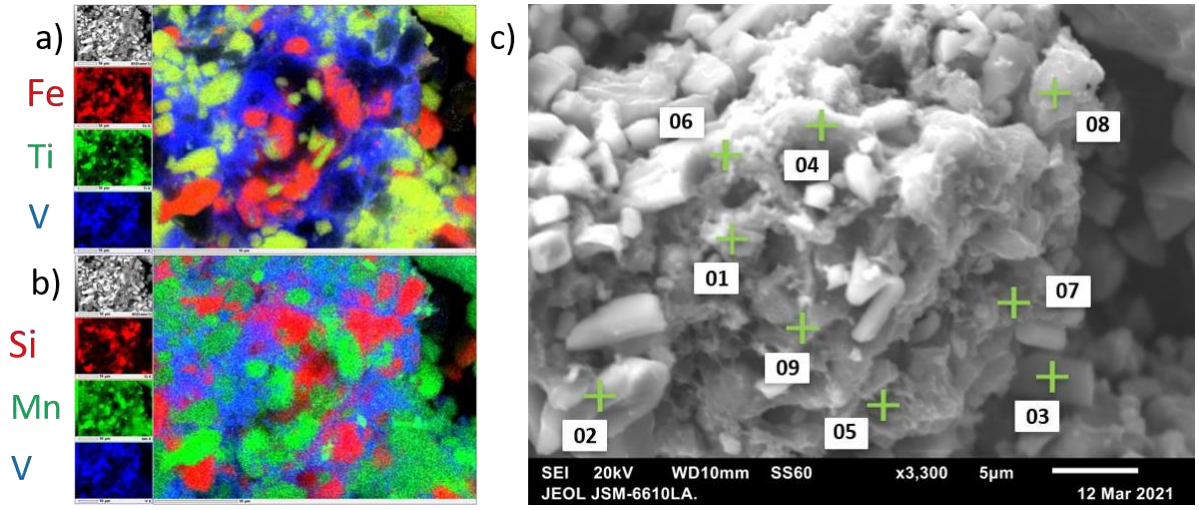

EDS Point	EDS Data for Element							Mineral Phase
	Fe	**Ti**	**V**	**O**	**Mn**	**Si**	**Mg**	
1	54.89	5.54	10.42	14.61	11.25	2.26	1.02	Mn-rich Hematite and vanadium
2	59.35	6.16	2.38	18.86	10.17	2.55	0.53	Mn-rich Hematite
3	34.69	22.59	4.45	28.25	5.73	3.65	0.64	Pseudobrookite
4	3.07	1.16	10.88	30.27	0.90	53.66	0.07	V_2O_5 and SiO_2
5	15.38	3.89	16.44	13.89	7.88	42.35	0.16	Manganese vanadate and Hematite/SiO_2
6	4.32	2.14	30.15	40.34	1.71	21.18	0.15	V_2O_5 and SiO_2
7	17.10	11.55	26.78	30.30	3.78	10.04	0.45	Vanadium-rich Pseudobrookite
8	2.09	1.27	4.56	52.68	0.57	38.74	0.09	SiO_2
9	55.28	5.51	9.00	17.37	9.06	2.71	1.07	Hematite and Manganese vanadate

Figure 3.28. *SEM maps of residue after leaching VRC roast (overnight, 1200 °C) with 1M HCl. a) elemental colour map (red: Fe, green: Ti, blue: V) b) elemental colour map (red: Si, green: Mn, blue: V) c) corresponding SEM image at x3300 with EDS points labelled. Table shows the mineral phases assigned to each EDS point, and the raw EDS data for each of the major elements in atomic% (rescaled to 100 %).*

Overnight Roast at 1200 °C 2M Leaching Residue

Next considered was the 2M HCl leaching residue. The XRD pattern showed the 3 major phases present in the 1M residue (Pseudobrookite, Hematite, and Cristobalite), with no indication of the presence of manganese(III) oxide. Yet again, no reflections were found indicating the presence of any manganese vanadate phase.

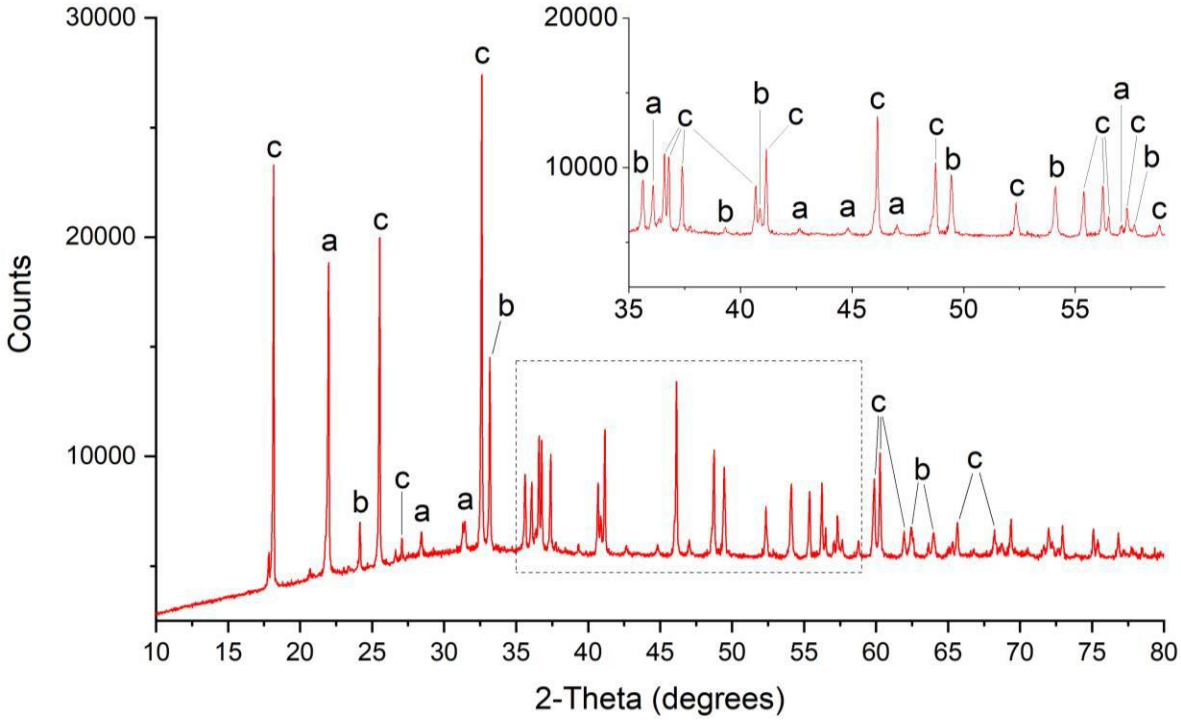

Figure 3.29. *XRD Pattern of residue after leaching roasted VRC (overnight, 1200 °C) with 2M HCl, with major reflections labelled a) Cristobalite, SiO_2 b) Hematite, Fe_2O_3 c) Pseudobrookite, $Ti_{1.10}Fe_{1.90}O_5$.*

Analysis of the EDS results for the 2M leaching residue follows. From the colour map, it appearedthat a portion of the vanadium was present in the Pseudobrookite phase, and Mn was present in the Hematitephase. EDS point 1 contained only V and O, and so likely was a particle of V_2O_5. EDS point 2 contained mostly Fe, with amounts of Ti, V, and Mn. This point was assigned as both Pseudobrookite and Hematite. EDS point 3 contained mainly Fe and Mn and was assigned to the Mn-rich Hematite phase. EDS point 4 contained mainly Fe, Ti, and Si, and was assigned to the phases Pseudobrookiteand SiO_2. Finally, EDS point 5 contained only Si, and was assigned to the SiO_2 phase.

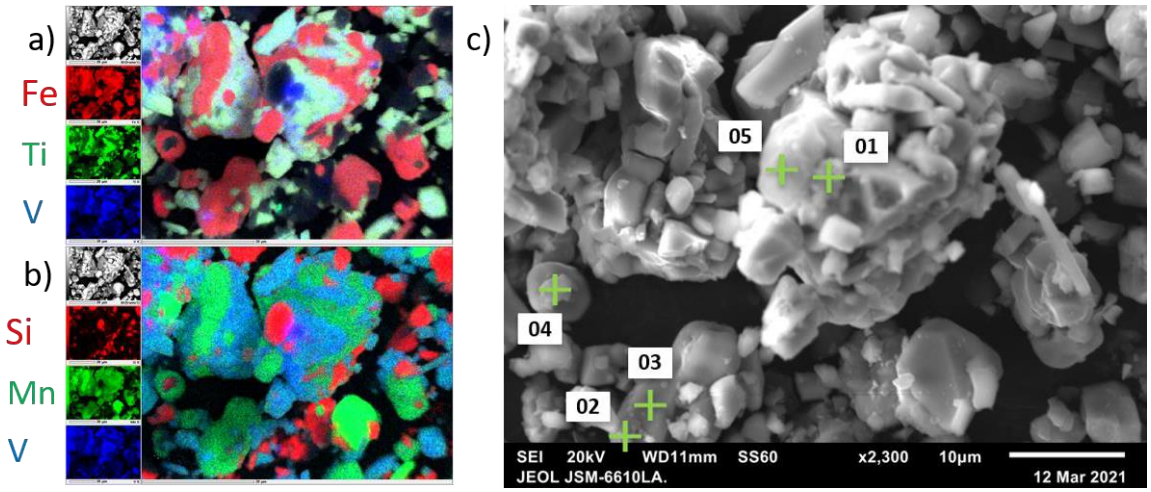

EDS Point	EDS Data for Element						Mineral Phase
	Fe	Ti	V	O	Mn	Si	
1	5.77	4.15	32.06	48.35	1.93	7.74	Vanadium
2	56.54	17.47	6.46	6.09	9.72	3.73	V-containing Pseudobrookite/Mn-rich Hematite
3	76.12	7.89	1.25	0.98	12.66	1.10	Mn-rich Hematite
4	21.77	8.78	1.01	29.68	3.48	35.27	Pseudobrookite and SiO_2
5	1.11	0.68	0.30	43.38	0.23	54.31	SiO_2

Figure 3.30. *SEM maps of residue after leaching VRC roast (overnight, 1200 °C) with 2M HCl. a) elemental colour map (red: Fe, green: Ti, blue: V) b) elemental colour map (red: Si, green: Mn, blue: V) c) corresponding SEM image at x2300 with EDS points labelled. Table shows the mineral phases assigned to each EDS point, and the raw EDS data for each of the major elements in atomic% (rescaled to 100%).*

Overnight Roast at 1200 °C 3M Leaching Residue

Finally, the 3M leaching residue is analysed. The XRD pattern of the residue showed no difference from the previous 2M residue, with the three main phases identified (Pseudobrookite, Hematite, and Cristobalite)

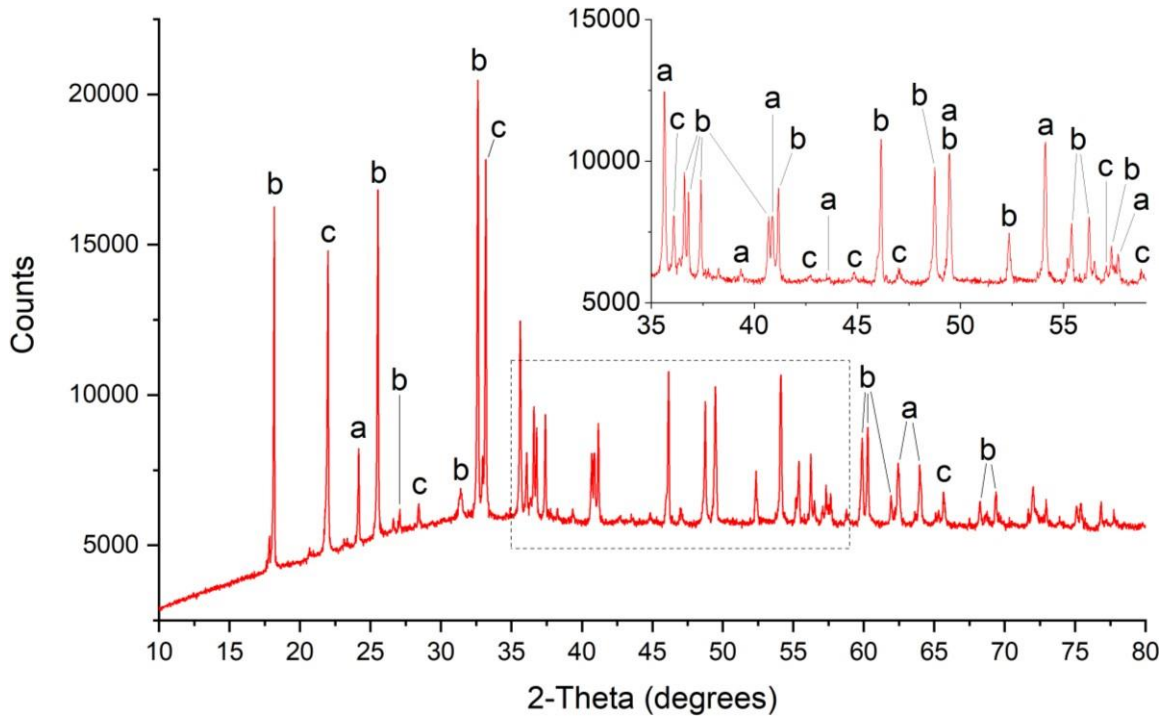

Figure 3.31. *XRD Pattern of residue after leaching roasted VRC (overnight, 1200 °C) with 3M HCl, with major peaks labelled a) Hematite, Fe_2O_3 b) Pseudobrookite, $Ti_{1.10}Fe_{1.90}O_5$ c) Cristobalite, SiO_2.*

The EDS results for the 3M residue is considered next. Each of the three phases present in the XRD could be identified. Two Hematite phases were identified, with one being particularly Mn-rich (EDS points 1 and 3). A Pseudobrookite phase could be identified (EDS point 2), as well as a SiO_2 phase (EDS point 4)

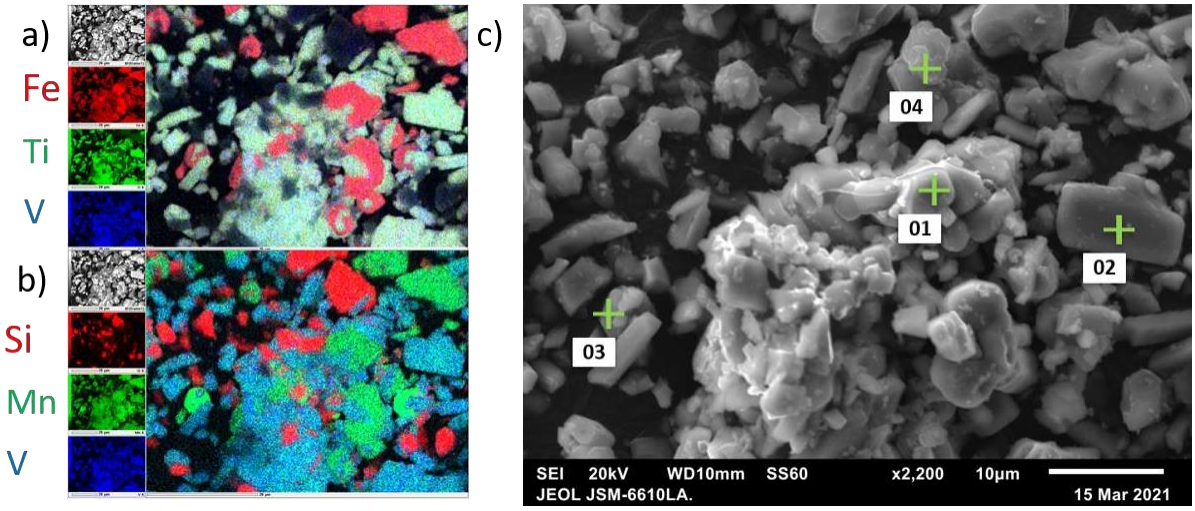

EDS Point	EDS Data for Element							Mineral Phase
	Fe	Ti	V	O	Mn	Si	Mg	
1	46.33	4.58	0.38	40.41	6.43	0.73	1.15	Hematite
2	28.38	22.67	1.03	39.30	5.80	1.51	1.29	Pseudobrookite
3	48.69	11.16	0.92	10.16	25.76	3.08	0.22	Mn-rich Hematite
4	1.59	0.63	0.07	61.93	0.28	35.47	0.03	SiO_2

Figure 3.32. *SEM maps of residue after leaching VRC roast (overnight, 1200 °C) with 3M HCl. a) elemental colour map (red: Fe, green: Ti, blue: V) b) elemental colour map (red: Si, green: Mn, blue: V) c) corresponding SEM image at x2200 with EDS points labelled. Table shows the mineral phases assigned to each EDS point, and the raw EDS data for each of the major elements in atomic% (rescaled to 100%).*

Summary

The main result, significant to the goal of this research, was the significant increase in the percentage of extraction of V after roasting. Pre-roast, the 4M leaching efficiency for the extraction of V was 58.88 %, which increased to 86.89 % after the roasting step. Additionally, the leaching efficiencies of Fe and Ti pre-roasting wass ~50 %, which decreased to less than 4 % after roasting. The cause for this was identified to benew phases formed upon roasting, with V mostly partitioning to the HCl-susceptible manganese vanadate phase, leaving Fe and Ti to form HCl-resistant Pseudobrookite and Hematite phases. Thiswas confirmed via analysis of the XRD and EDS of each of the leaching residues. After the roast, the material was found to be rich in a Mn- and V- phase, which was not present in any of the leaching residues. At 1M and 2M, small amounts of V-rich material was found to be located between particles of the acid-resistant minerals, but as no Mn was co-located with this V, it was found to be a different phase entirely, likely a vanadium oxide material. At all leaching concentrations, the predominant phases

found concurred with the XRD, with only Hematite, Pseudobrookite, and Cristobalite present. Any remaining V in the 3M and 4M experiments was found to be located in the Pseudobrookite phase. Furthermore, effective and selective leaching occurred with 4M HCl at 80 °C, reducing the cost in regards to acid consumed and equipment required compared to conc. HCl leaching. These results provide a clear pathway for the selective extraction of V from the VRC material: roasting at ~1000 °C, followed by leaching with HCl at a concentration around 4M. However, some amount of Ti and Fe was also extracted, so further purification is required.

3.3 Ironsand (IS)

3.3.1 Analysis of Starting Material

The VRC was originally intended to be utilised as a sounding board for extraction procedures that may be applied to the IS material, as the V content in the IS is much lower than that of the VRC. To this end, the IS was leached under the same conditions as the VRC experiments above, followed by a roasting procedure and leaching attempts of the roast. Before analysing these experiments, it is crucial to have an in-depth understanding of the starting material. To achieve this, XRF, XRD, and EDS were employed to determine the elemental composition of the material, as well as determine the mineral phases these elements are found in. It is appropriate to re-state at the start of this section that, for the sake of this research, IS refers to the fraction of natural ironsand which has had its Fe content amplified using magnetic and gravity separation.

The XRF results of the IS material are first considered (Table 3.10). The major element present is Fe, with Fe_2O_3 at 84.7 weight % in the analysis. The next largest components, in order of magnitude, are Ti, Al, Mg, and Si. The element of interest to this research, V, was only present in a very small quantity, with V_2O_5 at 0.58 weight % in the analysis. This poses a considerable challenge when trying to apply the leaching methods attempted for the VRC. In order to determine which mineralphases these elements exist in, the XRD and EDS results are next considered.

Table 3.10. *XRF major oxide analysis results for IS. Values are expressed as weight % on oven dried (110°C) basis. LOI = loss on ignition at 1000°C. Negative LOI indicates positive mass gain due to oxidation. Values for SO_3 and K_2O have been omitted due to low value (<0.03).*

	Fe_2O_3	MnO	TiO_2	CaO	P_2O_5	SiO_2	Al_2O_3	MgO	Na_2O	V_2O_5	LOI	SUM
IS	84.7	0.73	7.8	0.4	0.1	1.61	3.89	2.68	0.1	0.58	-3.26	99.38

The XRD pattern displayed one major phase (Figure 3.33). This was identified as TTM, with the formula $Fe(Fe_{1.04}Ti_{0.67})O_4$. From the literature presented in the introduction, this phase was expected to contain the V (see section 1.1.2). The other phase present in the XRD was only detected in comparably

minor amounts, and this was identified as a titano-hematite with formula $Ti_{0.14}Fe_{1.86}O_3$. Missing from the XRD analysis are any phases containing the elements Si, Al, and Mg. The EDS was consulted, and the XRD patterns of the HCl leaching residues are briefly invoked to reveal phases notyet present in the current XRD.

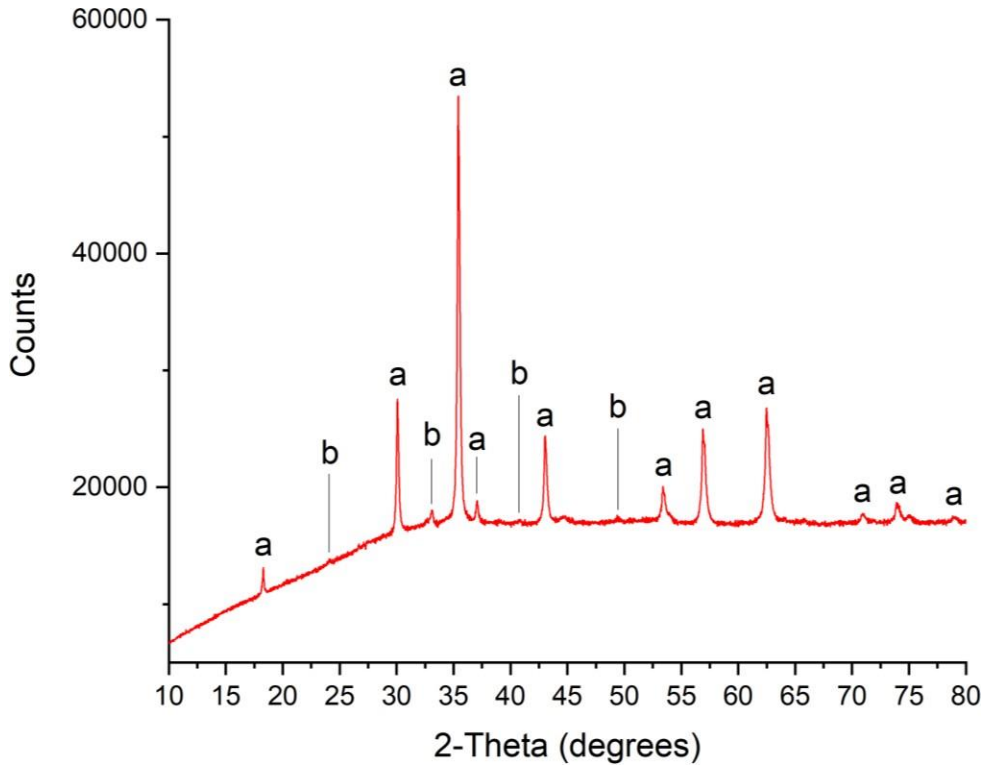

Figure 3.33. *XRD Pattern of IS with major peaks labelled a) Titanomagnetite, $Fe(Fe_{1.04}Ti_{0.67})O_4$ b) Hematite, $Ti_{0.14}Fe_{1.86}O_3$.*

The EDS was next considered. Based on the colour maps, the overwhelmingly predominant phase was the TTM phase, with varying amounts of Ti found within it (Figure 3.34.a) (EDS points 2 and3). Regions appearing only in red in the top left colour map were Hematite, as these contained little to noTi (EDS point 4). No regions of V concentration were found in the colour maps either, but the V that is present appeared to belong to the TTM phase (Figure 3.34.a). Some standout regions included the region in the centre-top of the map (Figure 3.34.b, green), which appeared to contain only Si. This was assigned to a SiO_2 phase, supported by the revealing of SiO_2 in the XRD patterns of the later IS leaching residues from which TTM had been selectively leached. Another region of interest in the colour map was the region at the top-left corresponding to a region of predominately Si and Ca (Figure 3.34.b, cyan). This was assigned to an Augite phase, which appeared in the leaching residue XRD patterns.The final region of interest was a Ca-rich phase at the bottom of the map (Figure 3.34.b, blue). This phase could not be identified using the XRD patterns of the leaching residues, indicating that this phase is leached. Thus, this remained an unidentified Ca-rich phase.

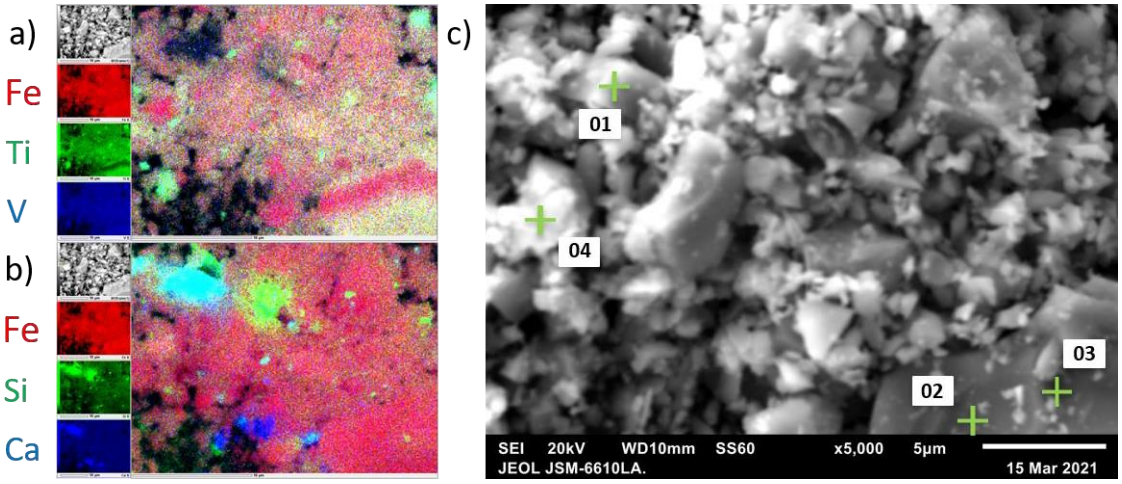

EDS Point	EDS Data for Element							Mineral Phase
	Fe	**Ti**	**V**	**O**	**Mn**	**Si**	**Ca**	
1	11.32	0.68	0.07	54.64	7.12	19.99	6.18	Augite
2	68.11	7.22	0.52	23.70	0.32	0.12	0.01	TTM
3	62.75	4.87	0.38	31.19	0.49	0.32	0.01	TTM
4	79.78	1.29	0.53	14.17	2.31	1.73	0.18	Hematite

Figure 3.34. *SEM maps of IS. a) elemental colour map (red: Fe, green: Ti, blue: V) b) elemental colour map (red: Fe, green: Si, blue: Ca) c) corresponding SEM image at x5000 with EDS points labelled. Table shows the mineral phases assigned to each EDS point, and the raw EDS data for each of the major elements (rescaled to 100 %).*

Summary

The major component of the IS material was Fe. Minor components were Ti, Ca, Si, and Mg. The V, of interest to this research, was present at a ~0.6 % weight percentage, which corroborated the literature presented in the introduction to this thesis (see section 1.1.1). The predominant crystalline phase in the material was TTM, with minor amounts of Hematite, SiO_2, and Augite. A Ca-rich phase could not be identified.

3.3.2 Leaching of Non-roasted Samples

Having analysed the starting material, one can consider the HCl leaching data. The procedure for these leaches was the same as that for the VRC material above. After adding the solid tothe 80 °C HCl, aliquots of the leachate were taken at fixed intervals, and the ICP-MS results of these aliquots are shown below (Figure 3.35.). The values reported in the ICP-MS results are given as concentrations, and these have been modified to show the amount leached as a molar percentage of theelement in the initial VRC material.

No significant difference was found in the leaching rates for the three main elements of interest, Fe, Ti, and V. As with the VRC leaching, Ti had a slower leaching rate than the other two, likely due to the presence of TiO_2 in the material, although this phase was not identified in the XRD. Another result of interest to this research was the increased % amount leached foreach element across the range of HCl concentrations. As for the VRC leaching, this was expected, as a higher acid strength leached more material across the timespan of the experiment. There were considerable differences in leaching rates between the 2M, 4M, and 8M experiments, but little difference between the 8M and conc. experiments. This indicated that at 8M, the maximum leaching amount appeared to have been reached for HCl leaching at 80 °C.

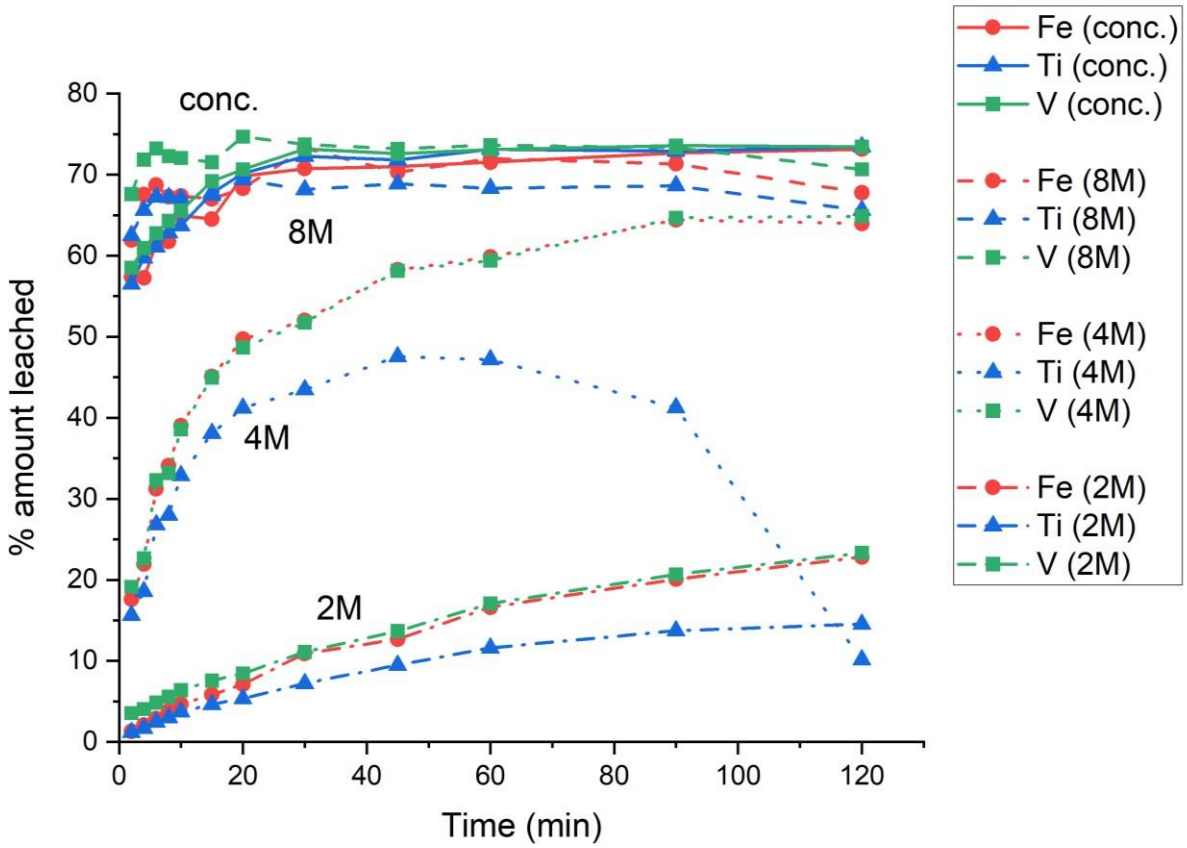

Figure 3.35. *HCl leaching of IS at 80 °C over the course of the experiment, comparing the effect of HCl concentration. The % amount leached is the moles of element leached compared to the moles of element in initial solid material.*

The final standout result from the above leaching data was the anomalous Ti leaching amount forthe 4M experiment. The Ti amount in the leachate increased until 45 min, at which point it decreased. The Ti likely existed in the leachate as $TiOCl_2$, and this is known to hydrolyse and precipitate as TiO_2.[80] This resulted in the sudden reversal of the trend in the Ti % amount leached. This was further backed up by the observation that a white precipitate was found in the leachate, as well as the presence of TiO_2 inthe EDS data for this leaching residue, which is soon considered in this section.

To more clearly observe the effect of HCl concentration on the total leaching amounts, the leaching efficiencies are given below (Table 3.11), and the final % amounts leached were plotted as a function of acid strength (Figure 3.36). The 4M Ti value has been kept in the chart but should be considered as an outlier. The leaching efficiencies for the range of experiments were comparable, indicating that the three elements Fe, Ti, and V, were found in the same TTM phase. The values between 8M and the conc. experiment were also comparable, indicating that the maximum leaching for 120 min at 80 °C was reached with the 8M HCl leaching. The key idea demonstrated in the graph was the factthat the largest difference in total leaching amount was between 2M and 4M HCl concentrations. While the 4M and 8M experiments had different leaching rates, the total leaching amount appeared to be comparable.

Table 3.11. *Leaching efficiencies for Fe, Ti, and V in IS leaching experiments. Values are the maximum percentage amount leached from solid material. The Ti value at 4M cannot be reported due to TiO_2 precipitation during course of the experiment.*

Sample	Fe Leaching Efficiency (%)	Ti Leaching Efficiency (%)	V Leaching Efficiency (%)
IS 2M Leach	22.81	14.57	23.31
IS 4M Leach	64.42	-	64.89
IS 8M Leach	71.98	68.88	73.65
IS conc. Leach	73.15	73.45	73.59

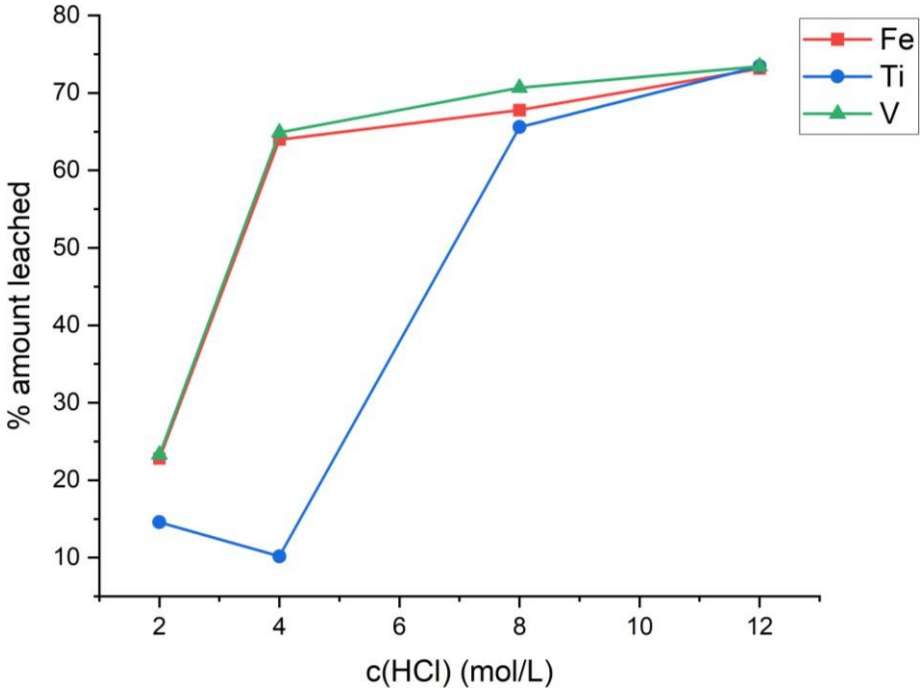

Figure 3.36. *Final extraction values at 2 hr as a function of HCl concentration. Outlying Ti result at 4M was due to TiO_2 precipitation during course of experiment.*

To complete the analysis of the leaching experiments, the leaching residues were analysed.These residues were first analysed by XRF to determine their elemental composition, and the results are shown below (Table 3.12). The Fe component appeared to be almost entirely leached across the range of experiments, with very little change observed in the 2M residue (84.7 to 83.80 weight %), and a substantial change observed in the conc. residue (84.7 to 13.92 weight %). The other elements which appeared to have been successfully leached across the range of experiments include Mn, Ti, and V. The anomalous Ti result for the 4M leaching residue (22.87 weight %) is due to the aforementioned TiO_2 precipitation. This also occurred in the 8M experiment, yet this is not evident in the ICP-MS analysis. This was due to the TiO_2 precipitation occurring after the final aliquot was taken from the leaching experiment, and it appeared as a white precipitate in the 8M leachate.

The elements retained in the leaching residues included Ca, Si, Al, and Mg. These were likely present in phases are resistant to HCl attack, such as SiO_2 and Augite. TheSiO_2 weight percentage value changed from 1.61 to 48.21 across the range of leaching experiments, which indicated a large portion of the TTM was leached in the conc. HCl leaching experiment. This should be reflected in the XRD and EDS analyses of the leaching residues.

Table 3.12. *XRF major oxide analysis results for IS and leached IS residues. Values are expressed as weight % on oven dried (110°C) basis. LOI = loss on ignition at 1000°C. Negative LOI indicates positive mass gain due to oxidation. Values for SO_3, Na_2O, K_2O, and P_2O_5 have been omitted due to low value (<1.0). Total mass submitted for 8M and conc.*

Sample	Fe_2O_3	MnO	TiO_2	CaO	SiO_2	Al_2O_3	MgO	V_2O_5	LOI	SUM
IS	84.7	0.73	7.80	0.40	1.61	3.89	2.68	0.58	-3.70	99.38
2M Leaching Residue	83.80	0.73	8.64	0.31	1.83	3.48	2.68	0.63	-2.90	99.4
4M Leaching Residue	63.28	0.57	22.87	0.83	5.22	3.19	2.41	0.63	0.04	99.48
8M Leaching Residue	21.00	0.72	17.95	5.08	37.54	6.66	5.54	0.29	2.31	98.52
Conc. Leaching Residue	13.92	0.4	9.16	6.24	48.21	7.93	6.13	0.19	3.93	97.91

2M Leaching Residue

To continue the analysis of the leaching residues, the XRD and EDS results of the 2M residue were considered. The titanomagnetite phase was still the only major phase identified in the XRD pattern (Figure 3.37). The Hematite phase present in the IS starting material was no longer present, and in its place, an iron oxide-hydroxide pattern was observed. This indicated that the Hematite had undergone leaching, and an iron oxide-hydroxide phase had been produced. This iron oxide-hydroxidephase was not likely to have been produced during the leaching, as the leaching occurred under acidic conditions. Thus, this phase was likely produced post-experiment, as the material oxidised on standing. No phases containing the other elements present in the IS material (Si, Ca, Mg) were identified in the XRD pattern.

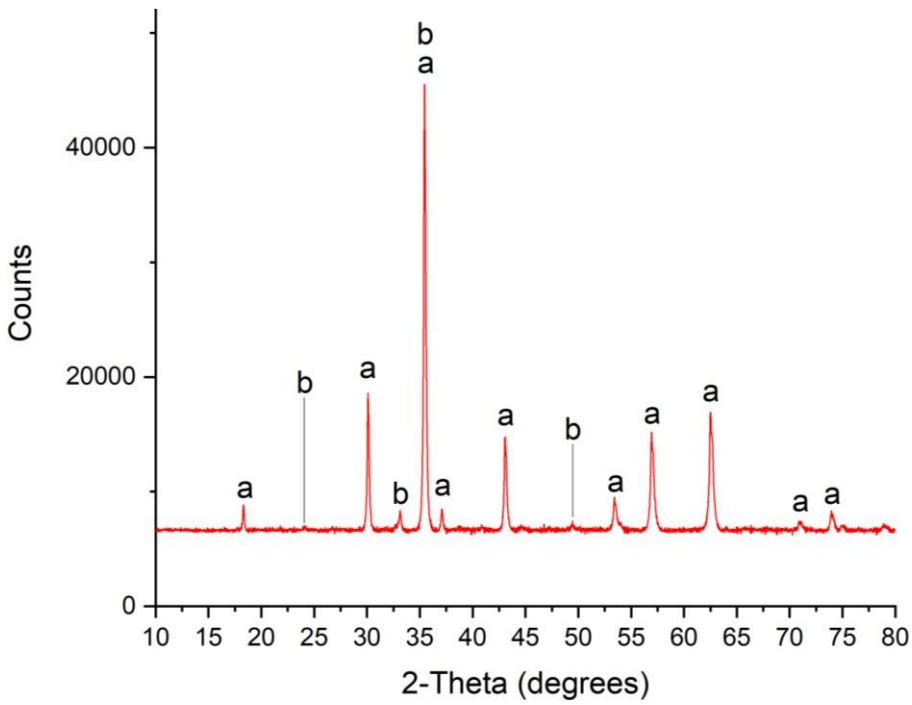

Figure 3.37. *XRD pattern of residue after leaching IS with 2M HCl, with major reflections labelled a)Titanomagnetite, $Fe(Fe_{1.04}Ti_{0.67})O_4$ b) iron oxide-hydroxide,$Fe_{1.9}O_{2.7}(OH)_{0.3}$.*

To further analyse phases present in the 2M leaching residue, the EDS of this material was considered (Figure 3.38). The colour maps indicated the predominance of Fe and Ti in the material,with some particles containing Si and Ca. Two EDS points were taken of particles high in both Fe and Ti, and assigned to the TTM phase (EDS points 1 and 4). By the colour maps, theamount of Ti in the TTM particles varied greatly between TTM particles. Two EDS points were taken of particles containing predominately Fe, and these were assigned to the iron oxide-hydroxidephase, in concordance with the XRD results (EDS points 2 and 3). The V in this material appeared to befound mainly in the TTM phase, as shown in the colour maps (Figure 3.38.a and b, blue).

The remaining EDS point contained amounts of Si and Ca, and was assigned to the Augite phase, which was present in later leaching residues, as well as in the EDS analysis of the IS starting material (EDS point 5). Regions containing only Si were present in the colour map (Figure 3.38.b, red), and assigned to an SiO_2 phase. Small regions containing only Ca were also noticed in thecolour map (Figure 3.38.b, green), and considered to be the same Ca-rich phase present in theIS starting material which could not be identified.

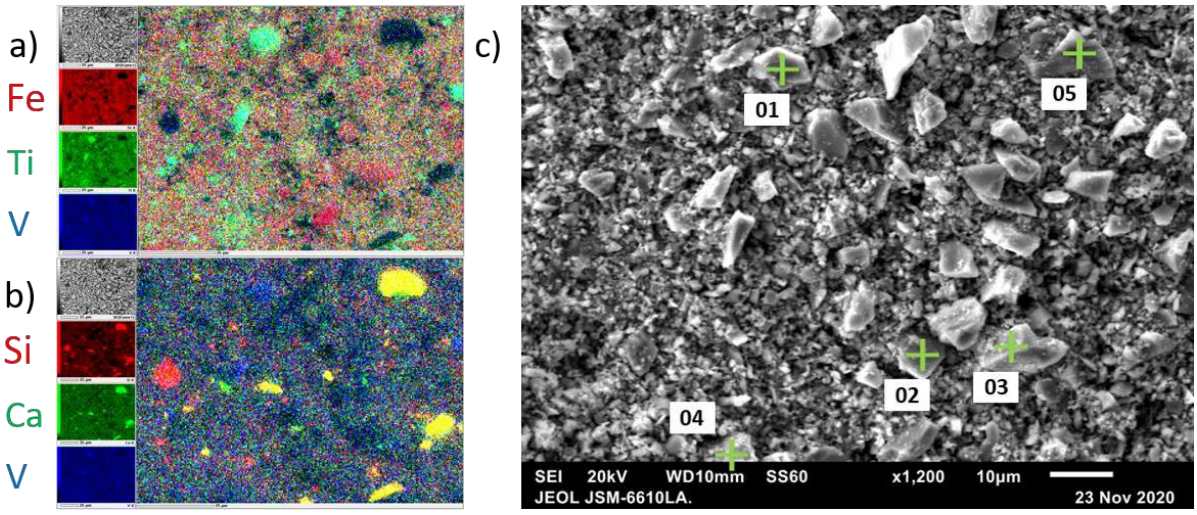

EDS Point	EDS Data for Element								Mineral Phase
	Fe	Ti	V	O	Mn	Si	Ca	Mg	
1	59.53	25.88	0.71	12.82	0.26	0.16	0.00	0.65	TTM
2	61.46	4.85	0.44	28.61	0.56	0.27	0.04	3.77	iron oxide-hydroxide
3	79.32	5.21	0.45	11.55	0.93	1.07	0.16	1.30	iron oxide-hydroxide
4	60.70	13.88	0.53	18.99	0.68	1.39	0.06	3.77	TTM
5	7.76	0.71	0.03	25.22	0.26	36.49	17.44	12.09	Augite

Figure 3.38. *SEM maps of residue after leaching IS with 2M HCl. a) elemental colour map (red: Fe, green: Ti, blue: V) b) elemental colour map (red: Si, green: Ca, blue: V) c) corresponding SEM image at x1200 with EDS points labelled. Table shows the mineral phases assigned to each EDS point, and the raw EDS data for each of the major elements in atomic% (rescaled to 100 %).*

4M Leaching Residue

The XRD pattern of the 4M residue still displayed theTTM phase as the dominant crystalline phase, and the iron oxide-hydroxide reflections appeared to have a greater relative height compared to the 2M residue (Figure 3.39). The peak reflection height of the TTM phase(in counts) dropped from ~45,000 to ~13,000, indicating that this phase was less predominant in the material, due to being leached. Still no evidence of the minor elements Si, Ca, and Mg, was foundin the XRD pattern.

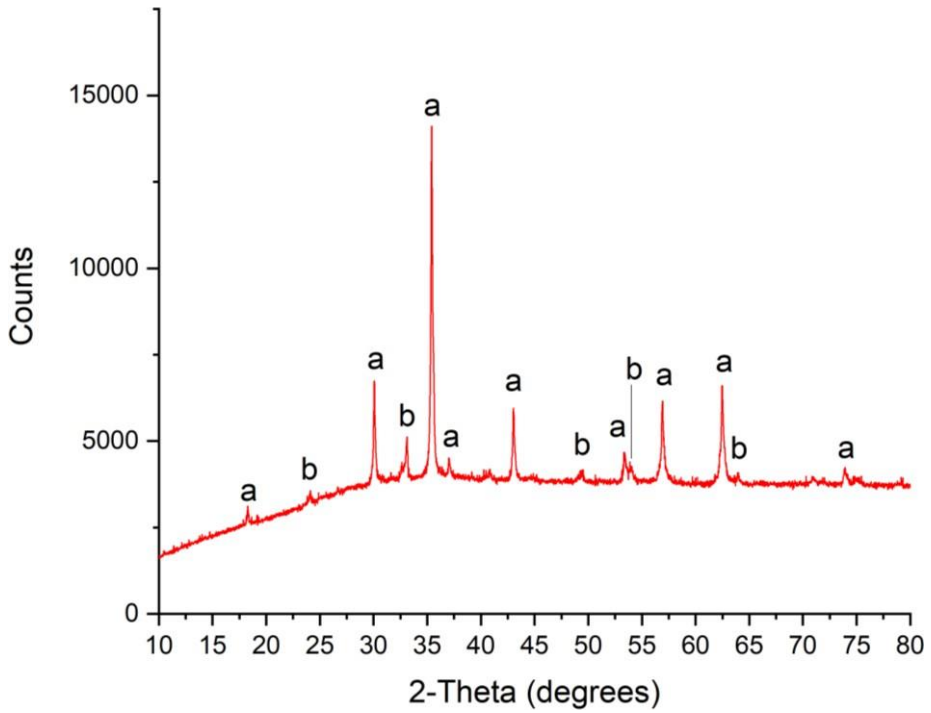

Figure 3.39. *XRD pattern of residue after leaching IS with 4M HCl, with major reflections labelled a)Titanomagnetite, $Fe(Fe_{1.04}Ti_{0.67})O_4$ b) iron oxide-hydroxide, $Fe_{1.9}O_{2.7}(OH)_{0.3}$.*

The EDS results for this phase indicated the presence of two main phases, a TTM phase and an iron oxide-hydroxide phase (Figure 3.40.a, red and green). EDS points were taken for both the TTM phase (EDS point 1) and for the iron oxide hydroxide phase (EDS point 3). For two of the TTM particles analysed, small amounts of Si were also found (EDS points 4 and 6), indicating the presence of SiO_2 deposits on the surface of the TTM particles. The V in this material appeared to be found mainly in the TTM phase, as shown in the colour maps (Figure 3.40.a and b, blue).

Two other mineral phases were identified in the EDS results. The first as a Ca and Si containing phase, found in all EDS maps of IS and its residues thus far. This was identified asAugite (EDS point 2). The other phase was a Ti-containing phase with very little Fe present, indicating a TiO_2 phase. No TiO_2 phase has yet been identified in the XRD patterns of any IS or leachingresidue material. This might be due to precipitation of TiO_2 occuring in this leaching experiment, and for the following 8M leaching experiment. The TiO_2 was precipitated as an amorphous hydrate, thus no TiO_2 XRD pattern was expected. The EDS colour map also indicated thepresence of Ca-dominant phases, found in all IS materials so far and not been identified yet (Figure 3.40.b, green).

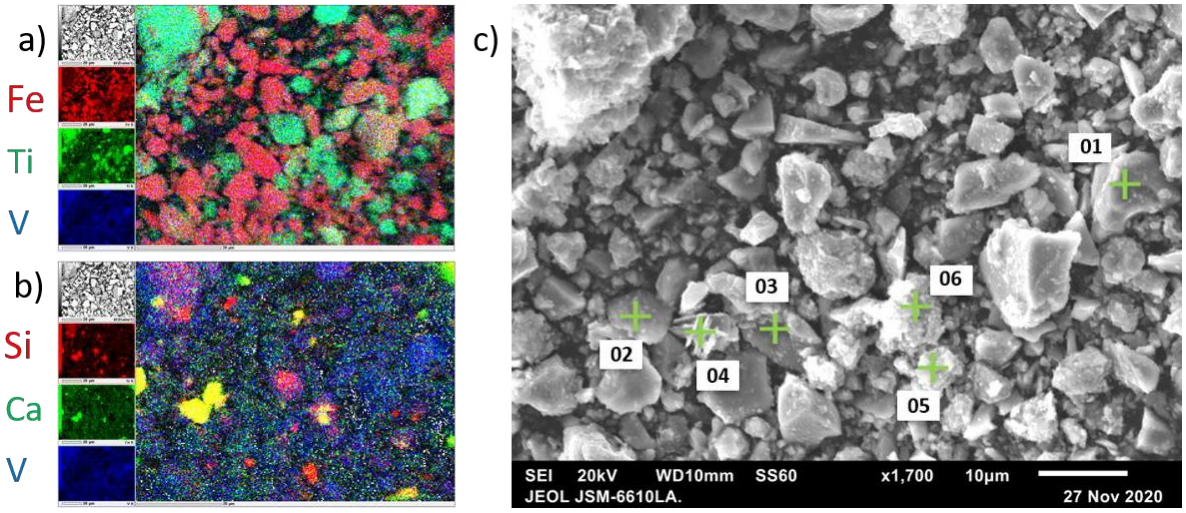

EDS Point	EDS Data for Element								Mineral Phase
	Fe	Ti	V	O	Mn	Si	Ca	Mg	
1	25.73	21.58	0.22	50.37	0.46	0.30	0.04	1.30	TTM
2	3.72	1.08	0.06	55.41	0.06	21.15	9.01	9.51	Augite
3	81.11	4.54	0.46	11.97	0.98	0.25	0.05	0.64	iron oxide-hydroxide
4	17.09	16.07	0.15	52.01	0.68	10.41	0.73	2.88	TTM with SiO_2
5	12.44	26.39	0.54	53.61	0.14	5.43	0.54	0.90	TiO_2 and TTM
6	21.35	8.14	0.34	55.23	0.07	12.08	1.71	1.08	TTM with SiO_2

Figure 3.40. *SEM maps of residue after leaching IS with 4M HCl. a) elemental colour map (red: Fe, green: Ti, blue: V) b) elemental colour map (red: Si, green: Ca, blue: V) c) corresponding SEM image at x1700 with EDS points labelled. Table shows the mineral phases assigned to each EDS point, and the raw EDS data for each of the major elements in atomic% (rescaled to 100 %).*

8M Leaching Residue

The XRD pattern of the 8M residue contained a large amorphous hump, indicative of the presence of a significant amount of amorphous material. The background hump wassubtracted from the pattern for ease of analysis (Figure 3.41). The XRD pattern appeared much more complex compared to the 2M and 4M residues, and the TTM phase was largely leached from the IS material, revealing the minor, HCl resistant phases. As such, the XRD results forthis material, as well as the following conc. HCl leaching residue material, were likely to be more subject to false positives due tolarge number of reflections present.

Reflections associated with TTM were still in the majority, and iron oxide-hydroxide remained present in the XRD pattern. The main minor phase of interest was Augite, which was suggested as a phase present inthe IS and its leaching residues up to this point. This XRD provided the justification for the earlier assignment of Augite in these materials. Another phase which appeared in the XRD pattern

was an Ilmenite phase,with the Fe substituted for a range of other metals.

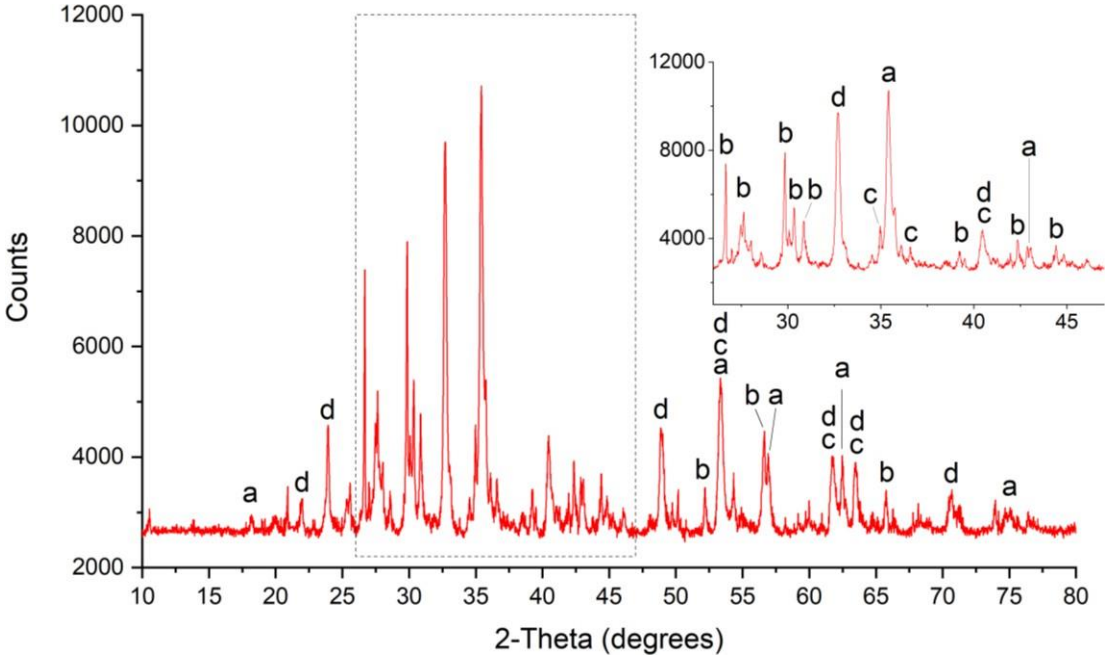

Figure 3.41. *XRD pattern of residue after leaching IS with 8M HCl, with major reflections labelled a)Titanomagnetite, $Fe(Fe_{1.04}Ti_{0.67})O_4$ b) Augite, $(Ca,Na)(Mg,Fe,Al,Ti)(Si,Al)_2O_6$ c) iron oxide-hydroxide, $Fe_{1.9}O_{2.7}(OH)_{0.3}$. d) Ilmenite, $FeTiO_3$.*

To confirm the XRD analysis, the EDS is considered. The colour maps indicate a lower amount of the two main phases (TTM and iron oxide-hydroxide) as compared to the 2M and 4M residues (Figure 3.42.a, red and green). The maps also indicated a higher presence of the Ca-containing Augite phase, as compared to the previous residues (Figure 3.42.b, green). The Si colourmap was lost during the analysis of this data, but an EDS point was taken of a particle, confirming the presence of Si (EDS point 1). The two phases previously identified in the 2M and 4M residues (TTM and iron oxide-hydroxide) were also identified in the EDS map (EDS points 2 and 3). The two remaining EDS points contained mostly Si, which indicated the presence of SiO_2 particles (EDS points 4 and 5). There also appeared to be particles containing mainly Mg present, but it was not known what these particleswere (Figure 3.42.b, red). They might be part of a Si-Mg phase, such as Enstatite ($MgSiO_3$), but this could not be determined without the Si EDS map.

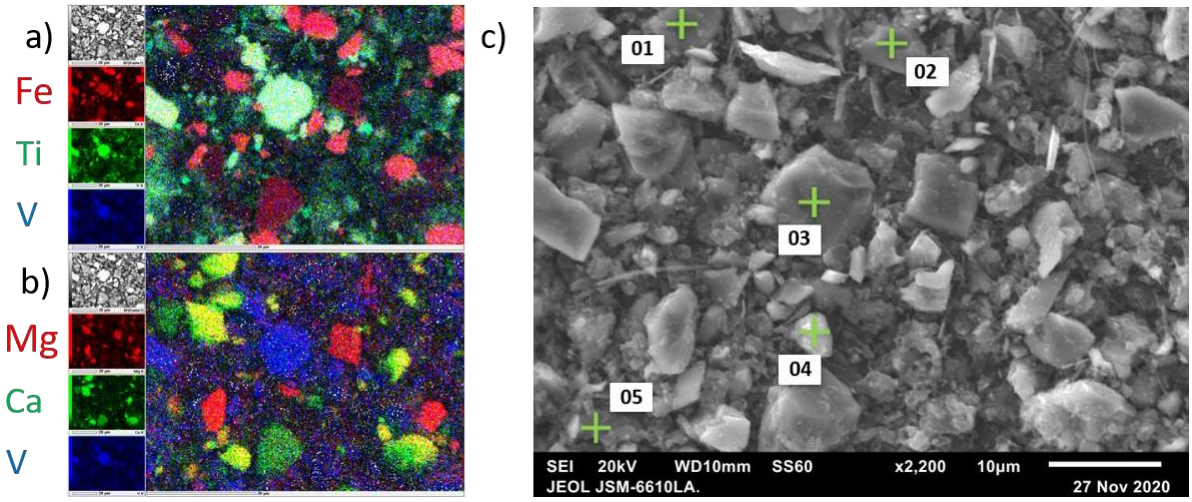

EDS Point	EDS Data for Element								Mineral Phase
	Fe	**Ti**	**V**	**O**	**Mn**	**Si**	**Ca**	**Mg**	
1	4.89	0.53	0.03	42.00	0.16	29.07	14.08	9.24	Augite
2	53.98	1.84	0.27	40.13	0.73	0.61	0.12	2.32	iron oxide-hydroxide
3	35.83	38.24	0.27	23.77	1.37	0.34	0.07	0.11	TTM
4	2.19	1.29	0.02	68.51	0.08	26.18	0.72	1.01	SiO_2
5	1.70	1.61	0.00	60.79	0.05	33.12	1.88	0.85	SiO_2

Figure 3.42. *SEM maps of residue after leaching IS with 8M HCl. a) elemental colour map (red: Fe, green: Ti, blue: V) b) elemental colour map (red: Mg, green: Ca, blue: V) c) corresponding SEM image at x2200 with EDS points labelled. Table shows the mineral phases assigned to each EDS point, and the raw EDS data for each of the major elements in atomic% (rescaled to 100 %).*

Conc. Leaching Residue

Similar to the 8M residue, the XRD pattern of this residue contained a large amorphous hump, indicating the presence of a significant amount of amorphous material, which has been subtracted as background (Figure 3.43.). The main finding in the XRDanalysis is the lack of reflections corresponding to TTM or iron oxide-hydroxide. This indicatedthat at least the majority of these phases was leached during the experiment. The main phases present in the pattern were Augite, as well as two newly found phases, Cristobalite and Quartz. These areSiO_2 minerals and were found in the EDS results for all residues. Thus, this justified the earlier assignment of these phases.

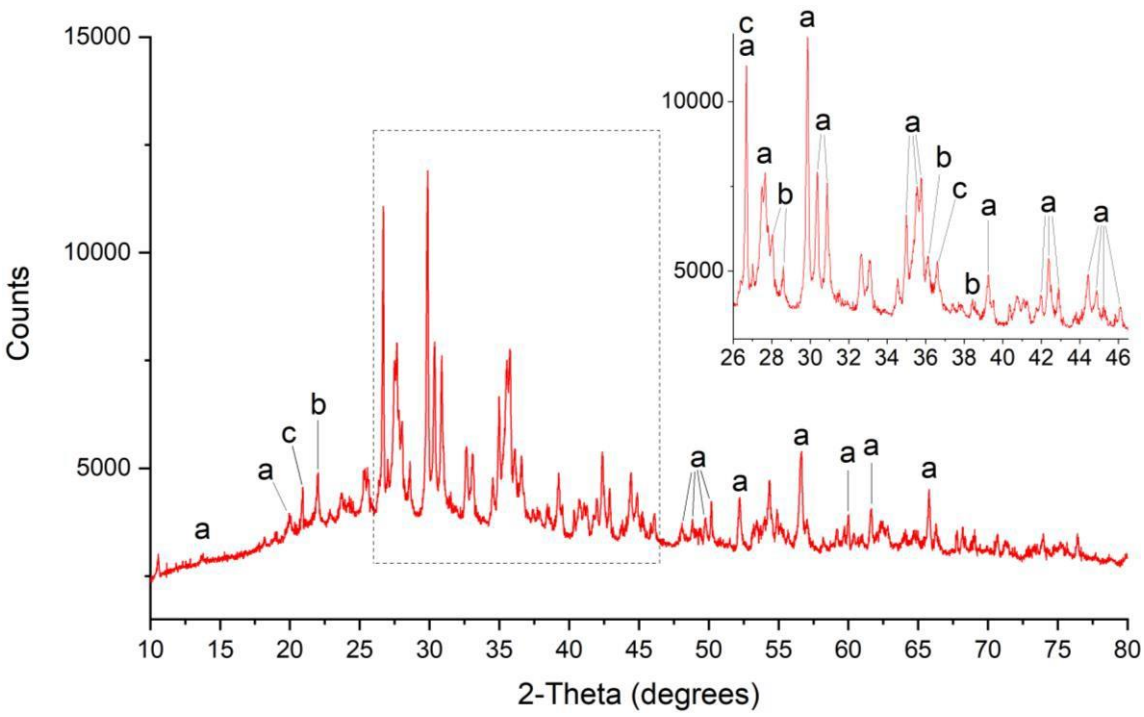

Figure 3.43. *XRD pattern of residue after leaching IS with conc. HCl, with major reflecctions labelled a)Augite, (Ca,Na)(Mg,Fe,Al,Ti)(Si,Al)$_2$O$_6$ b) Cristobalite, SiO$_2$ c) Quartz, SiO$_2$*

The EDS map of the conc. residue displayed some regions of Fe and Ti, indicating the presence of TTM in the residue (EDS point 1). There also appeared to be large particles of Si and Ca mineral, which were assigned as Augite (EDS point 3). Particles of SiO_2 could also be identified in the residue (EDS point 4). There were some small regions of the colour map which exhibited only the presenceof Ti, indicating that TiO_2 was present in the material (Figure 3.44.a, green). The remainder of the V found in the material appears to be found only in the remaining TTM phase (Figure 3.44.a and b, blue). There were also fibres of glass wool (SiO_2) present in the residue, which are likely artefacts from the sample filtration through a glass wool plug (Figure 3.44.b, red, and EDS point 2). A closer analysis of a particular particle was conducted at a higher magnification, shownin the green box below.

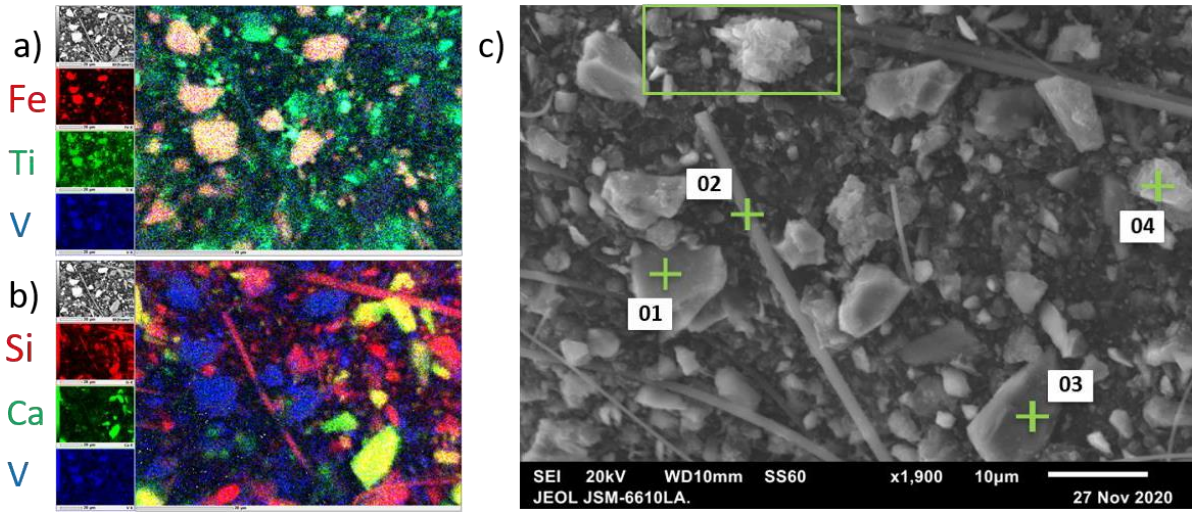

EDS Point	EDS Data for Element								Mineral Phase
	Fe	Ti	V	O	Mn	Si	Ca	Mg	
1	74.11	7.30	0.54	14.76	0.54	1.12	0.07	1.56	TTM
2	5.38	3.24	0.00	56.63	0.00	32.44	1.25	1.07	SiO_2
3	6.07	0.61	0.07	36.97	0.30	30.07	16.88	9.04	Augite
4	0.59	0.39	0.00	66.92	0.00	31.53	0.20	0.37	SiO_2

Figure 3.44. *SEM maps of residue after leaching IS with conc. HCl. a) elemental colour map (red: Fe, green: Ti, blue: V) b) elemental colour map (red: Si, green: Ca, blue: V) c) corresponding SEM image at x1900 with EDS points labelled. Table shows the mineral phases assigned to each EDS point, and the raw EDS data for each of the major elements in atomic% (rescaled to 100 %).*

Below is shown the higher magnification analysis of a particle. The particle appeared to be comprised of several mineral phases held together by SiO_2, based on the colour maps (Figure 3.45.a and b). EDS point 1 showed a region of Si, Ca, and Mg rich mineral, which was assigned as an Augite phase. EDS point2 was mainly Fe-containing, and assigned as iron oxide-hydroxide. This phase was not identified in the XRD but has precedent for existence due to its occurrence in the previous residues. Its inclusion in the acid-resistant SiO_2 phase shielded it from HCl attack. The central portionof this particle contained regions high in Si, Ca, and Mg, and was assigned as Augite. Theseparticles all appeared to be cemented by a SiO_2 phase, evidenced by EDS point 4.

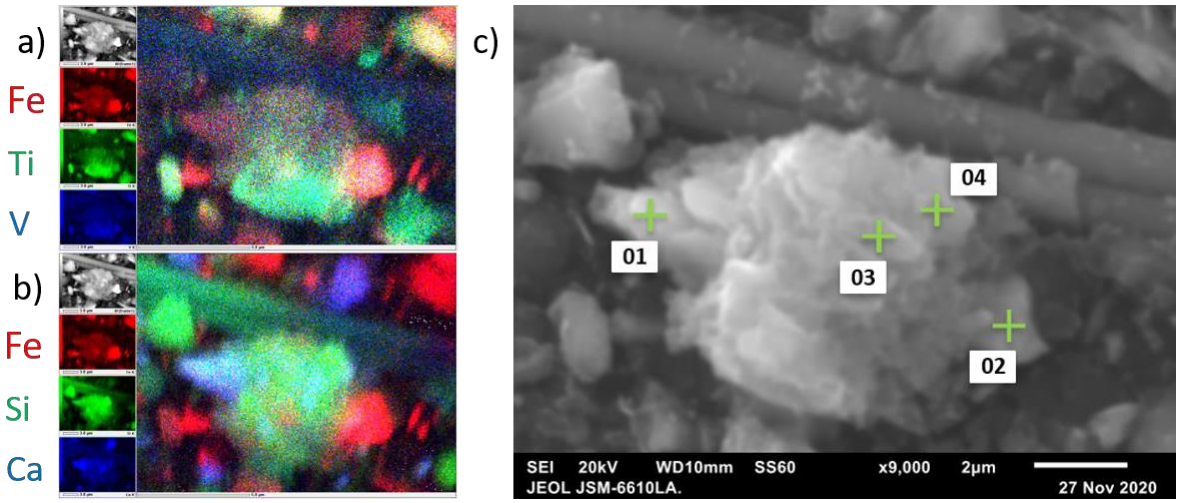

EDS Point	EDS Data for Element								Mineral Phase
	Fe	Ti	V	O	Mn	Si	Ca	Mg	
1	5.72	1.73	0.05	50.35	0.18	25.77	8.62	7.58	Augite
2	36.85	4.85	0.37	46.75	0.33	6.76	0.33	3.76	iron oxide-hydroxide
3	2.96	1.92	0.10	63.80	0.10	23.07	3.84	4.21	Augite
4	2.81	1.69	0.02	67.70	0.11	24.75	1.40	1.51	SiO_2

Figure 3.45. *SEM maps of residue after leaching IS with conc. HCl. a) elemental colour map (red: Fe, green: Ti, blue: V) b) elemental colour map (red: Si, green: Ca, blue: V) c) corresponding SEM image at x9000 with EDS points labelled. Table shows the mineral phases assigned to each EDS point, and the raw EDS data for each of the major elements in atomic% (rescaled to 100 %).*

Summary

The IS material was leached at a series of acid concentrations between 2M and conc. HCl. No considerable difference was found in the leaching rate or amount for Fe, Ti, or V, indicating that these were found in predominately the same phase, TTM. As the HCl concentration was increased, a higher %amount of these elements was leached over 120 min, starting at ~20 % for the 2M experiment, and peaking at ~70 % for the conc. experiment. In the 4M experiment, Ti precipitation was found to take place. XRF, EDS, and XRD analysis of the leaching residues indicated that the TTM and Hematite phases were leached, and an iron oxide-hydroxide phase was formed. The phases not leached were Augite, Quartz, and Cristobalite.

3.3.3 Roasting of Samples

Since the roasting of the VRC resulted in such a significant increase in V leaching, and a similar decrease in the leaching of both Fe and Ti, the same tactic was hypothesised to have a similar effect on the IS. To this end, the IS was roasted at 900 °C for 3 hours in air. The XRF results of the IS roast are

shown below, compared to that of the unroasted IS material (Table 3.13). No large differences were noticed in the XRF results, as expected for a roast. The LOI value has become positive, due to mass being lost in the roasting process. This indicated the oxidation of the elements in the IS material during roasting, as the unroasted IS took on oxygen during the XRF experiment, as demonstrated by the negative LOI value.

Table 3.13. *XRF major oxide analysis results for IS and IS roast (3 hr, 900 °C). Values are expressed as weight % on oven dried (110°C) basis. LOI = loss on ignition at 1000°C. Negative LOI indicates positive mass gain due to oxidation. Values for SO_3 and P_2O_5 have been omitted due to low value (<0.1).*

Sample	Fe_2O_3	MnO	TiO_2	CaO	SiO_2	Al_2O_3	MgO	V_2O_5	LOI	SUM
IS	84.7	0.73	7.8	0.4	1.61	3.89	2.68	0.58	-3.26	99.38
IS Roast	82.43	0.71	7.87	0.04	1.66	3.2	2.66	0.45	0.39	99.49

The XRD pattern displayed one major sets of reflections, due to Hematite (Figure 3.46). This indicatedthat the TTM converted into Hematite during the roasting process. The minor reflections in the pattern were found to be due to Pseudobrookite. This agreed well with the roasting of the VRC material, as Hematite and Pseudobrookite were found to be produced. No reflections indicated the presence of Mn, Ca, Si, Al, Mg, or V, so the EDS of the roasted material must be considered in order to locate these elements.

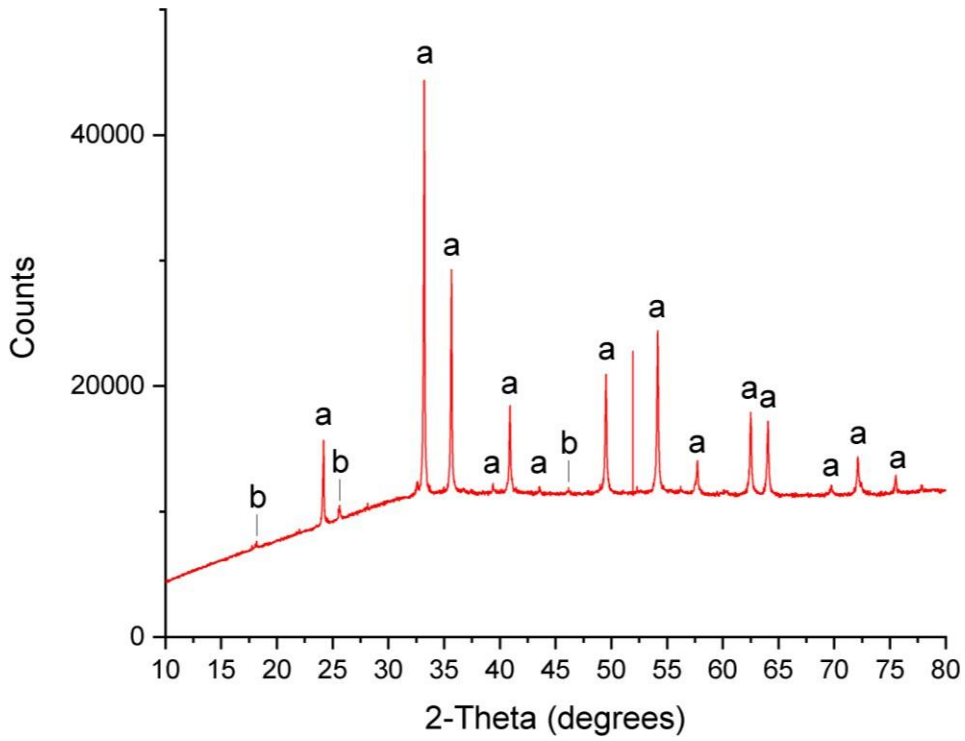

Figure 3.46. *XRD pattern of the IS after roasting at 900 °C for 3 hr, with major reflections labelled a) Hematite Fe_2O_3 b) Pseudobrookite Fe_2TiO5.*

The EDS results are shown below (Figure 3.47). The EDS colour map indicated that the major phase was a Fe and Ti containing phase (Figure 3.47.a, red and green). A point analysis was conducted on one of these particles, and it was assinged as a Ti-containing Hematite phase, as the Pseudobrookite phase was minor in the XRD. There were also regions containing mostly Fe, due to particles of Hematite (EDS point 2). Analysis of the colour maps indicated the presence of Si-rich regions(Figure 3.47.b, green). Previously, the 8M and conc. HCl leaching residue analyses were used to determine the nature of these phases. As no such leaching was conducted on this sample, one cannot say with confidence what these regions were. Likewise, there appeared regions of a Ca-rich phase (Figure 3.47.b, blue), as well as both Si and Ca containingphases (Figure 3.47.b, cyan).

Nevertheless, the most relevant result of this analyses was the presence of a V and Mn containing phase (Figure 3.48.a, blue, and EDS point 3). This particle seemed reminiscent of the manganese vanadate found in the VRC material, which was widespread in the VRC roast. The Mn:V ratio in this particle was approximately 5:6, and while this was not the 2:3 ratio found in the VRC roast, these values were comparable. For this reason, the particle was assigned as manganese vanadate. Importantly, only one small particle of this phase was located in the EDS analysisof this material. A higher magnification image of this region is presented in Figure 3.48.

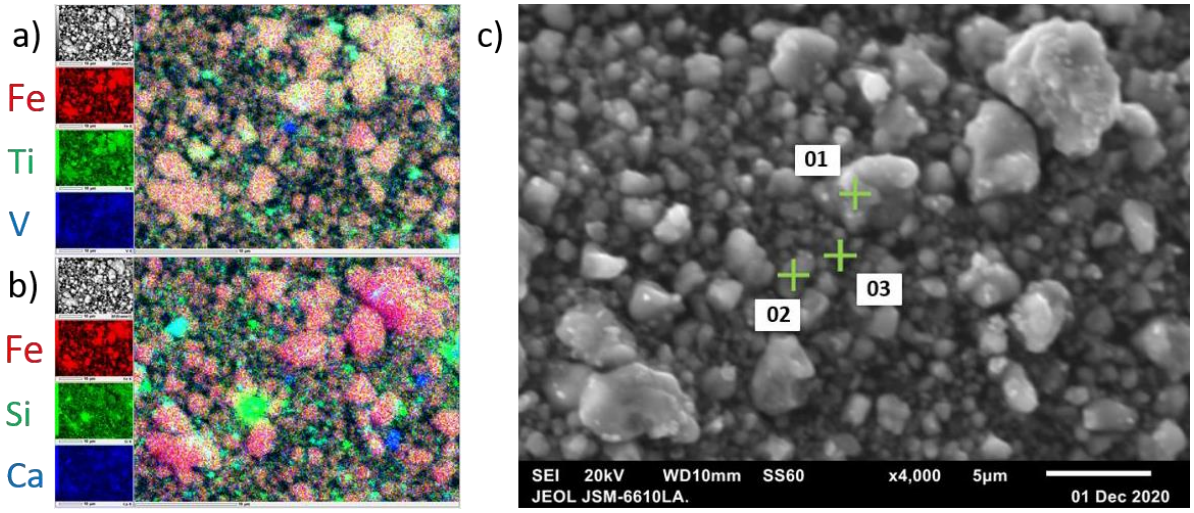

EDS Point	EDS Data for Element						Mineral Phase
	Fe	**Ti**	**V**	**O**	**Mn**	**Mg**	
1	46.26	5.11	0.47	44.71	0.44	3.02	Ti-containing Hematite
2	43.84	2.75	0.28	50.76	0.43	1.94	Hematite
3	11.23	1.63	14.41	59.09	12.04	1.60	Manganese vanadate

Figure 3.47. *SEM maps of IS roast (3 hr, 900 °C). a) elemental colour map (red: Fe, green: Ti, blue: V) b) elemental colour map (red: Si, green: Ca, blue: V) c) corresponding SEM image at x4000 with EDS points labelled. Table shows the mineral phases assigned to each EDS point, and the raw EDS data for each of the major elements in atomic% (rescaled to 100 %).*

The EDS image below shows a higher-magnification image of the V and Mn containing particle. The Mn:V ratio of the particle in the EDS point spectrum was still approximately 5:6. A small amount of Fe was also present in this analysis, but it is not known whether this was present in the mineral phase of this particle, an exclusion on the surface of the particle, or if the EDS spot was including a neighbouring particle. Additionally, the size of this particle was small, requiring a high-magnification image to analyse, and in this case was approaching the focal limit of the EDS instrumentation. Regardless,one should hope to see an increase in the leaching rate of V from the roasted sample if this phase was present in the roast in any significant amount.

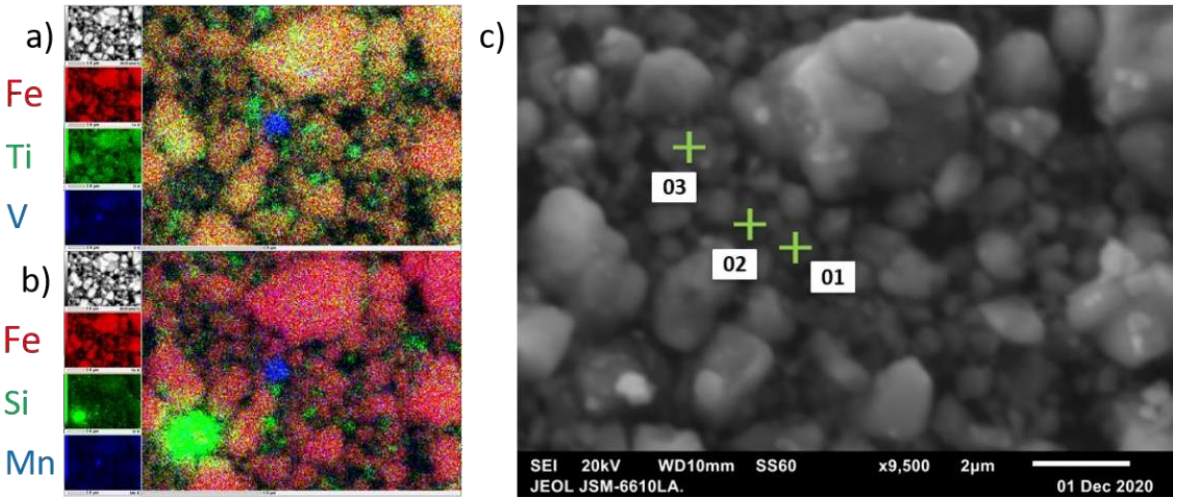

EDS Point	EDS Data for Element					Mineral Phase
	Fe	Ti	V	O	Mn	
1	11.27	1.50	14.38	61.08	11.77	Manganese vanadate
2	22.32	7.88	0.76	68.63	0.42	Pseudobrookite
3	33.13	3.33	0.25	62.99	0.30	Hematite

Figure 3.48. *SEM maps of IS roast (3 hr, 900 °C). a) elemental colour map (red: Fe, green: Ti, blue: V) b) elemental colour map (red: Si, green: Ca, blue: V) c) corresponding SEM image at x9500 with EDS points labelled. Table shows the mineral phases assigned to each EDS point, and the raw EDS data for each of the major elements in atomic% (rescaled to 100 %).*

3.3.4 Leaching of Roasted Sample

To determine the effect of roasting on the leaching behaviour of the IS, the material was leached with 4M HCl (120 min, 80 °C), and compared to the leaching of the unroasted material. The results are shown below (Figure 3.49). It is worth restating that the Ti leaching results were due to TiO_2 precipitation during the roasting experiment.

Generally, the leaching rate of each element (Fe, Ti, and V) decreased after the roasting procedure. This was because roasting of the IS formed more HCl-resistant phases (Pseudobrookite).The total % amount leached during the unroasted experiment was approximately 64 %, and this dropped to approximately 10 % for Fe and Ti after roasting. The most important difference was the V leaching curve after roasting. In the unroasted leaching, the V curve followed the Fe curve (no difference in leaching rate), which indicated that the V was locked up in the ferrous mineral. After roasting the V curve did not follow the Fe curve. In fact, the % amount extracted after roasting, while still much lower than the unroasted leaching, was ~30 %, compared to the ~10 % result for Fe and Ti.

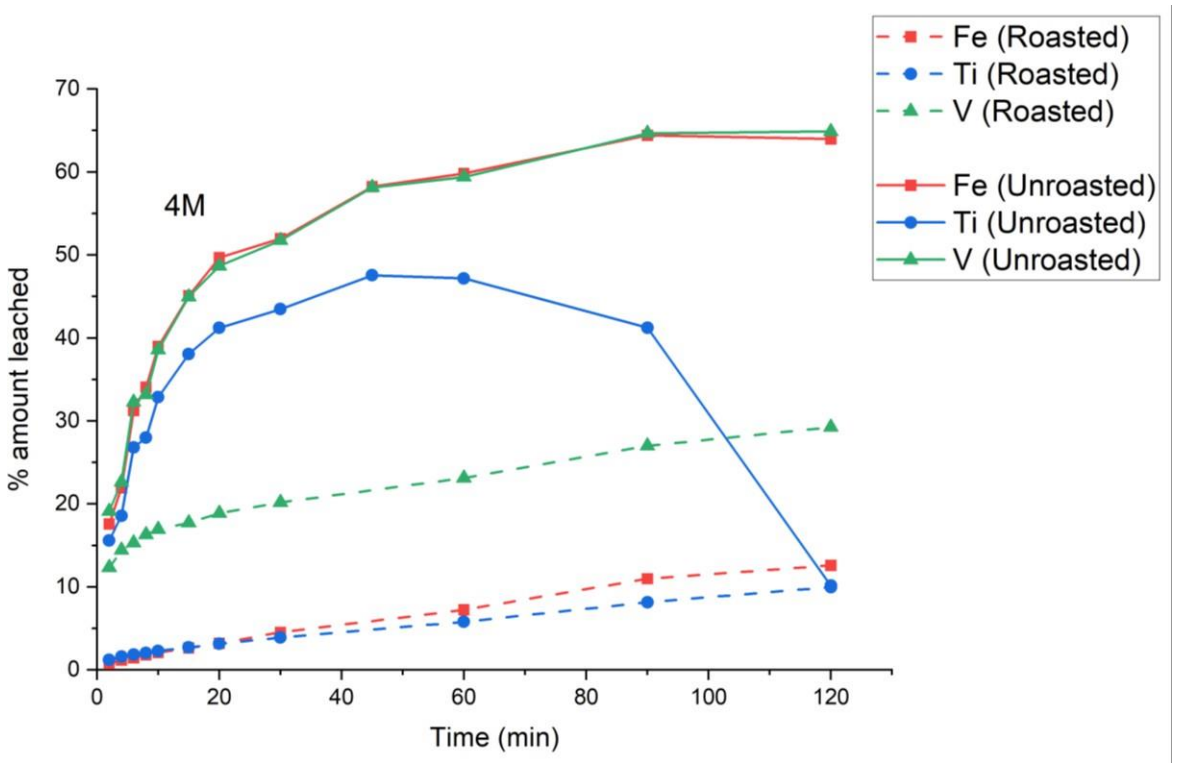

Figure 3.49. *4M HCl Leaching of roasted IS over time, compared to the 4M leaching of the unroasted material. The % amount leached is the moles of element leached compared to the moles of element in initial solid material.*

While the V leaching curve didn't follow the Fe curve, it did takeon roughly the same slope after the first few minutes. This was crucial, as it indicated that the V leached over the first few minutes was not bound in the Fe mineral phase, which was further evidenced by the steeper incline in the first few minutes. After this, the V was leached at the same rate as Fe, showing thatthis portion of V was found in the ferrous mineral phase. During the analysis of the roasted IS material, a smallamount of V and Mn containing mineral was found and assigned as a manganese vanadate. It was the presence of this phase which explained the above leaching results, as well as the shape and location of the leaching curve; one should expect this phase to be leached quickly, as in the case of the VRC leaching experiments. One should also expect to find V to still be present to some extent in the XRF results, andfurthermore, one should consider ways to optimise the partitioning of V from Fe in future roast experiments.

To complete the analysis of the roasting results, the leaching residue is considered. The XRF results showed the selective leaching of V from the roasted material (Table 3.14), as this was one of the only elements which decreased in weight % in the XRF results (along with Al). All other elements in the residue were either equal in weight % to the roasted starting material, or greater, indicating less leaching as compared to V. The value for Mn was equal to that of the roasted starting material, indicating some amount of leaching.

Table 3.14. *XRF major oxide analysis results for IS roast (3 hr, 900 °C) and its 4M HCl leaching residue. Values are expressed as weight % on oven dried (110°C) basis. LOI = loss on ignition at 1000°C. Values for SO_3, Na_2O, P_2O_5, and K_2O have been omitted due to low value (<0.08).*

Sample	Fe_2O_3	MnO	TiO_2	CaO	SiO_2	Al_2O_3	MgO	V_2O_5	LOI	SUM
IS Roast	82.06	0.71	7.55	0.38	1.57	3.43	2.61	0.58	0.25	99.29
IS 4M Leaching Residue	82.43	0.71	7.87	0.04	1.66	3.2	2.66	0.45	0.39	99.49

To continue the analysis of the leaching residue, the XRD was analysed (Figure 3.50). There appeared to be no difference between this pattern and that of the roasted IS starting material. The main phase was still Hematite, and minor reflections for Pseudobrookite were found. Still no evidence for the other minor elements were found in this pattern, so the EDS was considered.

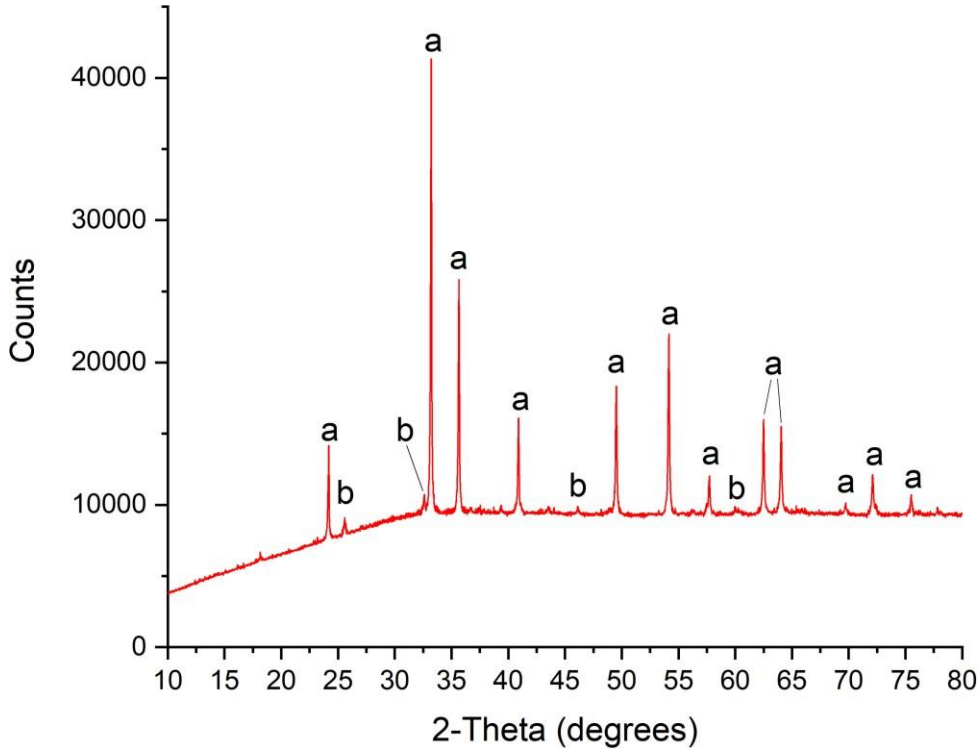

Figure 3.50. *XRD pattern of the residue after leaching of the roasted IS in 4M HCl, with major reflections labelled a) Hematite, Fe_2O_3 b) Pseudobrookite, Fe_2TiO5.*

The EDS colour maps with corresponding SEM image is shown below (Figure 3.51). The colour maps indicated the predominance of a Fe-containing phase, which was assigned to Hematite,as per the XRD results. (Figure 3.51.a and b, red). Some regions of Fe and Ti phase were also present, due to Pseudobrookite (Figure 3.51.a, red and green). Regions of Si-rich material were also found, which

were likely SiO_2. No evidence of SiO_2 was found in the XRD, so this assignment was unconfirmed. A region of interest was found in the lower right portion of the SEM image, where multipleparticles were stuck together. A higher magnification analysis of this particle shown in the green box was conducted, shown in Figure 3.52. below.

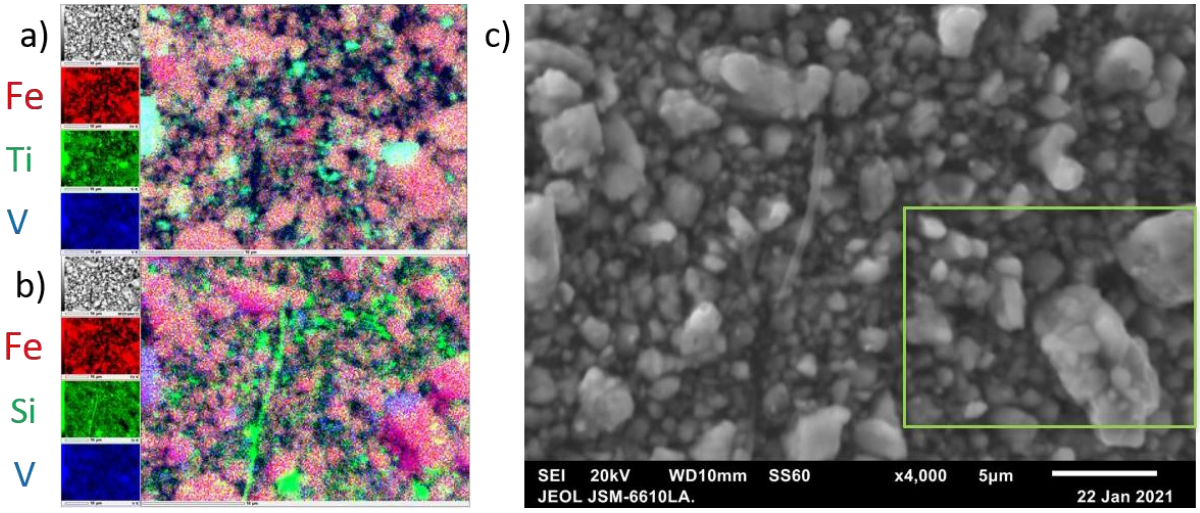

Figure 3.51. *SEM maps of residue after leaching IS roast (3 hr, 900 °C) with 4M HCl. a) elemental colour map (red: Fe, green: Ti, blue: V) b) elemental colour map (red: Fe, green: Si, blue: V) c) corresponding SEM image at x4000.*

Two main phases were found to be present in the higher magnification EDS image. The first of this was a Fe containing phase, assigned as Hematite (EDS point 1). The second was a Fe- and Ti-containingphase, assigned as Pseudobrookite (EDS point 2). The cluster of particles were mostly Hematite, with some Pseudobrookite near the top. No evidence of a Mn and Vcontaining phase was found in the EDS analysis of this material, and this was taken as an indicationthat any amount of this phase present was leached during the experiment. Based on theEDS colour map, it appeared that the remaining V found in the mineral was found within the Pseudobrookite phase.

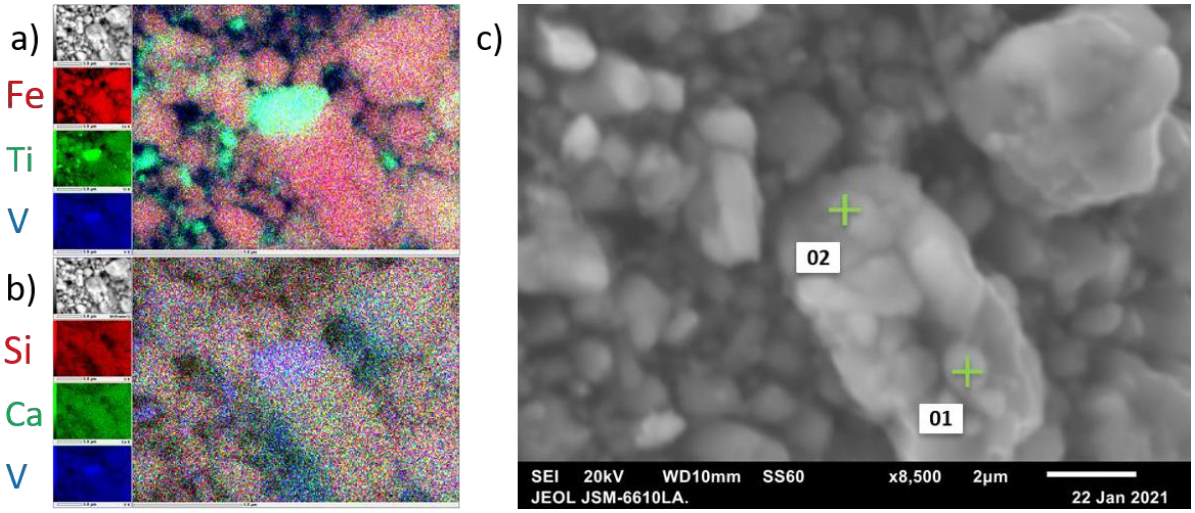

EDS Point	EDS Data for Element					Mineral Phase
	Fe	**Ti**	**V**	**O**	**Mn**	
1	38.49	3.11	0.23	57.89	0.28	Hematite
2	24.68	9.05	0.36	65.49	0.43	Pseudobrookite

Figure 3.52. *SEM maps of residue after leaching IS roast (3 hr, 900 °C) with 4M HCl. a) elemental colour map (red: Fe, green: Ti, blue: V) b) elemental colour map (red: Si, green: Ca, blue: V) c) corresponding SEM image at x8500 with EDS points labelled. Table shows the mineral phases assigned to each EDS point, and the raw EDS data for each of the major elements in atomic% (rescaled to 100%).*

Summary

The IS material was roasted, which formed a main phase of Hematite and a minor phase of Pseudobrookite from the original TTM phase. A small particle of Mn- and V-rich mineral was found and assigned to the same manganese vanadate phase formed in the VRC roast. This roastedIS material was leached with 4M HCl, and it was found that the leaching rate and % amount leachedfor Fe, Ti, and V decreased compared to the unroasted material, due to the formation of HCL-resistant phases during roasting. Notably, the V % amount leached was higherthan that for the other elements. For Fe and Ti, the value dropped from ~64 % to ~10 %, whereas the relative value for V was ~30 %. This indicated the selective leaching of V over Fe and Ti, and due to the shape of the leaching curve, it was found that this was due to the formation of a new V phase which was highly sensitive to HCl. This was assumed to be the manganese vanadate phase formed during roasting, and observed for the roasts of the VRC. In future experiments, the formation of any vanadate phase should be encouraged by millingand prolonged roasting

4 Conclusions

This study explored the potential for extracting V from two materials: VRC and IS. The extraction was conducted with an HCl leach, for 120 min at 80 °C, and at a range of HCl concentrations.

The main component of the VRC was found to be Jacobsite. with minor components of Ilmenite, Cristobalite, Rhodonite, Olivine, and TiO_2. The elemental composition of the material showed similarities with VRC materials studied elsewhere, with the exception of the richness of Mn in the VRC investigated. Of particular note was the presence of a small amount of a Mn and V rich phase, which was identified as a manganese vanadate, $Mn_2V_2O_7$. The VRC material was leached at a range of HCl concentrations, and no selective dissolution of V was observed. As the concentration of HCl was increased, a higher degree of extraction was observed. The spinel phases (Jacobsite, TTM) were selectively leached over the other phases, including TiO_2, SiO_2, Augite, and Rhodonite. In these results, no way to separate the Fe, Ti, and V was found using direct HCl leaching. An attempt was made to precipitate Fe and Ti while leaving V in solution, and this was found to be unsuitable for V extraction, as the V co-precipitated.

Two sets of VRC roasts were produced, one at 900 ℃ for 3-hr, and the other at 1200 ℃ overnight. No noticeable difference could be found in their XRD pattern, XRF data, or EDS maps. The main phases of the VRC were converted into Hematite, Pseudobrookite, Rutile and Mn_2O_3 upon roasting. Importantly, the existence of a manganese vanadate, $Mn_2V_2O_7$, was demonstrated. During the roasting process, V and Mn partitioned from the Ti and Fe and formed this phase. The roasts were also leached in HCl, and a dramatic increase in the extraction of V after roasting was observed, while the relative extraction of Fe and Ti decreased. This was due to the formation of the acid-sensitive $Mn_2V_2O_7$, and the acid-resistant Pseudobrookite. These results provide a clear pathway for the selective extraction of the V from the VRC material: roasting at ~1000 °C, followed by leaching with HCl at a concentration around 4M. However, some amount of Ti and Fe was extracted also, so further purification is required.

The leaching and roasting experiments were repeated with the IS material. The composition of this material was found to be mainly TTM, with minor amounts of Hematite, SiO_2, and Augite. It was found that the V was present in a very small relative amount in this material. The IS material was leached in HCl, and no considerable difference was found in the leaching rate or amount for Fe, Ti, or V. This indicated that there is no way to separate the V from the Fe and Ti by direct leaching. In the 4M experiment, Ti precipitation was found to take place. The IS was roasted at 900 ℃ for 3 hours in air forming Hematite and Pseudobrookite. A small particle of a manganese vanadate phase was also found. Upon leaching, it was found that the % amount leached for Fe, Ti, and V had decreased. Significantly, the percentage of V leached was higher than that for the other elements. This provided evidence of a pathway fo V extraction from the original IS material.

5 Future Directions

Before moving the research in this thesis onto larger scale with the intention of testing these results for industry, some important factors need to be considered. While this thesis provides a significant key result (a method of selectively extracting the V from these materials) a few questions remain. First, it is not known what species the Fe, Ti, and V are in solution after being leached from the solid material. This can be further understood via solution-based analysis of the leachates, such as UV-vis spectroscopy.

A high-resolution identification of the present phases and how they are arranged in the material can be considered for future research in this area, to better understand the dissolution of the mineral phases, and the formation of new phases. A better understanding of the mineral phases present in the material will aid in the fine-tuning of any potential industrial processes based on these results.

5.1 Further Separation of V

In this research, the vanadium was successfully extracted from the VRC with a leaching efficiency of 86.89 % after roasting at 900 °C for 3 hours. However, V was coextracted with a majority of the Mn from the original material. In order to bring a product to market, it would be most efficient to produce a puresingle-element product, such as V_2O_5 or MnO_2. To this end, a future research direction for this thesis should be an attempt at separating the V and Mn from the leachate into their pure elemental components.

Further to this, small amounts of Fe and Ti were also extracted during the HCl leaching process. A line of future research should include the optimisation of the roasting and leaching procedures to minimise this unwanted extraction. A post-leaching treatment of the leachate should also be considered to purify the V from the Fe and Ti impurities.

5.2 Combination with H_2 Reduction

As the NZ steel industry seeks to move away from coal as its main source of reductant, in order to work toward the national goal of carbon net-neutrality by 2050, the capacity for H_2 to replace coal with another source of reduction is being extensively researched. This is a goal of the co-supervisor of this thesis, Dr. Chris Bumby.[81] In the H_2 reduction process, the VRU process will still be applicable and will generate a VRC slag. The results of this thesis should be replicated with this material, as it may contain different phases or impurities which will need to be considered.

6 References

1. Christie, T.; Brathwaite, B. *Mineral Commodity Report 15 — Iron*; Institute of Geological and Nuclear Sciences Ltd; **2006**.

2. Orpin, A.; Bostock, H.; Nodder, S.; Barnes, P.; Lamarche, G. In *Resource evaluation, exploration and current prospecting interests of west coast ironsands, North Island, New Zealand*, 2009.

3. Lawton, D. C.; Hochstein, M. P., Geophysical study of the Taharoa ironsand deposit, west coast, North Island, New Zealand. *New Zealand journal of geology and geophysics* **1993,** *36* (2), 141-160.

4. Baker, E.; Gaill, F.; Karageorgis, A.; Lamarche, G.; Narayanaswamy, B.; Parr, J.; Raharimananirina, C.; Santos, R.; Sharma, R., Chapter 23. Offshore Mining Industries. 2014; pp 1-25.

5. Carter, L., Ironsand in continental shelf sediments off western New Zealand—a synopsis. *New Zealand Journal of Geology and Geophysics* **1980,** *23* (4), 455-468.

6. Wang, Z.; Pinson, D.; Chew, S.; Rogers, H.; Monaghan, B. J.; Zhang, G., Interaction of New Zealand Ironsand and Flux Materials. *ISIJ international* **2016,** *56* (8), 1315-1324.

7. Martin, W. R. B., The iron and titanium ores of New Zealand: Occurrence, composition, attempts to use and status today with special reference to ironsands. *New Zealand engineering* **1955,** *10* (10), 317-336.

8. Thorp, D.; Cutten, C. W.; MacArthur, N. A.; Griffiths, S. J. *Ironsand Concentration Processes At New Zealand Steel Limited*

9. Ingram, J.; La Roche, J., Steel from Ironsand. In *Evolving Auckland*, Wily Publications: 2011; pp 245-261.

10. Hogan, D.; Williamson, B., In *New Zealand is different: chemical milestones in New Zealand history*, Clerestory: Christchurch, 1999; p 261.

11. Pearce, C. I.; Henderson, C. M. B.; Telling, N. D.; Pattrick, R. A. D.; Vaughan, D. J.; Charnock, J. M.; Arenholz, E.; Tuna, F.; Coker, V. S.; Laan, G. v. d., Iron site occupancies in magnetite-ulvospinel solid solution: A new approach using XMCD. *The American mineralogist* **2009**. (LBNL-3328E; Journal ID: ISSN 0003-004X; AMMIAY; TRN: US1004573), Medium: ED.

12. Beckett-Brown, C. E.; McDonald, A. M., The crystal-chemistry of Ni-bearing spinel-group minerals; chemical, geological, and exploration implications. *Canadian mineralogist* **2018,** *56* (1), 77-94.

13. Lujan Ganuza, M.; Ferracutti, G.; Gargiulo, M. F.; Castro, S. M.; Bjerg, E.; Groller, E.; Matkovic, K., The Spinel Explorer-Interactive Visual Analysis of Spinel Group Minerals. *IEEE transactions on visualization and computer graphics* **2014,** *20* (12), 1913-1922.

14. Xue, Z.; Shen, Y.; Chu, L.; Wang, Y.; Zhang, Y.; Sun, Z.; Wang, J.; Zeng, Y.; Li, P.; Zhu, S., NaCl- induced nickel- cobalt inverse spinel structure for boosting hydrogen evolution from ethyl acetate and water. *Journal of materials chemistry. A, Materials for energy and sustainability* **2019,** *7*

(4), 1700-1710.

15. Santos-Carballal, D.; Roldan, A.; Grau-Crespo, R.; de Leeuw, N. H., First-principles study of the inversion thermodynamics and electronic structure of FeM2X4 (thio) spinels (M = Cr, Mn, Co, Ni; X = O, S). **2015**. *Physical Review B* 91 (19) , 195106.

16. Okube, M.; Oshiumi, T.; Nagase, T.; Miyawaki, R.; Yoshiasa, A.; Sasaki, S.; Sugiyama, K., Site occupancy of Fe 2+ , Fe 3+ and Ti 4+ in titanomagnetite determined by valence-difference contrast in synchrotron X-ray resonant scattering. *Journal of synchrotron radiation* **2018,** *25* (Pt 6), 1694.

17. Gilligan, R.; Nikoloski, A. N., The extraction of vanadium from titanomagnetites and other sources. *Minerals engineering* **2020,** *146*, 106106.

18. Li, R.; Liu, T.; Zhang, Y.; Huang, J.; Xu, C., Efficient Extraction of Vanadium from Vanadium-Titanium Magnetite Concentrate by Potassium Salt Roasting Additives. *Minerals (Basel)* **2018,** *8* (1), 25.

19. Fischer, R. P., *Vanadium resources in titaniferous magnetite deposits*. U.S. Govt. Print. Off.: Washington, **1975**.

20. Sharp, R. M.; Cann, N. K.; McFadzean, D., NZ's Iron and Steel Industry - an Historical Perspective. *New Zealand engineering* **1990,** *45* (4), 9-15.

21. Ingram, J. H., Pioneering a Process (The Development of New Zealand Steel Limited's Unique Iron/Steel Making Process*). Institution of Engineers*, Australia: Barton, ACT, **1988**; pp i-xi.

22. Steel, N. THE IRONMAKING PROCESS. https://www.nzsteel.co.nz/new-zealand-steel/the-story-of-steel/the-science-of-steel/the-ironmaking-process/. (accessed 2020-09-11).

23. Henley, R. G.; Chubb, T.; Graham, C., The Commissioning, Operation and Development of the Vanadium Recovery Unit at NZ Steel. Chemical Engineering Group (New Zealand): Auckland, N.Z, 1990; pp 207-214.

24. Petranikova, M.; Tkaczyk, A. H.; Bartl, A.; Amato, A.; Lapkovskis, V.; Tunsu, C., Vanadium sustainability in the context of innovative recycling and sourcing development. *Waste management* **2020,** *113*, 521-544.

25. Wanty, R. B.; Goldhaber, M. B., A method for the determination of vanadium and iron oxidation states in naturally occurring oxides and silicates. *Talanta* **1985,** *32* (5), 395-398.

26. Sweatman, W.; Wake, G.; Fullard, L.; Bruna, M., Recovering vanadium during the production of steel from iron sand. *ANZIAM Journal* **2012,** *53*, 1.

27. Treviño, S.; Díaz, A.; Sánchez-Lara, E.; Sanchez-Gaytan, B. L.; Perez-Aguilar, J. M.; González-Vergara, E., Vanadium in Biological Action: Chemical, Pharmacological Aspects, and Metabolic Implications in Diabetes Mellitus. *Biological Trace Element Research* **2019,** *188* (1), 68-98.

28. Langeslay, R. R.; Kaphan, D. M.; Marshall, C. L.; Stair, P. C.; Sattelberger, A. P.; Delferro,M., Catalytic Applications of Vanadium: A Mechanistic Perspective. *Chemical reviews* **2019,** *119* (4),2128-2191.

29. Henry, E. R., Researches on Vanadium. Part II. *Philosophical transactions of the Royal Society*

of London **1869,** *159*, 679-692.

30. Pourret, O.; Dia, A., Vanadium. In *Encyclopedia of Geochemistry*; W. M. White. Ed; Springer, **2016**;

31. Bauer, G.; Güther, V.; Hess, H.; Otto, A.; Roidl, O.; Roller, H.; Sattelberger, S.; Köther-Becker, S.; Beyer, T., *Vanadium and Vanadium Compounds*. Ullmann's Encyclopedia of Industrial Chemistry, 2017.

32. Costigan, M.; Cary, R.; Dobson, S.; World Health, O.; International Programme on Chemical, S., Vanadium pentoxide and other inorganic vanadium compounds. World Health Organization: Geneva, 2001.

33. Christopher, W. W., The Road to the Model T: Culture, Road Conditions, and Innovation at the Dawn of the American Motor Age. *Technology and culture* **2007,** *48* (3), 497-523.

34. Baker, M. J., Ford: how the model T revolutionised an industry. In *The Business & Management Collection, Henry Stewart Talks*;. **2018**; https://hstalks.com/bm/3728/ (accessed 2020-011-23)

35. Skyllas-Kazacos, M.; Cao, L.; Kazacos, M.; Kausar, N.; Mousa, A., Vanadium Electrolyte Studies for the Vanadium Redox Battery—A Review. *ChemSusChem* **2016,** *9* (13), 1521-1543.

36. Choi, C.; Kim, S.; Kim, R.; Choi, Y.; Kim, S.; Jung, H.-y.; Yang, J. H.; Kim, H.-T., A review of vanadium electrolytes for vanadium redox flow batteries. *Renewable & sustainable energy reviews* **2017,** *69*, 263-274.

37. Cunha, Á.; Martins, J.; Rodrigues, N.; Brito, F. P., Vanadium redox flow batteries: a technology review. *International Journal of Energy Research*, **2015,** *39* (7), 889-918.

38. Liu, Z.; Zhang, Y.; Dai, Z.; Huang, J.; Liu, C., Coextraction of vanadium and manganese from high-manganese containing vanadium wastewater by a solvent extraction-precipitation process. *Frontiers of Chemical Science and Engineering* **2020,** *14* (5), 902-912.

39. Cai, Z.; Feng, Y.; Li, H.; Zhou, Y., Selective Separation and Extraction of Vanadium(IV) and Manganese(II) from Co-leaching Solution of Roasted Stone Coal and Pyrolusite via Solvent Extraction. *Industrial & Engineering Chemistry Research* **2013,** *52* (38), 13768-13776.

40. Wen, J.; Jiang, T.; Sun, H.; Yu, T., Novel Understanding of Simultaneous Extraction of Vanadium and Manganese from Vanadium Slag and Low-Grade Pyrolusite Based on Selective Oxidation–Reduction Roasting. *ACS Sustainable Chemistry & Engineering* **2020,** *8* (15), 5927-5936.

41. Smith, J. F.; Carlson, O. N., The Mn−V (Manganese-Vanadium) system. *Journal of Phase Equilibria* **1982,** *2* (4), 473-478.

42. Schwarz, B.; Forster, J.; Goetz, M. K.; Yücel, D.; Berger, C.; Jacob, T.; Streb, C., Back Cover: Visible-Light-Driven Water Oxidation by a Molecular Manganese Vanadium Oxide Cluster (Angew. Chem. Int. Ed. 21/2016). *Angewandte Chemie (International ed.)* **2016,** *55* (21), 6344-6344.

43. Dobley, A.; Ngala, K.; Yang, S.; Zavalij, P. Y.; Whittingham, M. S., Manganese Vanadium Oxide Nanotubes: Synthesis, Characterization, and Electrochemistry. *Chemistry of Materials* **2001,** *13* (11), 4382-4386.

44. Abbood, H. A.; Abbood, H. A.; Ahmed, K. A. M.; Ahmed, K. A. M.; Ren, Y.; Ren, Y.; Huang, K.; Huang, K., MnV2O6·V2O5 cross-like nanobelt arrays: synthesis, characterization and photocatalytic properties. *Applied Physics A* **2013,** *112* (4), 901-909.

45. Zoellner, B.; Gordon, E.; Maggard, P. A., A small bandgap semiconductor, p-type MnV2O6, active for photocatalytic hydrogen and oxygen production. *Dalton Transactions* **2017,** *46* (32), 10657-10664.

46. Chuan-Cang, Z.; Fa-Min, L.; Peng, D.; Lu-Gang, C.; Wen-Wu, Z.; Huan, Z., Synthesis, structure and antiferromagnetic behaviour of brannerite MnV2O6. *Chinese physics B* **2010,** *19*, 067503.

47. Viegas, J. s. I.; Moreira, R. L.; Dias, A., Polymorphism and Optical–Vibration Properties of MnV2O6·nH2O (n = 0, 2, 4) Prepared by Microwave Irradiation. *Crystal growth & design* **2019,** *19* (6), 3233-3243.

48. Liao, J. H.; Leroux, F.; Piffard, Y.; Guyomard, D.; Payen, C., Synthesis, Structures, Magnetic Properties, and Phase Transition of Manganese(II) Divanadate: Mn2V2O7. *Journal of Solid State Chemistry* **1996,** *121* (1), 214-224.

49. Krasnenko, T. I.; Zhuravlev, N. A.; Rotermel, M. V., Stabilizing the triclinic structure of Mn2V2O7 via isovalent cationic substitution. *Bulletin of the Russian Academy of Sciences. Physics* **2013,** *77* (3), 246-248.

50. Knowles, K. M.; Vickers, M. E.; Sil, A.; Han, Y. H.; Jaffrenou, P., X-ray powder diffraction and electron diffraction studies of the thortveitite-related L phase, (Zn,Mn)2V2O7. *Acta crystallographica. Section B, Structural science* **2009,** *65* (2), 160-166.

51. Yan, Q.; Li, G.; Newhouse, P. F.; Yu, J.; Persson, K. A.; Gregoire, J. M.; Neaton, J. B., Mn2V2O7: An Earth Abundant Light Absorber for Solar Water Splitting. *Advanced energy materials* **2015,** *5* (8), 1401840.

52. Li, M.; Zheng, S.; Liu, B.; Wang, S.; Dreisinger, D. B.; Zhang, Y.; Du, H.; Zhang, Y., A Clean and Efficient Method for Recovery of Vanadium from Vanadium Slag: Nonsalt Roasting and Ammonium Carbonate Leaching Processes. *Mineral processing and extractive metallurgy review* **2017,** *38* (4), 228-237.

53. Ellingham, S. T. D.; Thompson, T. J. U.; Islam, M., Scanning Electron Microscopy–Energy-Dispersive X-Ray (SEM/EDX): A Rapid Diagnostic Tool to Aid the Identification of Burnt Bone and Contested Cremains. *Journal of forensic sciences* **2018,** *63* (2), 504-510.

54. Newbury, D. E.; Ritchie, N. W. M., Is Scanning Electron Microscopy/Energy Dispersive X-ray Spectrometry (SEM/EDS) Quantitative? *Scanning* **2013,** *35* (3), 141-168.

55. Wolfgong, W. J., Chapter 14 - Chemical analysis techniques for failure analysis: Part 1, common instrumental methods. Elsevier Ltd: **2016**; pp 279-307.

56. Konopka, J. F., Quantitative Analysis of Oxygen in Metal Oxides with SEM/EDS by Direct Measurement of all X-ray Peaks. 2012; Vol. **2012**, pp V23C-2831.

57. Goldstein, J. I.; Newbury, D. E.; Michael, J. R.; Ritchie, N. W. M.; Scott, J. H. J.; Joy, D. C.,

Scanning Electron Microscopy and X-Ray Microanalysis. 4th ed. 2018. ed.; Springer New York: New York, NY, **2018**.

58. Chen, P., *Table of key lines in x-ray powder diffraction patterns of minerals in clays and associated rocks*. Dept. of Natural Resources: Bloomington, Ind, **1977**.

59. Shinoda, K.; Matsubara, E.; Waseda, Y., *X-Ray Diffraction Crystallography: Introduction, Examples and Solved Problems*. 1. Aufl. ed.; Springer-Verlag: Berlin, Heidelberg, **2011**.

60. Nijenhuis, J. t.; Gateshki, M.; Fransen, M. J., Eleventh European Powder Diffraction Conference. In *Possibilities and limitations of X-ray diffraction using high-energy X-rays on a laboratory system*, Oldenbourg Wissenschaftsverlag: **2015**; pp 163-170.

61. Dzubay, T. G., *X-ray fluorescence analysis of environmental samples*. Ann Arbor Science Publishers: Ann Arbor, Mich, **1977**, 310, pp 324-325.

62. Marguí, E.; Grieken, R. v., *X-ray fluorescence spectrometry and related techniques : an introduction*. Momentum Press: New York, New York, **2013**.

63. Thomas, R., *Practical guide to ICP-MS a tutorial for beginners*. 3rd ed. ed.; Taylor & Francis: Boca Raton, **2013**.

64. Kustel, G., *Roasting of gold and silver ores : and the extraction of their respective metals without quicksilver*. New ed. ed.; A.J. Leary: San Francisco, **1880**.

65. Ingraham, T. R.; Kerby, R., Roasting in extractive metallurgy a thermodynamic and kinetic review. *Canadian Metallurgical Quarterly* **1967,** *6* (2), 89-119.

66. Wen, J.; Jiang, T.; Xu, Y.; Cao, J.; Xue, X., Efficient extraction and separation of vanadium and chromium in high chromium vanadium slag by sodium salt roasting-(NH4)2SO4 leaching. *Journal of industrial and engineering chemistry (Seoul, Korea)* **2019,** *71*, 327-335.

67. Hebei Iron and Steel Co Ltd, Chengde Branch Applies for Patent on Method for Extracting Vanadium from Vanadium Solution Through Vanadium Slag Sodium Salt Roasting Vanadium Extraction Process. *Global IP News. Chemical Patent News* **2016**.

68. Zheng, H.; Zhang, W.; Guo, Y.; Gao, Q.; Shen, F., Transformation of Vanadium-Bearing Titanomagnetite Concentrate in Additive-Free Roasting and Alkaline-Pressure Leaching for Extracting Vanadium (V). *Minerals (Basel)* **2019,** *9* (3), 197.

69. Sedneva, T.; Lokshin, E.; Gromov, P.; Kopkova, E.; Shchelokova, E., Decomposing the Titaniferous Magnetite Concentrate with Hydrochloric Acid. *Theoretical Foundations of Chemical Engineering* **2011,** *45*, 753-763.

70. Zhang, A.; Monaghan, B.; Longbottom, R.; Nusheh, M.; Bumby, C., Reduction Kinetics of Oxidized New Zealand Ironsand Pellets in H2 at Temperatures up to 1443 K. *Metallurgical and Materials Transactions B* **2020,** *51*, 492-504.

71. Kasia, P., TIVAN extraction process underpins TNG project. *Industrial Minerals* **2013**.

72. Ondrey, G., A new metals-recovery process moves to the pilot scale. *Chemical engineering* **2014,** *121* (12), 12.

73. Wilson, A. M.; Bailey, P. J.; Tasker, P. A.; Turkington, J. R.; Grant, R. A.; Love, J. B., Solvent

extraction: the coordination chemistry behind extractive metallurgy. *Chemical Society Reviews***2014,** *43* (1), 123-134.

74. Yang, F.; Li, X.; Han, L.; Gao, F.; He, C.; Wei, Y., Solvent Extraction of Vanadium from Sodium Carbonate–Sodium Bicarbonate Solution Using Aliquat-336. *Mining, Metallurgy & Exploration* **2020,** *37* (5), 1667-1672.

75. Liu, F.; Ning, P.-G.; Cao, H.-B.; Zhang, Y., Measurement and modeling for vanadium extraction from the (NaVO3+H2SO4+H2O) system by primary amine N1923. *The Journal of chemical thermodynamics* **2015,** *80*, 13-21.

76. Ye, G.; Hu, Y.; Tong, X.; Lu, L., Extraction of vanadium from direct acid leaching solution of clay vanadium ore using solvent extraction with N235. *Hydrometallurgy* **2018,** *177*, 27-33.

77. Jiang, D.; Song, N.; Liao, S.; Lian, Y.; Ma, J.; Jia, Q., Study on the synergistic extraction of vanadium by mixtures of acidic organophosphorus extractants and primary amine N1923. *Separation and purification technology* **2015,** *156*, 835-840.

78. Tavakoli, M. R.; Dreisinger, D. B., Separation of vanadium from iron by solvent extraction using acidic and neutral organophosporus extractants. *Hydrometallurgy* **2014,** *141*, 17-23.

79. Martins, A. H., Vanadium Precipitation From Sulfate Acid Solutions. *Canadian metallurgical quarterly* **2000,** *39* (1), 15-22.

80. Huang, Z., Hydrolysis of Titanic Acid in Hydrochloric Acid Solution for Synthesis of TiO2 Powder with Controlled Particle Size: Processes, Morphology, and Kinetics Study. M.S. Thesis, University of Utah, Utah, USA, **2017**.

81. Bumby, C., Hydrogen - an alternative reductant? https://stirringthepot.podbean.com/e/hydrogen-an-alternative-reductant/ (accessed 20-11-21)